Flinders
UNIVERSITY

School of Computer Science, Engineering and Mathematics

Sensitivity of a strain measurement technique to detect disc injury using radiostereometric analysis

Submitted by

Vasanthi Pendyala

2131653

Studying Master in Biomedical Engineering

Supervised by Dr. John Costi

Submitted to the School of Computer Science, Engineering and Mathematics in the Faculty of Science and Engineering in partial fulfilment of the requirements for the degree of Master in Engineering (Biomedical) at Flinders University- Adelaide, Australia

Submitted on May 8th 2018

Disclaimer

I certify that this work does not incorporate without acknowledgement any material previously submitted for a degree or diploma in any university and that to the best of my knowledge and belief. It does not contain any material previously published or written by another person except where due reference is made in the text.

Vasanthi Pendyala Date

P. Vasanthi 08/05/2018

Acknowledgement:

I would like to express my sincere thanks to my supervisor Dr. John Costi without whom I could never have accomplished my project. I am very thankful to all members of engineering services for their support. My gratitude to Flinders University for providing me all the guidelines to accomplish my work. Special thanks to Dhara Amin who helped throughout the testing process, and parents who believed in me and finally to all my professors, lecturers and friends who directly or indirectly help me finish my project.

Abstract

The intervertebral disc (IVD) is a vital element of the spine in the human body. It helps in the spine movement and acts as a shock absorber. When there is an annular tear or any damage to the disc, there will be a change in its internal strains. One way of calculating internal strains is by placing radiographic end plate markers, circumferential markers and a grid of wires in the disc and then calculating the displacement of the markers by reconstructing a 3D image by digitising the digital radiographs of the disc using the radio-stereometric analysis (RSA). The primary objective of the experiment was to study how sensitive the internal strain measurement technique in detecting the internal strains in different stages of disc injury. Bovine tail intervertebral discs were used in this study, as they are similar to human intervertebral disc composition, geometry and are also cost effective.

Five healthy bovine intervertebral discs marked with radiographic endplate markers, circumferential markers, and a wire grid were inserted into the disc, and 6 degrees of freedom (DOF) testing was performed followed by taking x-rays after each DOF. In this study, three different states of the disc are subjected to test. The three states are as follows:

Case 1: Testing the disc in its uninjured state,

Case 2: Testing with a minor injury (5mm width and depth rim lesion),

Case 3: Testing with a significant injury (5mm depth and 10mm width rim lesion).

In each case, the disc was subjected to 6DOF testing. The injury induced onto the disc in this study was a rim lesion, and the 6DOF in which the disc was stimulated are left axial rotation, right lateral bending, extension, flexion, flexion rotation, and compression at 0.1Hz. The 3D reconstructed outputs of x-rays taken after each DOF are compared with the 3D reconstructed outputs of x-rays taken at the neutral position of the disc. In total 18 test results were collated for each disc. From 6DOF Hexapod testing output data the stiffness and hysteresis loss ratio (mechanical properties) of the disc of the disc are also calculated. The mechanical properties of the disc in each DOF were compared in the three test cases.

There were no significant changes within-subjects effects observed between the stiffness and hysteresis loss ratio values ($p > 0.05$) of the disc in its different test cases. The reconstructed 3D images of the IVD after each DOF were compared to IVD in neutral position for the three test cases. Displacement of the wire intersection points was calculated. An intra-observer variability (repeatability) test was conducted to check for the user error that might affect the final results of the specimen.

Hence, it was concluded that there was no change in the mechanical properties of the disc after performing the 6DOF testing. The maximum value of user error calculated from the intra-observer repeatability study is about 0.29 mm. The change in the radius of the disc periphery after inducing an annular tear explains that the RSA technique was able to detect the changes occurring in the disc, by experimenting on different ranges of disc injuries and more number of samples gives an accurate sensitivity of the technique.

Table of Contents

LIST OF FIGURES

LIST OF TABLES

1 Introduction

The intervertebral disc (IVD) is present in between two adjacent vertebral bodies of the spine. In total, the human spine consists of 23 intervertebral discs. IVD is made up of fibrous cartilage and serves as shock absorbers while allowing the spine to twist and bend (Humzah and Soames, 1988). The IVD is degenerative when there is a repetitive complex movement in the spine like lifting heavy loads. The IVD acts as a viscoelastic material (Virgin 1951). Disc degeneration and low back pain are common problems (Newell et al., 2017). The disc mechanics is an important aspect to understand the functioning and degeneration of the disc (Krag et al., 1987). IVD internal strains are calculated experimentally by tracking the small metal beads and wires inserted into the intact disc using stereo-radiographs (Krag et al., 1987; Costi et al., 2007). The primary objective of this study is to determine how sensitive the strain measurement technique is to detect disc injury using radio-stereometric analysis (RSA), as the previous studies have not mentioned anything about the sensitivity of strain measurement technique.

2 Literature Review

2.1 Intervertebral disc

There are twenty-three discs in the human spine: five in the lumbar region (lower back), twelve in the thoracic region (middle back) and six in the cervical region (neck). The spine (also known as vertebrae) is composed of 24 bones. These 24 bones are connected to each other with muscles and ligaments to form spinal column by which the body perform functions and gain shape. The spinal cord (bundle of nerves) is protected by spinal column, which sends signals to the other parts of the body (Wilke et al., 1997).

The intervertebral discs' make up a quarter of the vertebral column. There are no discs between Coccyx, Atlas (C1), and Axis (C2). These discs are non-vascular and consequently based on the end-plates to diffuse required nutrients. The cartilaginous coatings of the end-plates help to keep the discs in position.

The intervertebral discs are made of a fibrocartilaginous material that helps the backbone's shock captivating system, which shields the vertebral column, brain, and many other structures. The intervertebral discs permit extension and flexion (spinal motion). Single disc motion is reserved, but the significant motion may be attainable when the discs are connected to each other (Bogduk et al., 1981, White and Panjabi, 1978). The outer portion of the intervertebral disc is made up of annulus fibrosus, which is a very strong material. The inner portion is made of a jelly-like matter called mucoprotein gel. This internal part is also called nucleus pulposus (Figure 1) (White and Panjabi, 1978).

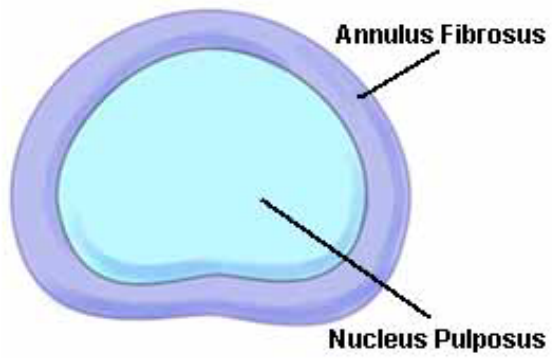

Figure 1: Axial (top) view of the intervertebral disc (White and Panjabi, 1978)

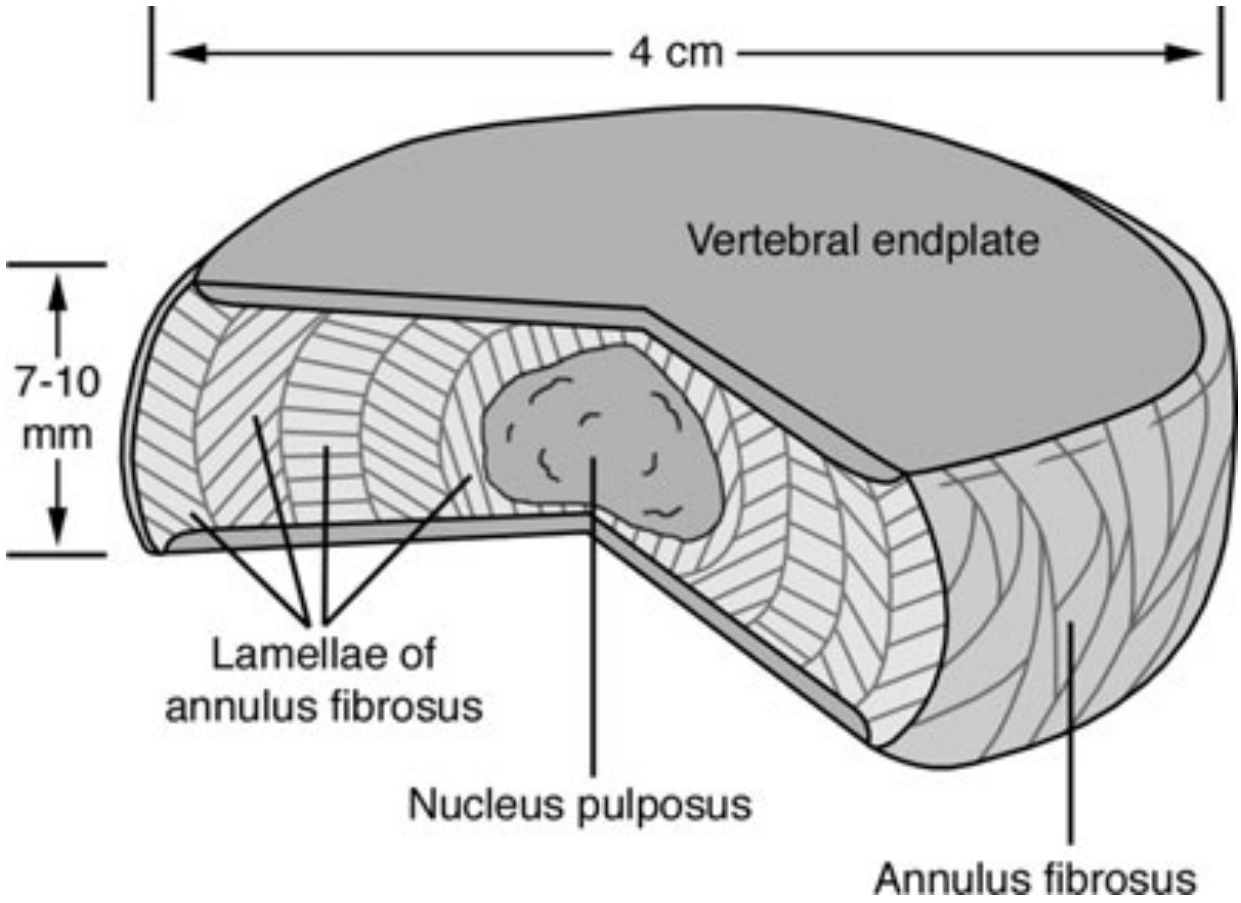

Figure 2: Showing the structure of the intervertebral disc (Raj, P. Prithvi, 2008)

When there is an effect from activity, intervertebral discs between each of the vertebrae in the vertebral column absorbs the shock. They also shield the nerves, which pass between the intervertebral discs and spine. Intervertebral discs are soft and compressible and are present between the vertebrae that make the whole spine. These disc acts as shock absorber for the spinal column. By applying pressure on the spine, the mucoprotein gel moves inside the outer covering and redistributes to absorb the pressure's impact. With the increase in age of a person, the gel loses its moisture, and the shock absorption power of the spine decreases. The outer layer of intervertebral disc weakens with age and can tear apart which causes long-lasting back pain for some people (Bainville et al., 1997).

Degenerative disc disease (DDD) is not a disease, but simply a term used to describe the natural breakdown of the intervertebral disc as the person becomes older. Degenerative disc disease

can happen across the spine, but it mostly takes place in the discs present in the lumbar region (lower back) and the cervical region (neck).

The variation in the discs with age can result in neck or/and back pain:

Osteoarthritis: The collapse of the cartilage tissue that cushions and protects joints.

Herniated disc: An uncharacteristic swelling or breaking open of a vertebral disc.

Spinal stenosis: The tightening of the spinal canal, the open space in between the vertebral column that grasps the spinal cord.

2.2 Annulus fibrosus structure

The annulus fibrosus is the tough circular external portion of the intervertebral disc, which surrounds the internal gel core known as the nucleus pulposus. The annulus fibrosus is composed of collagen fibres (both type I as well as II). These fibres are present in layers as a lamella, with a concentric arrangement pattern. The collagen fibres are embedded in a matrix made of hydrated proteoglycans with lesser quantities of elastin, small proteoglycans, and minor collagens. The type I collagen fibres are present in greater concentration near the outer edge of the ring, in order to provide strength to the structure (Tavakoli, Elliott and Costi, 2016).

The lumbar disc annulus fibrosus and its inherent structure were examined in detail in earlier decades when its function and composition were not well understood. Marchand and Ahmed carried out a breakthrough study in 1990, where they made use of a layer-by-layer peeling mechanism to investigate numerous cut surfaces of the disk microscopically. The specimen samples of the annulus fibrosus from subjects of different ages were taken from disc L2-3 and L4-5. They were purposefully dehydrated in a controlled environment to aid visual contrast between the translucent matrix and the opaque white collagen fibre bundles. Then the annulus structure was closely examined in relation to its circumferential and radial locations.

Their study divulged several new features of its structure. The authors found that apart from the transition zone, the annulus fibrosus is made of 15-25 distinct layers. Approximately half the layers have termination or origination points, contributing to irregularities in the lamellae. Furthermore, they discovered two mechanisms causing layer interruptions at the irregular

regions. The authors discussed that the thickness of each individual layer differs circumferentially as well as radially, growing with age. Lastly, the authors concluded that 20-62 fibre bundles make up the height of the disc, while the mean inter-bundle space was 0.22mm.

Guerin and Elliott published a study in 2007, which compared the contributions of the structure of the annulus fibrosus to tissue mechanical behaviour (Guerin and Elliott, 2007). Guerin and Elliott used an anisotropic nonlinear hyper-elastic annual fibrosus structural model and concluded that the amplification of the traditional models of non-linearity could be denoted to interfaces between the collagen fibres and the matrix. These interactions are enabled by the minor collagens and elastin crosslinks.

The stiffness of the annulus fibrosus structure and composition allow it to withstand complex loads and compressive forces, while the nucleus pulposus behaves as a shock absorber (Youssef, Lopez and Kabo, 2017). The pressure from any force is distributed evenly across the discs due to the annulus fibrosus behaving in an inhomogeneous, anisotropic and nonlinear mechanical manner, meaning that the structure functions as a protective lamina (Iatridis, 2016). Damage could otherwise occur to the vertebrae lying below, or to their endplates, because of the development of stress concentrations.

2.2.1 Different types of Annulus injuries

The intervertebral disc's strongest component is the annular disc, which connects each vertebra to the other. These fibres disperse pressure across the disk and the nucleus within the disc absorbs the shock of physical impacts, thus protecting the spine. Like any other portion of the body, the disc is also potentially vulnerable to injury. The annulus can undergo ruptures or tears on any area of the disk.

If there is a tear without any rupture of disc material, this is termed an annular tear. An annular tear of the fissure is the outcome of a traumatic or degenerative change occurring in the intervertebral disc. The tears are in fact breakages or separations within the collagen fibres, which constitute the annulus fibrosus. Tears in the annulus fibrosus compromise disc integrity, leading to pathological changes such as bulging and prolapse. The result of annular tears is compression of structures within and surrounding the annular fibrosis. A herniation is when an

annular tear introduces a channel for the disc's internal components to exit the annular fibrosis. Annular tears have been reported to result in premature disc degeneration, degeneration of facet joints and end-plates.

Tears involving the outer third disk are called circumferential tears (also known as delamination). These tears are often caused by compression of older discs. They are extremely painful due to that region being highly innervated. Circumferential annular tears heal over time, leaving a scar tissue, however, that area remains prone to tears and injuries in the future (Gallucci et al., 2011).

Radial tears are an outcome of fibre breakage as they extend from the nucleus to end-plate of the disc. Radial tears often occur as a natural ageing process and are usually symptomless; however, they greatly contribute to the imminent degeneration.

Horizontal tear of the disc are known as transverse tears and are often seen alongside radial tears. These small tears signify the initial stage of age-related disc distortion. Peripheral rim tears are painful and are more commonly exhibited by the anterior annulus. They are due to either trauma or the annular bony attachment avulsing near the cartilaginous endplate. These rim lesions are present in the outermost annular fibres where they insert into the bony ring apophysis. It is proposed by Wang et al. (2012) that rim lesions contribute to the onset of disc degeneration, vertebral endplate and facet joints degeneration. Rim lesions self-repair to a certain degree with the creation of fibrocartilaginous and fibrovascular tissue.

Annular tears are even experienced by people as young as 15 years old (Maxfield, 2010). Growth as well as an increase in stress cause structural defects to normally peak in middle age. The cause of most annular tears is ageing and natural disc degeneration. However, traumatic injuries also result in annular tears; for instance, due to injuries experienced while playing high-impact sports. Treatment of annular injuries involves physiotherapy, anti-inflammatory medications, analgesic medications, and a combination of rest and low-impact exercises. Surgery will be considered in a rare case (Guterl et al., 2013).

2.2.2 Changes in stiffness of the disc with degeneration

Intervertebral discs are prone to degeneration with age. The vertebral disc has stiff exterior thanks to the tough collagen fibres, which constitute the annular fibrosis. This lamellar structure or the gel-like nucleus pulposus that it houses do not escape age-related deterioration and its mechanical qualities and thus function inevitably suffer. Adams and Roughley (Adams and Roughley, 2006) discussed that these degenerative changes are the contributing factors to a number of orthopaedic impairments for the middle aged and the elderly, such as neck and back pain and stiffness of the spine. Some factors responsible for age-related degeneration include poorer nutrition, the death of viable cells and cell senescence, matrix protein modifications and accumulation of broken down matrix molecules, as well as matrix fatigue failure.

Galbusera and colleagues in 2014, denoted morphological deterioration of the disc to a reduction in water content and collapse of intervertebral space, along with annular injuries such as tears (Galbusera et al., 2014). The researchers discussed that spine flexibility is connected to these changes. Degenerative changes to the nucleus pulposus and annulus fibrosus alter their biomechanical properties. The structural properties are also deteriorated due to such alterations to their material constitutions (Kepler et al., 2013). The degenerative changes also alter the viscoelastic properties of the entire disc and bring about the instability of the motion segment and structural failure.

The degenerative process is believed to be initiated in the nucleus pulposus, whose proteoglycan concentration decreases, and collagen type change from type II to type I, making it a far more fibrotic tissue. The nucleus gradually dehydrates, losing its hydrostatic pressure feature, and becomes stiff, diminishing its shock absorbing properties. Consequently, the load mechanics are also altered as the nucleus becomes stiff and not able to distribute the load effectively (Costi, Hearn and Fazzalari, 2002).

Urban and Roberts in 2003, reported that the vertebral disc demonstrates age-related degenerative changes earlier than all other human body connective tissues. Skeletal maturation and growth make the boundaries between the annular fibrosus and nucleus pulposus less significant, and the nucleus pulposus becomes stiffer and more fibrotic with age, losing its gel-

like properties. The disc structures become more irregular and disorganized with age, and consequently, the annular lamellae begin to bifurcate and interdigitate, with the elastic and collagen networks going haphazard. This causes the elastic response of the annulus to vary. The cleft formation is frequently noticed within the disc, alongside the formation of fissures, especially in the nucleus. Degeneration also results in greater blood supply and innervation to the discs (Urban et al., 2003).

The nucleus pulposus demonstrates cell proliferation and granular changes, which results in the formation of clusters. Simultaneously, cell death is also ongoing and necrotic and apoptotic cells become evident. Dynamic viscoelastic testing demonstrates that the elastic modulus of the annular fibrosus increases as degeneration increases. Along with elastic anisotropy, the permeability aspect of the disk is also altered due to the influences of age and diminishing of the water content, resulting in the decrease of disc height.

Tears in the annular fibrosus, which occur due to age, heal with the formation of fibrous scar tissue, hardening the lamella to such an extent that the functional spinal unit loses its flexibility. Although the annular fibrosus is meant to be stiff, its stiffness should not compromise spinal movements and functions (Inoue and Orías, 2011). Similarly, the nucleus also becomes stiffer and the discs fail to perform both their functions of ensuring proper spinal mobility and protecting the vertebra from contact and injury.

2.2.3 Techniques used to calculate internal disc strains:

I. Compression, Flexion and Lateral Bending Method:

   In this method 18 degenerated and healthy intervertebral discs were selected, and flexion, compression, extension and lateral bending were applied on these discs. The position of the wires that were placed in the mid-traverse plane was documented using the craniocaudal radiographs at loaded and unloaded steps. Radial and the circumferential strains from the lateral, anterior and the posterolateral were compared between the degenerated and the healthy IVDs when the load was applied on them (Tsantrizos et al., 2005).

II. Imaging under Mechanical Load Method:

Custom made load frame was build using the non-magnetic material so that the axial compression loads can be applied to the disc while it is being scanned by the MR scanner. The samples were kept in a fix position so that any damage caused by bending or torsion can be avoided. The imaging was done using the 3T MR scanner. Mid-sagittal images of the high-resolution were obtained with the help of the T2- weighted turbo spin-echo sequence. Another image having the details of mid-coronal was also obtained from the neutral loaded samples. The samples were tested with flexion, axial compression, extension positions and neutral in an arbitrary order (O'Connell, Vresilovic and Elliott, 2010).

Direct measurement of intervertebral disc maximum shear strain in six degrees of freedom Costi et al found that lateral shear and compression produce the maximum shear strain per mm of displacement and the combination of a lateral bending and flexion motion might cause the highest rate of disc injury (Costi et al., 2007). The shear strains are calculated using a strain measurement technique using radiographic analysis.

Detailed information of the procedure was followed to calculate the internal strains by Costi et al., 2007 as this project follows the identical procedure to study the sensitivity of the strain measurement technique to detect disc injury using radio-stereometric analysis.

Nine samples of human lumbar discs from three male spines were used in the study of disc and two adjoining hemi-vertebrae. The determination of disc grade was done based on the Thompson's criteria (Thompson et al., 1990). If seven of the disc have to be of grade 1, that means that they are in excellent condition and only two of them are in between grade of 2-3, this means that early signs of degeneration are shown only in the nucleus (Thompson et al., 1990). Specimens of the disc were preserved at a very low temperature (-80˚C) before they can be prepared for the testing phase by very careful dissection of the tissue present around them.

Radiographic markers were used for marking the lower endplate of each of the disc. The end plate at the lower end was marked with the help of lead beads of 1.5 mm length. One of the lead beads were placed at the center of the endplate at a diameter of 2mm tunnel

that was formed by drilling of vertebral bodies. Drilling was continued unless the resistance felt to be increasing which indicated that the endplate has touched. The margins of the endplate were affixed with the help of four peripheral beads (right, left, anterior, posterior). As seen during the dissection phase that cyanoacrylate was used to fix the beads into position. The periphery of the disc was marked by using an elastic band and after that the ends are glued together. With the passage of about 15-20 mins, 5mm length tantalum wire segments were inserted in the band after equal intervals. The increase in the tension of elastic band avoided contact to the concave posterior regions of that disc, the markers were present at the ±20 ˚ at the posterior side of the disc and therefore that region was ignored from any further analysis. After the process of marking is done, wires were introduced through each of the disc by threading it by the help of 18G needle. The alignment of every wire was accomplished with a rotation and translation stage.

By the addition of the wires, hemi-vertebrae were implanted in a radiolucent cup with the aid of polymethylmethacrylate cement. The use of this device made sure that the superior and the inferior surface of the cup is in suitable position. The lateral and axial radiographs from every embedded specimen were taken off. The reason of taking of these specimens was to ensure that the geometric center of the disc was in relevance to the cups. This identified position was then used as the rotation center for rotational tests. The tank was then filled with the adjustment protest for the stereo-radiography, which has almost 2 mm distance across the lead das that are mounted on it in the familiar positions. Before testing, every specimen was equilibrated in the bath with a 100 N compressive preload for three hours. After equilibration, stereo-radiographs of the specimen were taken and this position was considered as the underlying datum position.

Stereo-sets of radiographs were filtered utilizing a flatbed scanner at 650 dpi determination (0.044 mm/pixel). 90% certainty interim (90% CI) exactness RMS digitizing mistake was 0.044 mm (0.017 mm). In every film, points of interest were recognized and physically digitalized utilizing Matlab software. The DLT (DirectLinearTransformation) technique as actualized in Matlab schedules reconfu.m and dltfu.m was utilized for the stereo-remaking of the 3-D directions of every historic point. Coordinating endplate dabs were recognized by

the Hungarian technique (Matlab capacities condass.m and hungarian.m supportively given by N. Börlin), and coordinating plate fringe markers (tantalumwires in flexible group) from every film were dictated by the utilization of heuristic coordinating calculations.

Distinguishing coordinating recreated the midlines of the wires focuses on the wires by introducing along the relating pictures to discover insignificant DLT mistakes. In this manner, the nearest approaches ('crossing points') of wires were figured to characterize focuses for following tissue relocations.

Removals measured at the self-assertive positions (labeled focuses in every circle) were used first to insert value in institutionalized matrix locations with the goal that they could be arrived at the midpoint of b/w specimens. The general, regular, two-dimension planar matrix included 148 four-nodded quadrilateral components by a sum of 174 hubs. The fringe was characterized by a twelfth request polynomial fitted through found the middle value of directions of the fringe (flexible band) markers in un-dislodged (datum) positions. Relative 3-D relocations of all directions (wires, endplate dots and circumferential markers) between uprooted places of the specimens were ascertained and standardized by the separate information removal (mm/mm) or rotation (mm/°).

For movements that were thought to be symmetrical about the mid sagittal plane (axial rotation, horizontal twisting and parallel shear) the dislodging information for the two reciprocal movements were pooled, in the wake of representing contrasts in sign, and the outcomes are exhibited as though they were just for positive relocations (left axial rotation (+Rz), right sidelong bowing (+Rx), and left horizontal shear (+Ty)).

Mean provincial MSS values at each of nine anatomical districts were characterized by dividing the framework. These areas were: front (10 hubs), left/right anterolateral (8 hubs each), left/right horizontal (6 hubs every), core (15 hubs), left/right posterolateral (8 hubs each), and posterior (8 hubs). Territorial contrasts in MSS inside every uprooting or rotation were distinguished by a restricted ANOVA and Bonferroni-balanced post-hoc correlations. Measurable investigations were performed to assess territorial contrasts having the biggest MSS just, since shear is viewed as an imaginable tissue disappointment paradigm and is

gotten from foremost strains by the equation (P1-P3)/2. For each info removal, the districts with the biggest MSS were distinguished, and the biggest provincial MSS qualities were pooled wherever a few locales had values that were not altogether unique in relation to each other.

To distinguish the physiological rotations and removals that may put the plate at most serious hazard for substantial tissue strains and harm, the mean (95%CI) of the pooled local MSS were increased by the greatest announced physiological lumbar segmental movement for each DOF. Utilization of the biggest intersegmental movement (as opposed to qualities particular to every anatomical level) spoke to the 'assuming the worst possible scenario' intra-discal strains. The subsequent percent MSS for each DOF were then measurably thought about. The MSS at the extremes of physiological movement are alluded to as physiological MSS.

2.3 Radiostereometric Analysis

RSA is a method used to determine the accurate wear and migration of the orthopedic implants that includes the arthroplasties of the hip (Bottner et al., 2005). It is a straightforward concept through which the precise location of two different objects in relevance to each other in the 3D is measured. In the analysis of radiostereometric, the location of the original object is remade with the help of two 2D x-ray films shown in figure 3.

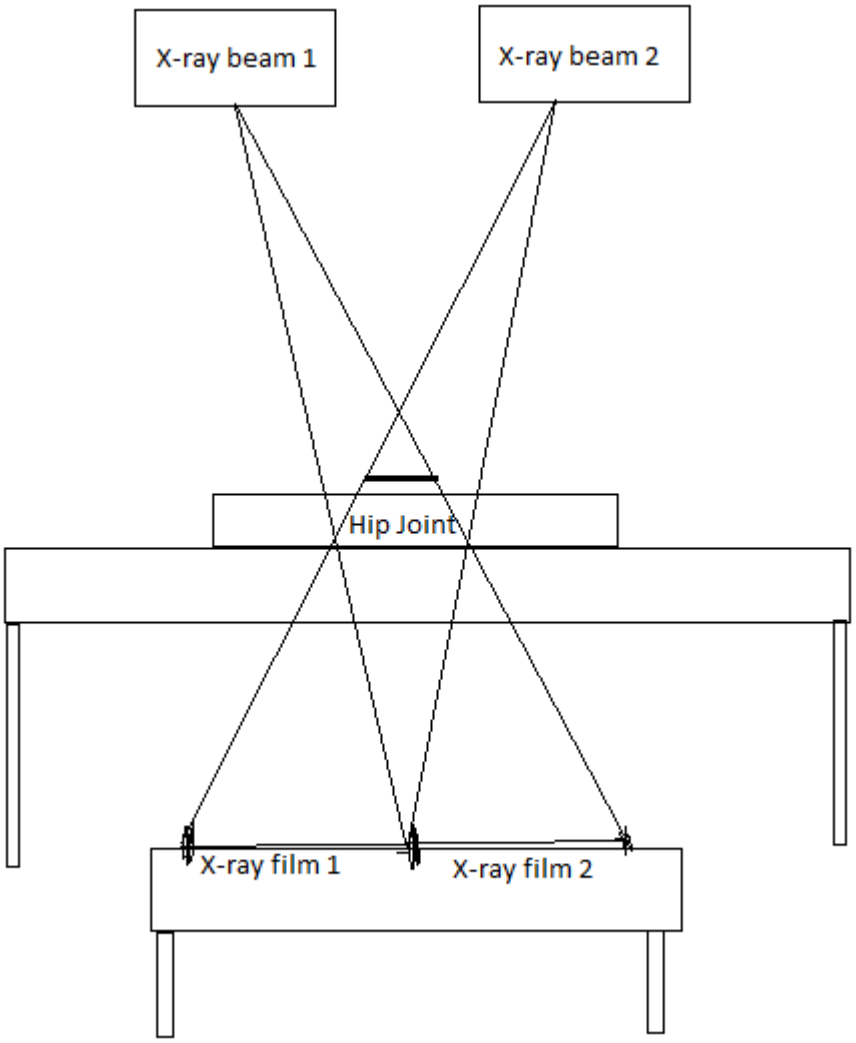

Figure 3: Showing the x-ray setup used to take the image ((Bottner et al., 2005))

To rebuild the position of the segments in the human body, every segment is marked with the help of using tantalum beads. The segment movement after that is measured with localising each of the segments in a coordinate system (Bottner et al., 2005). It is a very powerful

technique that is used in the surgery hospitals. The information that is acquired from the RSA technique can show the precise amount of position change occurring from the time of implant of the prosthesis, which helps the surgeon in determining the lifespan of an implant.

2.3.1 Accuracy of RSA

RSA has long been heralded as a reliable method of accurately evaluating the wear and degree of migration of orthopaedic implants. AP and ML x-ray images of any prosthesis are used by RSA to determine its 3D measurements. Bojan et al., 2015, emphasised in their recent study of RSA precision that it is necessary to determine the most accurate measure of following patients' progress and conducting research to improve orthopaedic implant design and technology (Bojan et al., 2015).

A study by Solomon et al. assessed whether RSA findings are precise and reliable in a tibial plateau fracture mode or not in 2010. They measured rotation and translation accuracy by using displacement-controlled stages, while precision was gauged via dynamic double examinations. The authors found that RSA is highly precise and accurate i.e., +/- 16 µm at 95% confidence interval assess fragment movement of a lateral tibial plateau fracture, and encouraged imminent RSA clinical fracture studies (Solomon et al., 2010).

Pineau et al. also carried out a quantitative study in 2010 to determine the accuracy of RSA when measuring femoral head migration in the cup of a dual mobility implant. Machined polyethylene liners with different layers of concentric wear were used in this model of RSA implant penetration measurement. Three examiners with differing levels of experience analysed the RS films of four liners while blinded to the concentric wear. The results established that model-based RSA is accurate enough to become the means of reference for measuring hip prosthesis wear in vivo (Pineau et al., 2010).

In 2012, Stilling et al carried out a phantom study to compare the accuracy of two methods of model-based RSA (2D and 3D) with a plain radiographic assessment of polyethylene wear (PolyWare). The study found that a 3D measurement of RSA methods accuracy is 0.2mm and for PolyWare accuracy is 0.3mm. When compared PolyWare with RSA methods, PolyWare is less accurate than RSA ($p=0.036$) (Stilling et al., 2012).

A literature review conducted in 2017 by Ten Brinke et al explored the accuracy of RSA measurements of upper limb implants (Ten Brinke et al., 2017). The review concluded that although RSA is a highly accurate technique for measuring early migration of orthopaedic implants, the rotation measurement precision was lacking in some components.

There is a possibility of the accuracy of RSA results to be compromised by human errors. To investigate this, Lin et al. conducted a study to evaluate the errors, which occur due to improper lower limb poses at the time of RSA. The research found that dorsal flexion induces image overlapping and reduces the accuracy of RSA by 0.3 to 10 times (Lin et al., 2017). Therefore, the authors recommended that whilst taking X-ray images for RSA, the limb should be held taut and vertical, with minimal flexion so that the quality of the projected X-rays does not distort RSA result findings.

From the studies of RSA accuracy it is apparent that researchers and medical practitioners have a similar opinion regarding RSA as the most accurate means of tracking the progress of orthopaedic implants. However, it was also pointed out that there is a possibility of the RSA results being incorrect due to image overlapping or limb poses; therefore, those conducting the analysis should ensure such errors in the account.

3 Objective

The objectives of the project are:

- To determine how sensitive the internal strain measurements using RSA are in detecting disc injury.
- To determine the repeatability/precision of the digitizing technique.
- To determine mechanical properties of the disc.

4 Methods

Five bovine tail FSUs were tested in total for this project, however the results of four FSUs were considered due to some technical issues. Each FSU testing was done in a sequence as shown in the flow chart below:

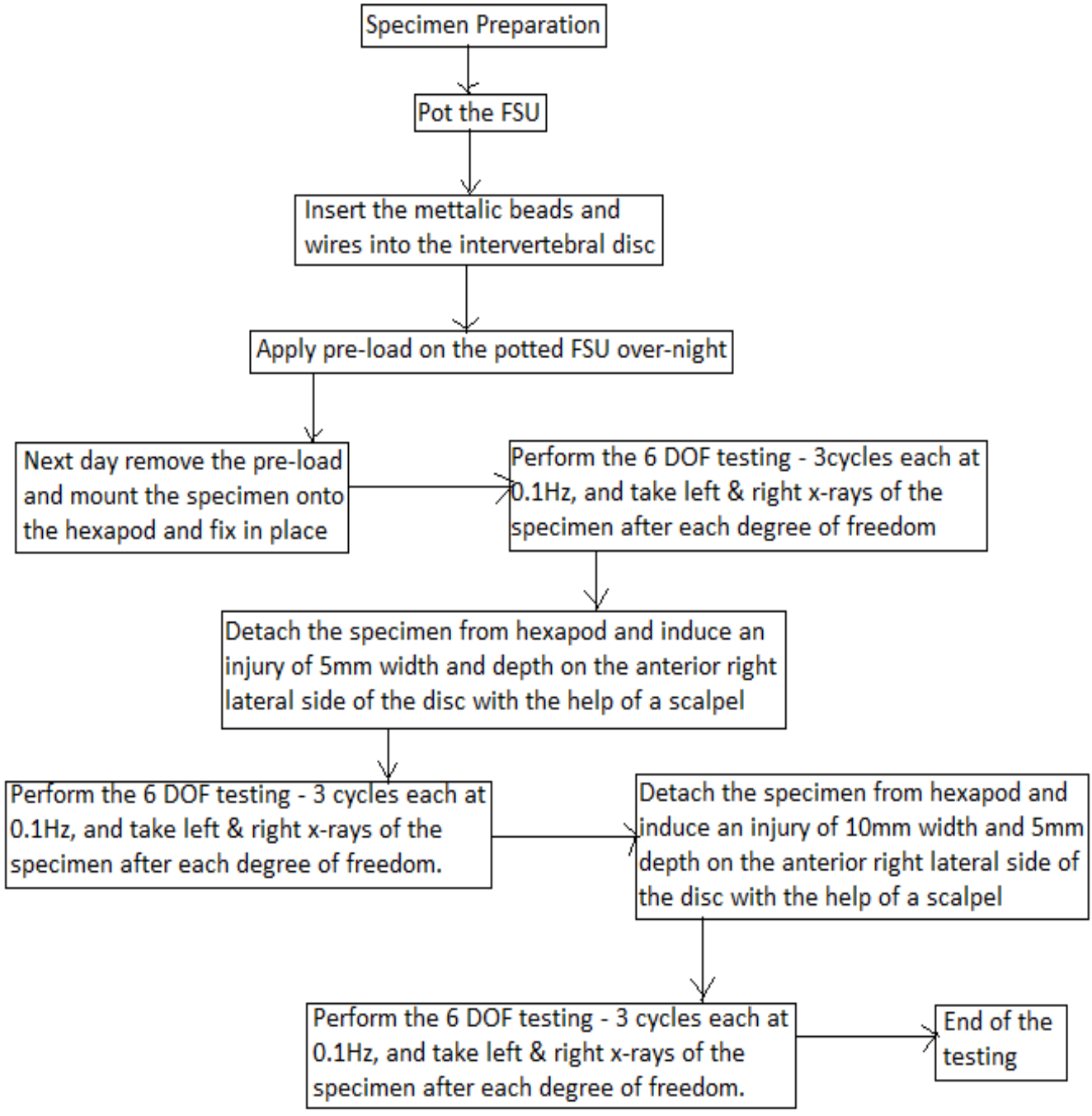

Figure 4: Showing the procedure followed for testing an FSU

4.1 Testing procedure

The following procedure is followed for all the five specimens.

1. Obtained bovine tails of freshly exterminated cows from the local abattoir.
2. Stored them at -20^{0}C in the freezer until the day of cleaning.
3. On the day of specimen cleaning: Allowed the specimens to thaw for three hours outside on a bench top. After the specimens are thawed well, all the soft tissue surrounding the intervertebral disc was cleaned. Each bovine tail was cut into two functional spinal units (FSU), FSU consists of an intervertebral disc intact with the adjacent vertebra (Figure 5). FSUs were wrapped with a saline soaked gauge and well maintained in a zip lock bag labeled with specimen id and date at -20^{0}C in the freezer until the day of specimen preparation for testing.

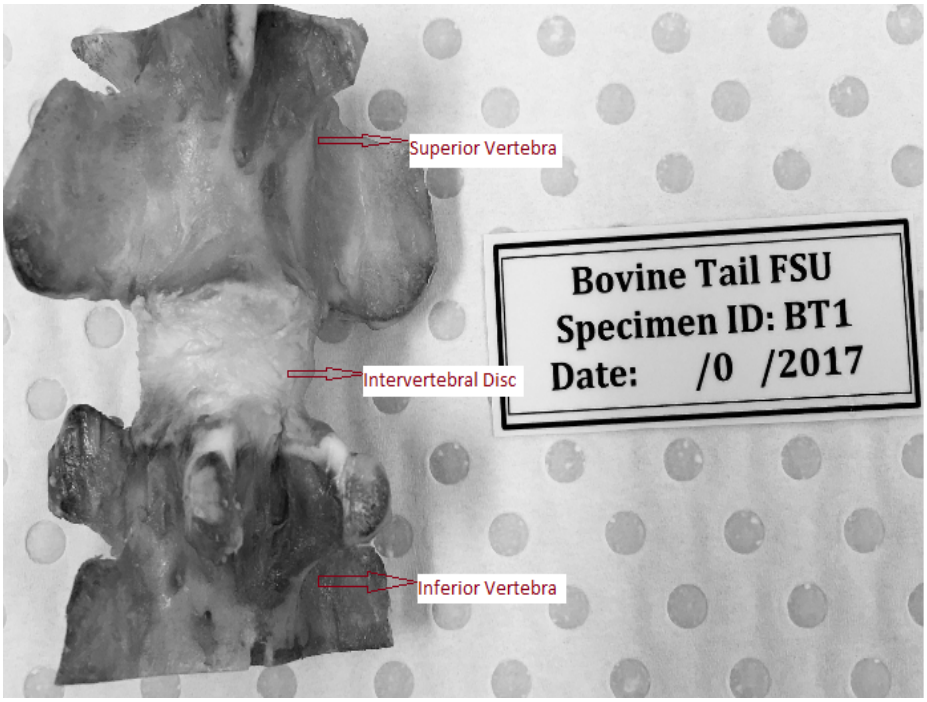

Figure 5: Image of an FSU

4. On the day of specimen preparation:
   a. Allowed the specimen to thaw on a bench top for two hours. Took the following (Table 1) FSU measurements using Vernier caliper.

Superior endplate anterior width (mm):	Superior endplate lateral width (mm):
Inferior endplate anterior width (mm):	Inferior endplate lateral width (mm):
Height of the superior vertebra (mm):	Height of the inferior vertebra (mm):
Height of the intervertebral disc (mm):	
Total FSU height (mm):	

Table 1: Measurements to be taken from the FSU before potting

b. With the help of a small hand drill, 1.5mm lead beads are placed on the endplates of the disc. Superior and inferior endplate has five beads marked on each. The beads are placed on the anterior, posterior, right lateral, left lateral periphery of the intervertebral disc endplate, and one at the centre of the endplate. The centre beads on the superior and inferior vertebra are placed by running a hand drill down the centre of the vertebra for a length (superior and inferior vertebra height respectively) measured before. Fixed the beads in place with the help of superglue**.** Figure 6 shows the lead beads fixed on the intervertebral disc periphery of the FSU.

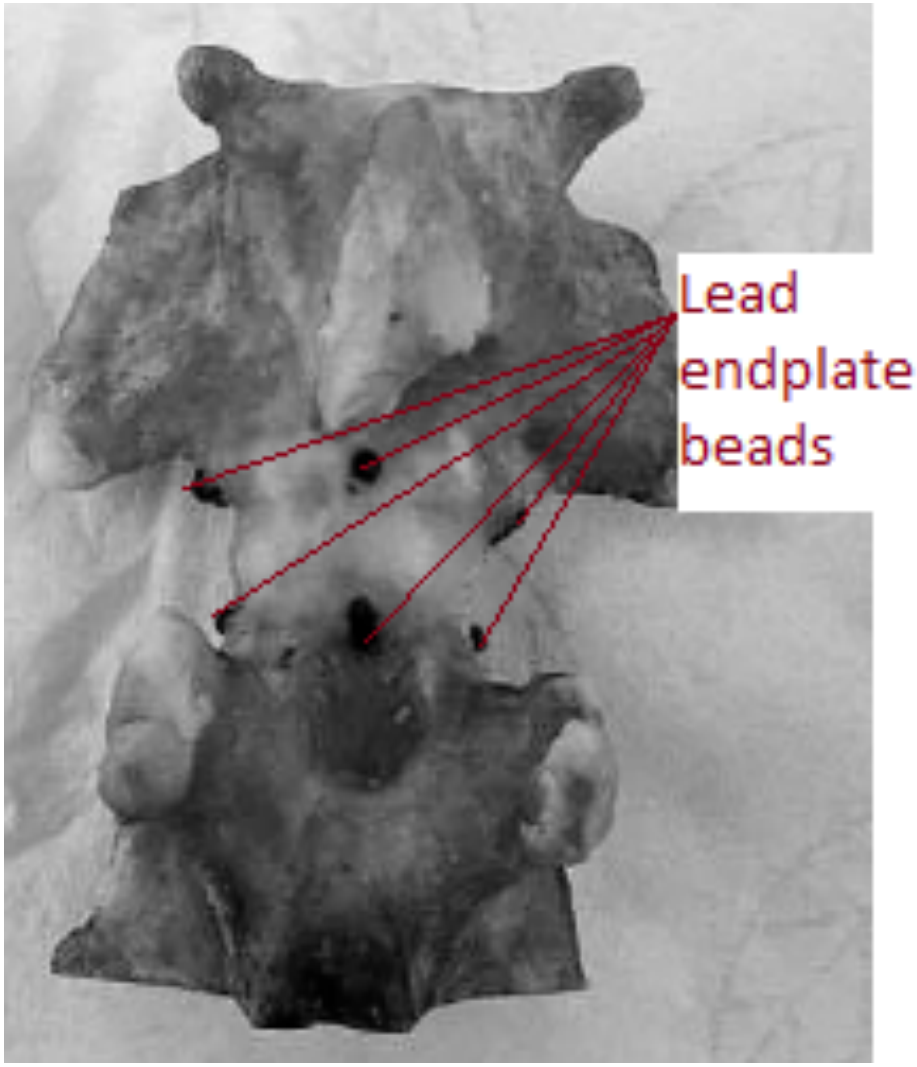

Figure 6: Showing the endplate beads placed on the FSU

For performing 6 degrees of freedom testing in the hexapod robot, the superior and inferior endplates of the FSU need to be potted into nylon cups.

c. First, the inferior vertebra was potted into the bottom cup after which the tantalum wires and circumferential markers are inserted into the intervertebral disc.

d. The inferior vertebra of the FSU was potted into nylon cups of 120mm diameter.

Required equipment: bench coat, alignment rig, alignment plates, potting cups, nylon screws (M6 X 60mm), mixing bowls, self-curing acrylic liquid and powder, gloves.

Attached the bottom cup to the bottom alignment plate, anterior facing forward. Placed IVD centre of the specimen at the centre of the cup and tightened the screws until they keep the FSU in place, at the centre of the cup.

Prepared the PMMA by mixing 71ml acrylic liquid and 179g acrylic powder and poured the solution into the bottom cup and waited for 15-20 minutes while the PMMA cured.

Figure 7: Acrylic powder and liquid used to make PMMA

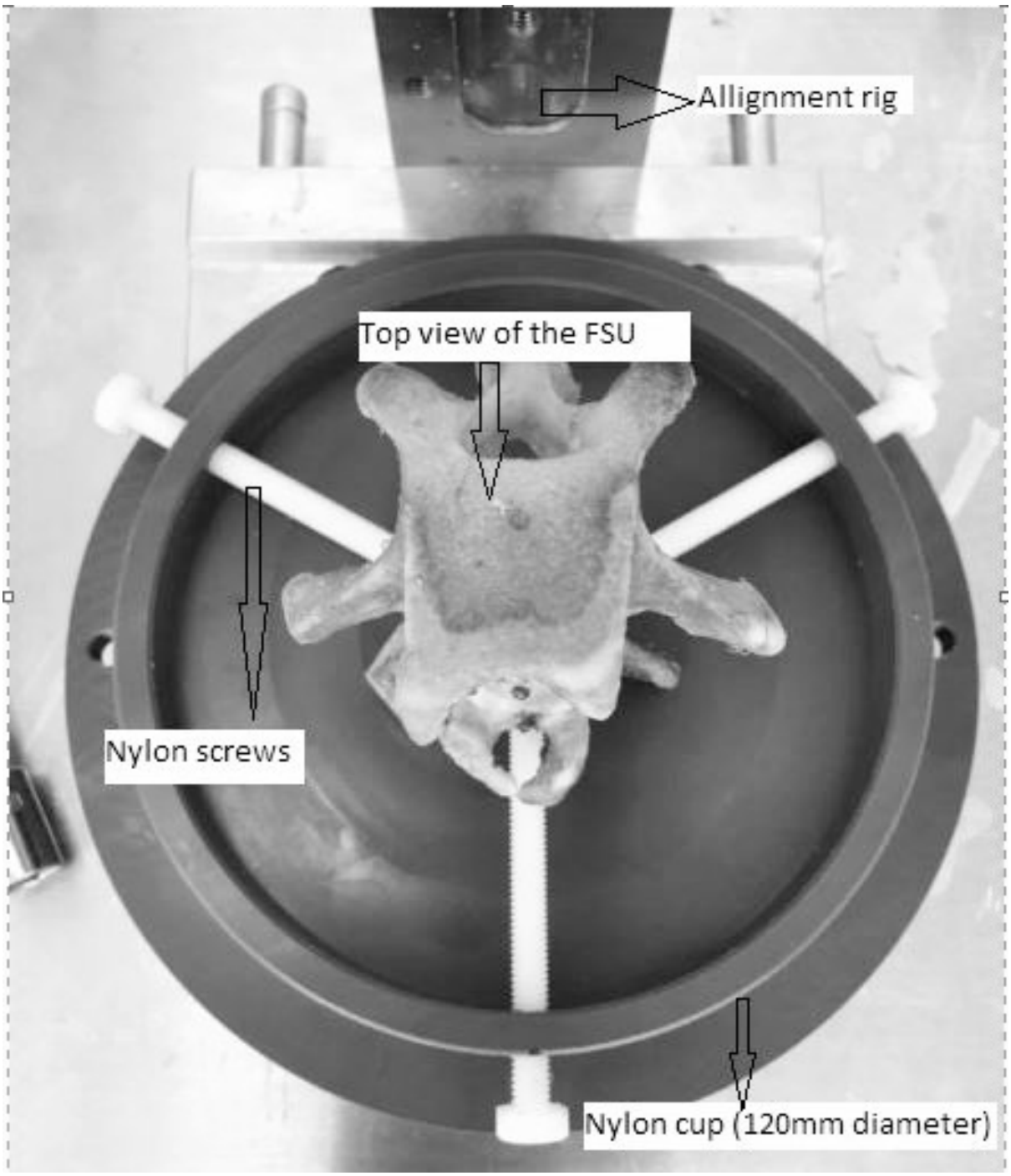

Figure 8: Top view of the FSU setup for potting inferior vertebra

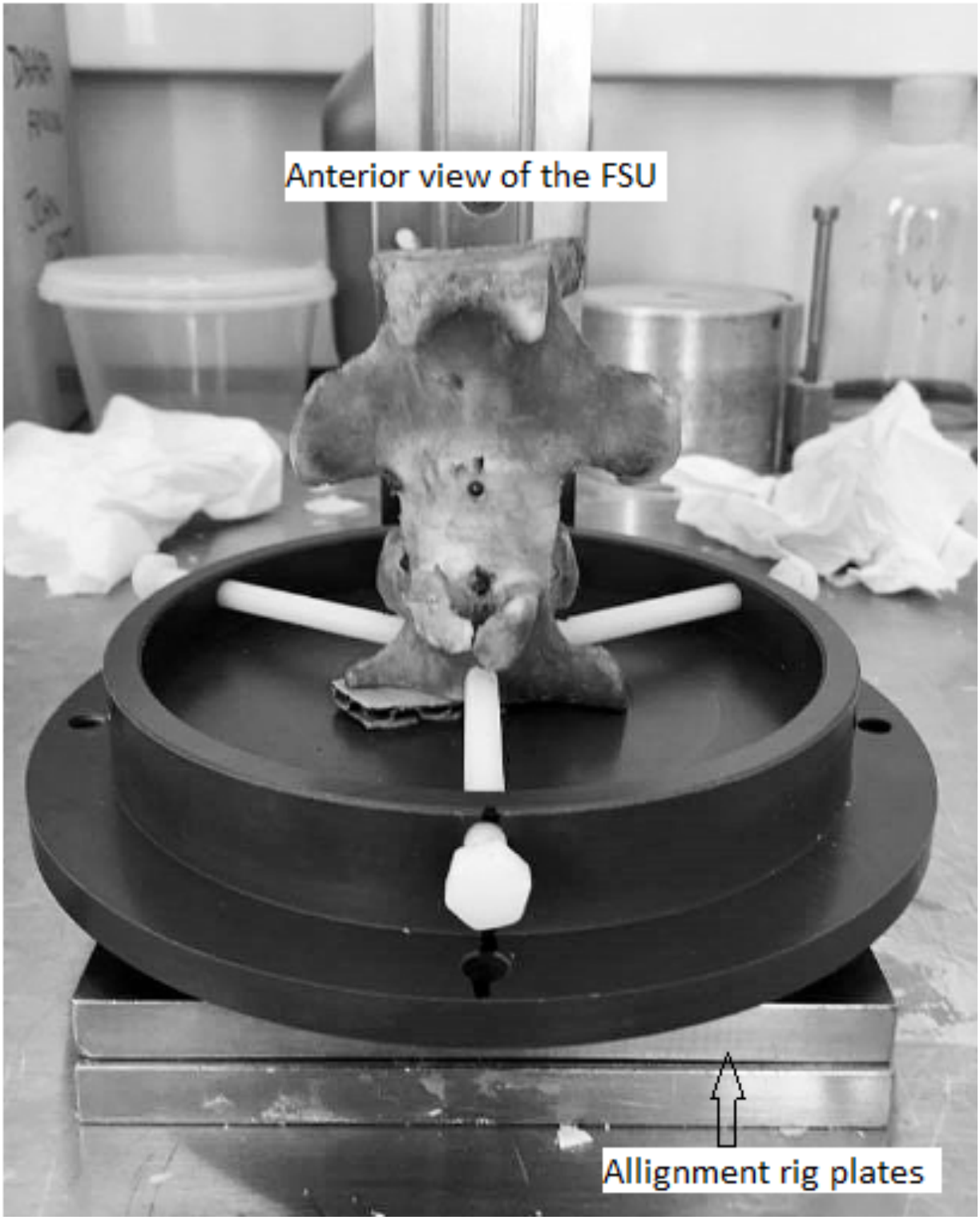

Figure 9: Anterior view of the FSU setup for potting inferior vertebra

e. After the PMMA has cured, measurements are taken for geometric offsets (x, y, and z-offsets) of the disc. The geometric offsets are used for testing in hexapod (Figure 10). The offsets are calculated as follows (table 2).

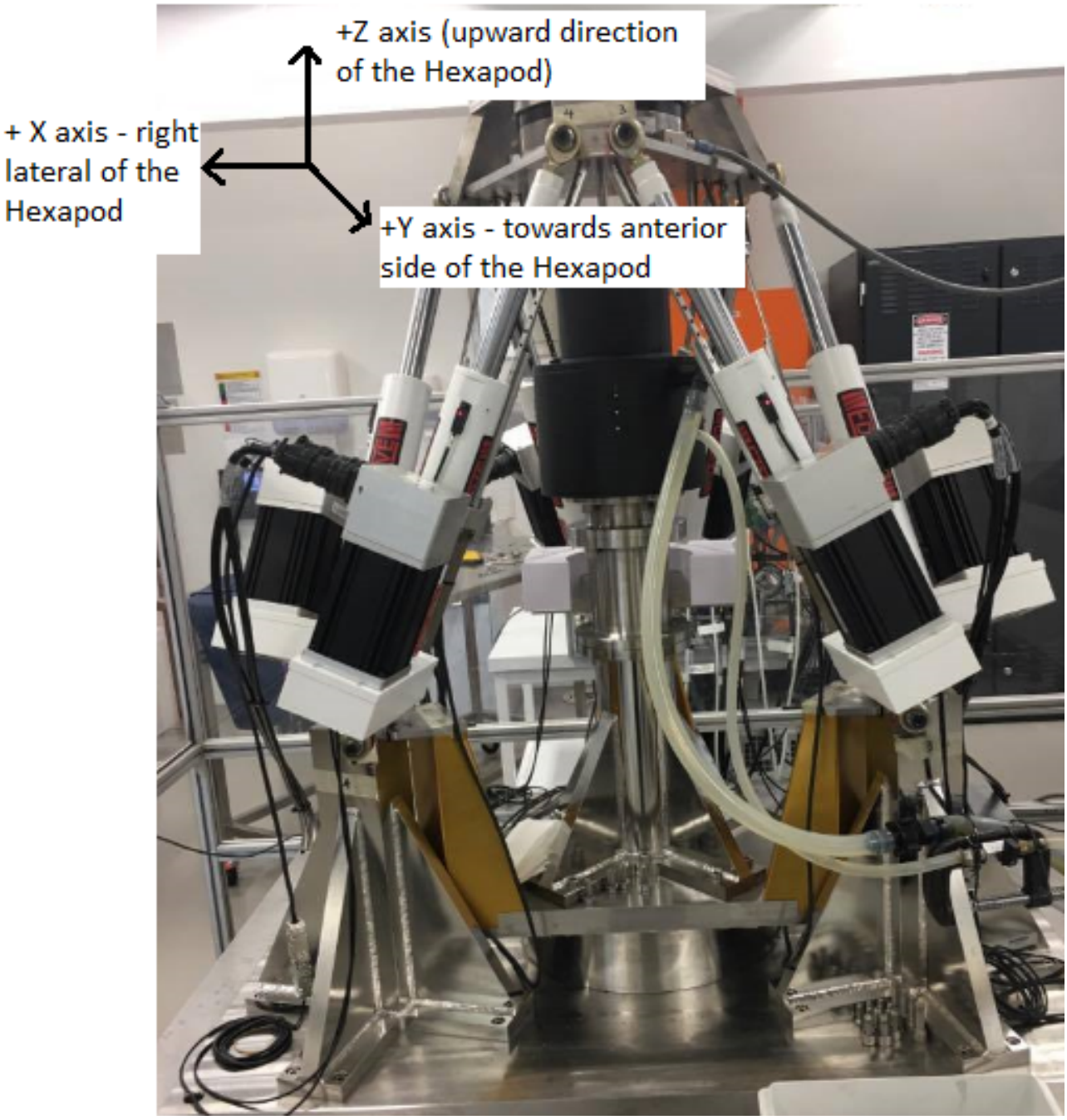

Figure 10: Axis direction of the hexapod robot

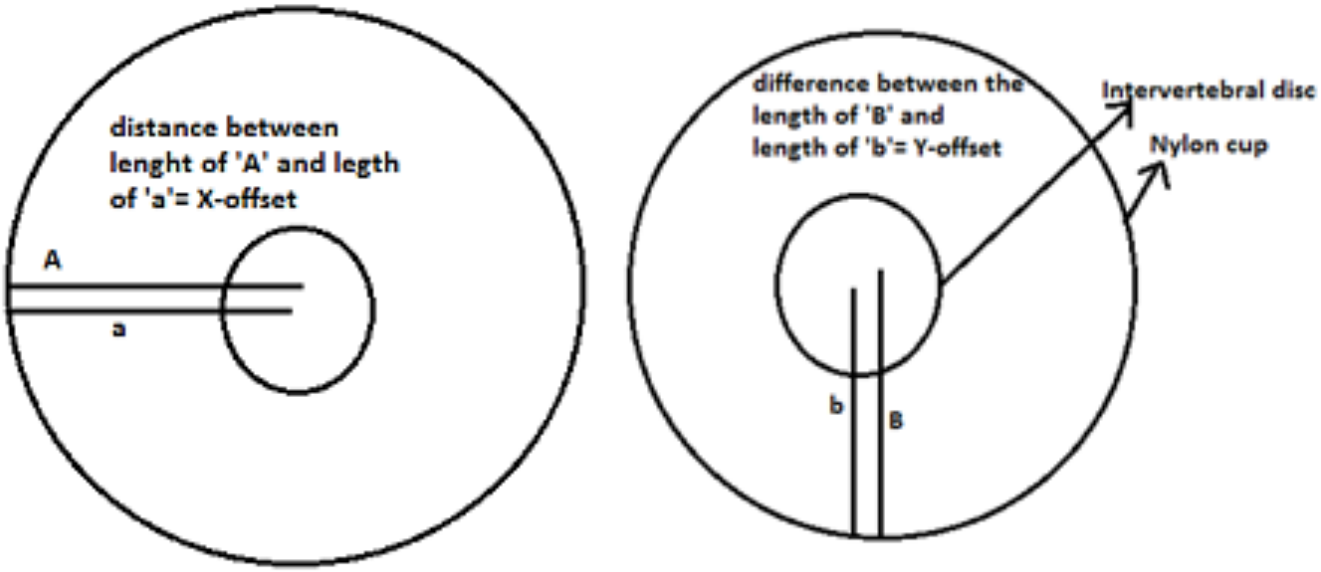

Figure 11: Calculation of X and Y- offsets

X-offset = distance between the centre of the disc and centre of the cup in the x-axis direction (mm).
Y-offset = distance between the centre of the disc and centre of the cup in the y-axis direction (mm).
Z-offset = height of the coupling plate of the hexapod (mm) + height of the top cup (mm) + height of the spacer (mm) + PMMA level to the middle of the disc (mm)

Table 2: Showing how to calculate the X, Y, and Z offsets for the hexapod system

f. A wire grid of 2X2 is inserted into the disc with the help of needles.

A stencil paper having grid lines at 45^0 angles was placed in a place on the bottom cup border. The wires are placed at an angle of 45^0 taking the guidance of the stencil paper. Eight circumferential markers are placed on the periphery of the disc. All the endplate beads, wires, circumferential markers are secured in place with the help of super-glue (Figure 12).

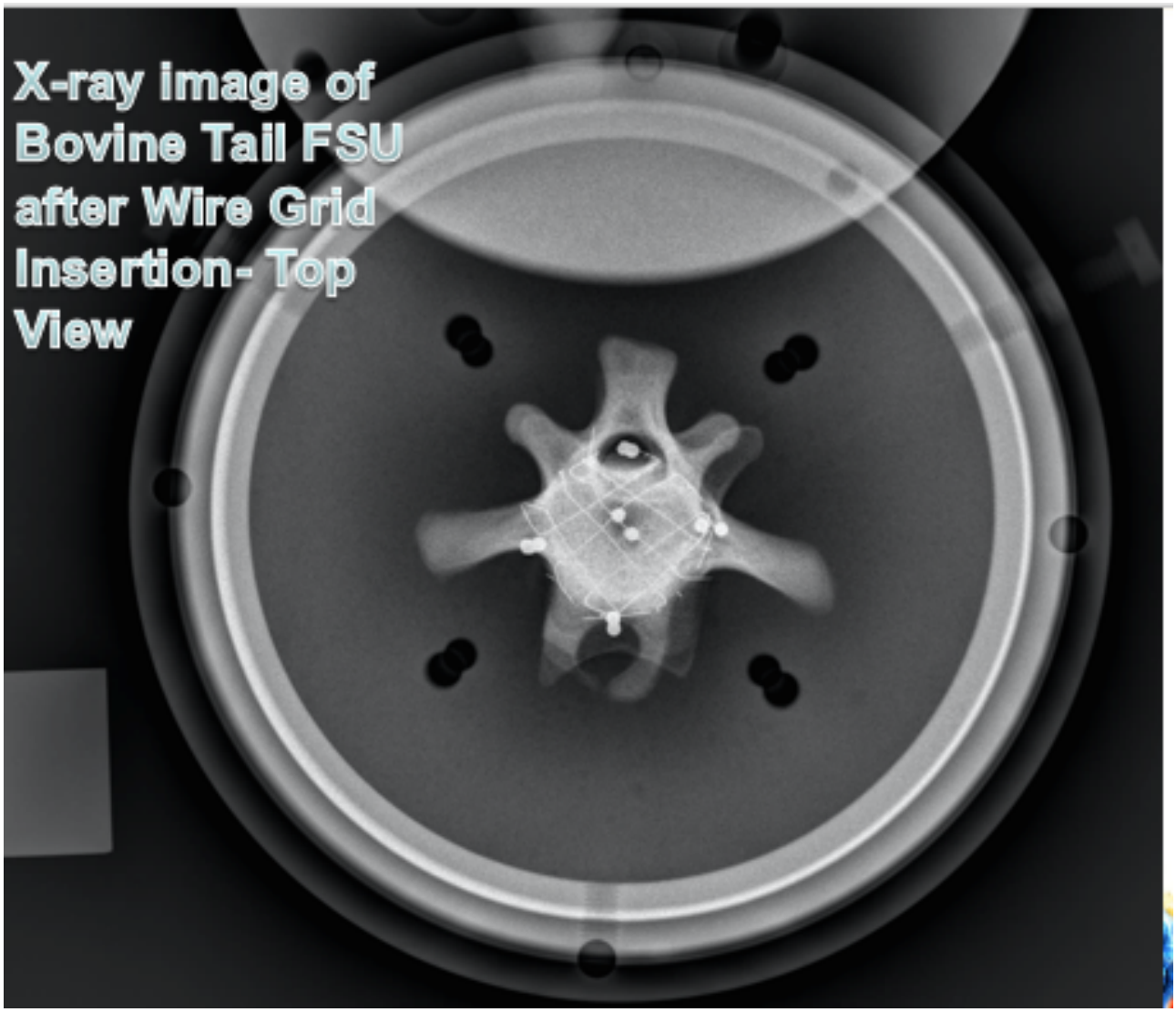

Figure 12: X-ray image of the FSU with wires, endplate beads, and circumferential markers

g. Potted the superior vertebra into the top nylon cup (Figure 13).

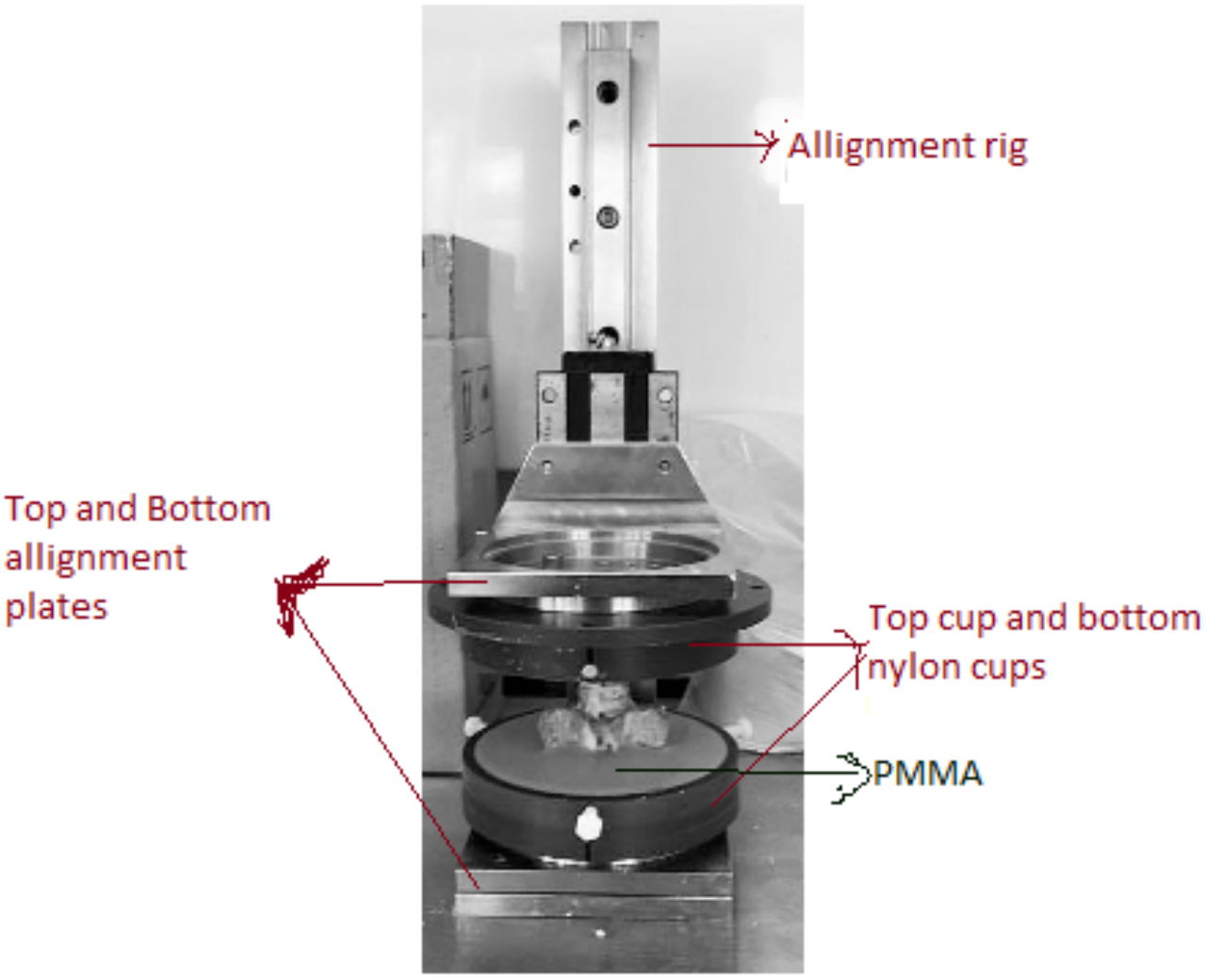

Figure 13: FSU after potting

h. Applied pre-load on the potted FSU to get it back to its normal physiological range of activity (Adams 2151-2156). The pre-load is based on the disc area measurements taken and substituting the values in the following equation for 18 hours (overnight):

$$pre - load = \frac{0.1}{1.5} * area\ of\ the\ bovine\ intervertebral\ disc\ (N) \ldots\ldots\ldots eq\ 1$$

While pre-loading the disc was kept hydrated with PBS (phosphate buffered saline). Figure 14 shows an image of the intervertebral disc soaked in a PBS

solution and with pre-load on it. On an average pre-load of 45N is applied on the FSU.

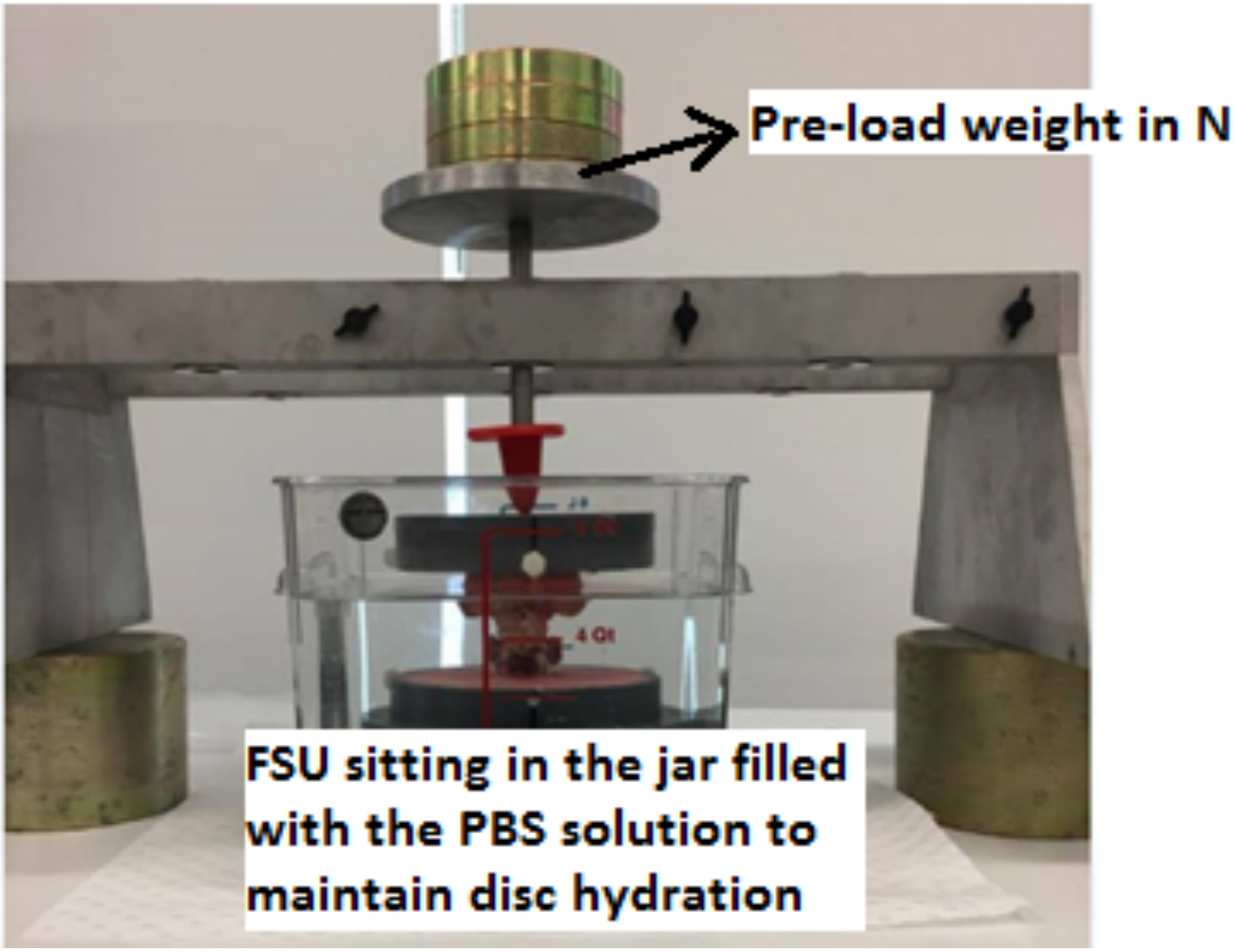

Figure 14: Hydrating the FSU while an over-night preload is applied

5. On the day of 6 DOF (degree of freedom) testing:
   a. The testing is done using the customized six-degree-of-freedom (6-DOF) hexapod robot (F. Fraysse et al., 2014). The specimen is fixed into a bath and then mounted onto the hexapod (Figure 15). The bath is then fixed to the hexapod base, and the bath is filled with 0.15M phosphate buffered solution (PBS) and maintained at room temperature to keep the disc hydrated.

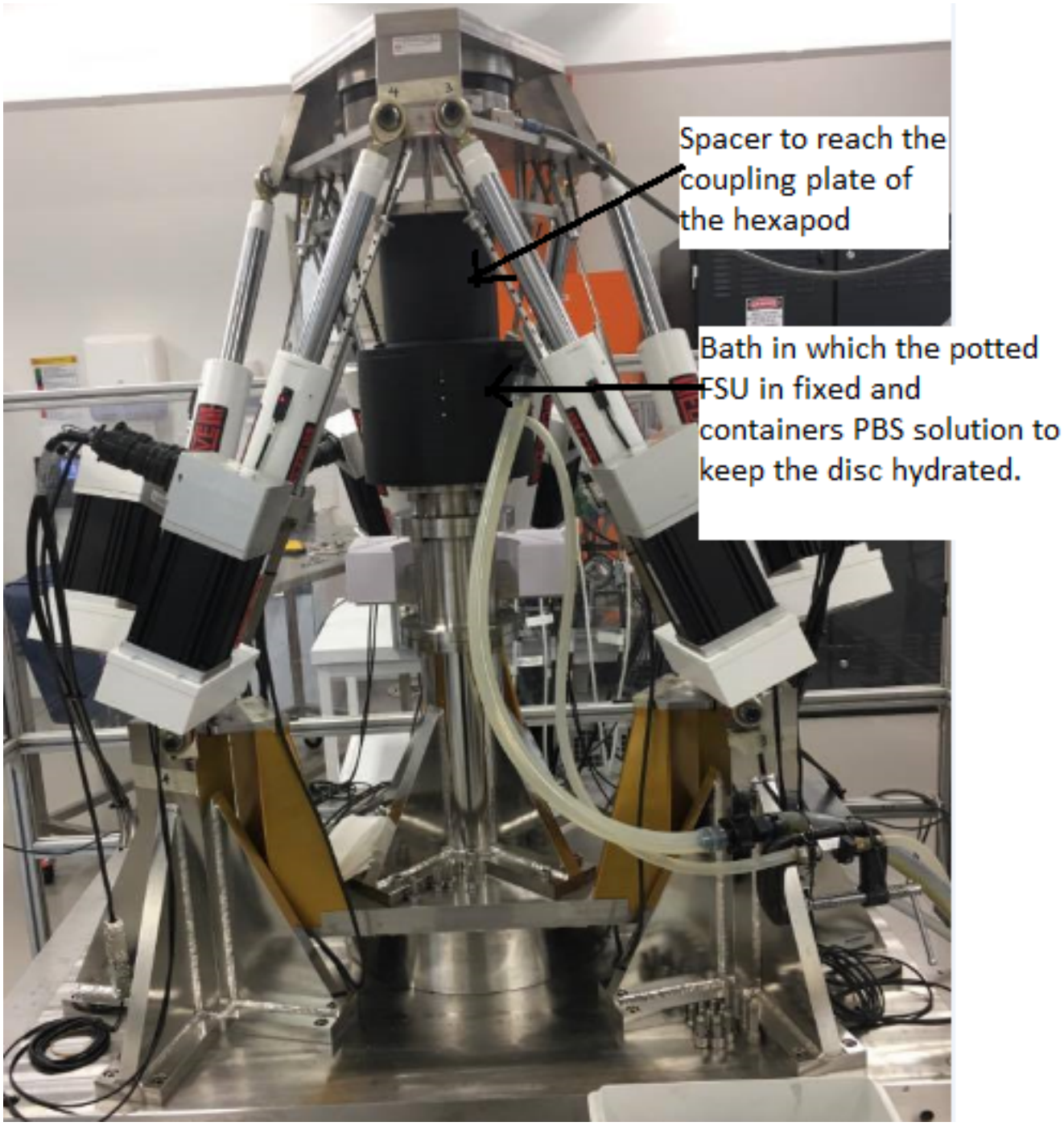

Figure 15: Hexapod robot with the specimen fixed to it

b. The testing of the FSU is done in three different cases:

Case 1: Uninjured disc inserted with lead beads, tantalum wires, and circumferential markers.

Case 2: Disc (inserted with lead beads, tantalum wires, and circumferential markers) with an induced annular tear of 5mm width and depth.

Case 3: Disc (inserted with lead beads, tantalum wires, and circumferential markers) with an induced annular tear of 10mm width and 5mm depth.

c. The 6 degrees of freedom in which the testing is done are left axial rotation (Rz), right lateral bending (Ry), extension (Rx), flexion (Rx), flexion (Rx)+ rotation (Rz), and compression (Tz). All the tests are done in position control mode, as the bovine tail is very floppy. The magnitude of the rotation in the experiment tests were chosen based on the studies conducted by (Amin et al., 2016), (Pearcy and Tibrewal, 1984), and (Costi et al., 2008). The active range of axial rotation and lateral bending at intervertebral joint in human is 2^0 and 3^0 respectively (Pearcy and Tibrewal, 1984).

The sequence of tests done: the test sequence mentioned below in table 3 is done for all the three cases. In total 18 tests are done on each FSU (6 tests for each case).

Test number	Direction	Test type	Hz	Cycles	Magnitude
1	Left Axial Rotation (Rz)	Dynamic	0.1	3	2^0
2	Right lateral bending (Ry)	Dynamic	0.1	3	3^0
3	Extension (Rx)	Dynamic	0.1	3	2^0
4	Flexion (Rx)	Dynamic	0.1	3	-5^0
5	Flexion + rotation (Rx)	Dynamic	0.1	3	$(-13^0) + (-2^0)$
6	Compression	Dynamic	0.1	3	-0.6 MM

Table 3: Showing the tests done in sequence

d. After each test, the specimen was then moved into the maximum position of the respective test done and left, and right x-rays are taken. For example: After performing the dynamic test in left axial rotation for 3cycles at 0.1Hz specimen is moved back to 2^0 in the left axial rotation direction and positioned to take x-ray images of the specimen. The x-ray beam was rotated to 56^0 angle to the specimen to attain a proper x-ray image (Figure 16).

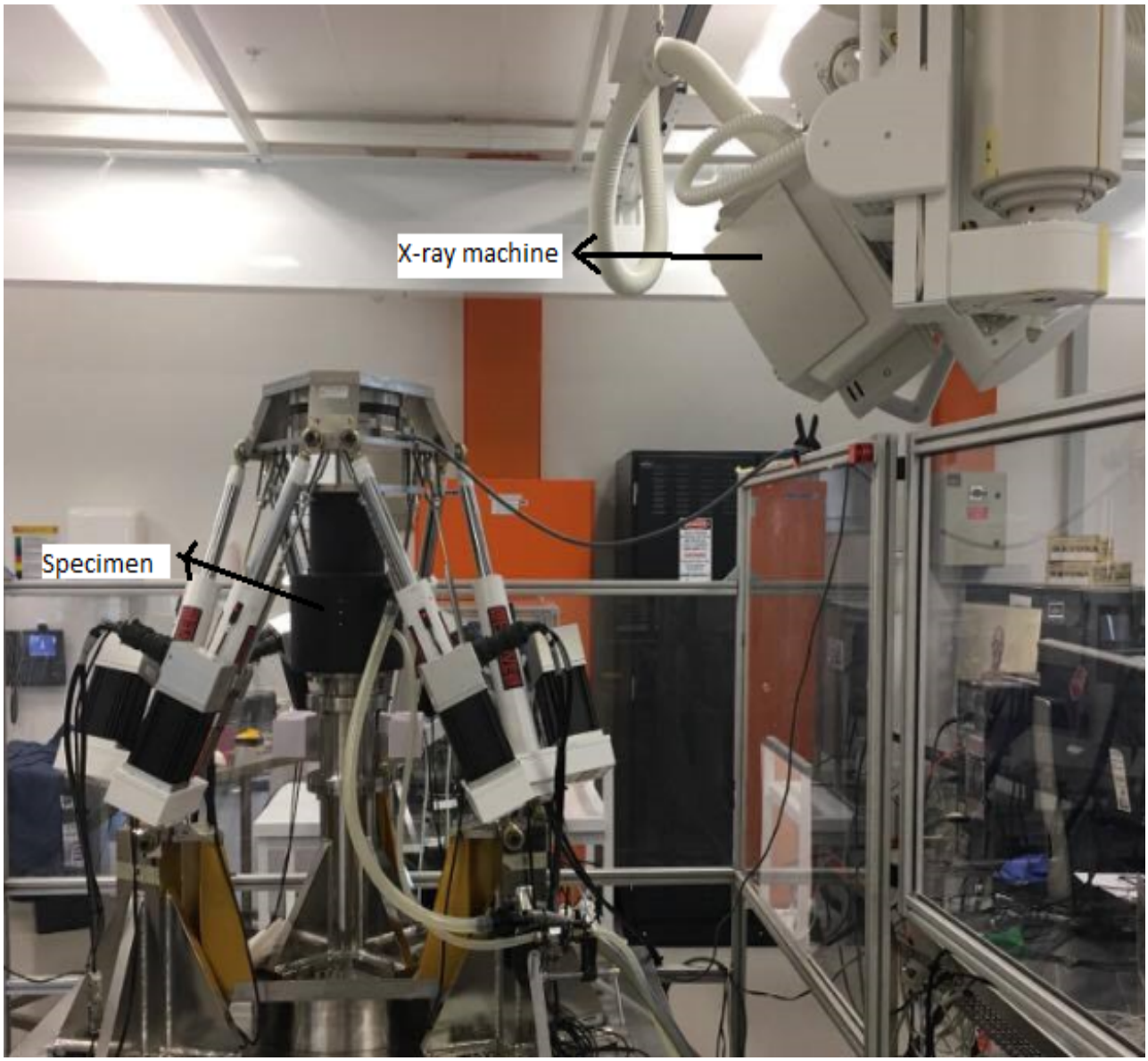

Figure 16: X-ray setup

e. The PBS liquid is drained first and then unbolted the specimen from the hexapod robot.

f. The specimen was detached from the hexapod, and an annular tear of 5mm width and depth was induced on the right anterolateral side of the disc Figure 17). The injury is parallel and adjacent to the inferior endplate of the upper vertebra (Osti et al., 1990). The induced peripheral annular tear in this experiment is performed based on the paper published by (Osti et al., 1990). A disc with healthy nucleus might have a peripheral tear, as peripheral tears are usually caused due to trauma in the anterior annulus regardless of disc degeneration (Osti et al., 1992).

Figure 17: Annular tear made on the disc

g. The specimen was fixed back into the bath and mounted onto the hexapod and filled the bath with PBS to keep the disc hydrated.
h. The test was repeated as shown in table 4 and took a left and right x-ray of the specimen after each test while holding the specimen in position.
i. After completing all the six tests (Table 4) detach the specimen from the hexapod robot and make another annular tear just beside the previous one by the 5mm depth and 5mm width.
j. Then fixed the specimen back into the hexapod robot and followed the sequence of tests and left, and right x-rays of the specimen after each test.
k. After completing the test (Table 4), the specimen was detached from the hexapod robot, and all the data from the hexapod computer was collected.
l. Before starting the testing sequence (Table 4) left and right x-rays of the specimen are taken at the neutral position for all the three cases.

The specimen preparation took about 4 hours and then it was pre-loaded for 18 hours, and 6 DOF testing in the hexapod took about 3 hrs. Total testing time for one specimen was 25hrs. There is no relaxation in between each test as all the tests are done in position control mode. The output data from the hexapod computer was collected; stiffness and hysteresis loss ratio of the FSU from the final loading cycle are calculated and compared to study the mechanical behaviour of the specimen in different test conditions. The x-rays taken after each test are digitised, by picking the required reconstruction points manually using the DLT technique using the Matlab software (Reinschmidt et al., 1997) to reconstruct a 3D image. The end plate beads and the circumferential markers were identified by the Hungarian method and heuristic matching algorithms respectively (Costi et al., 2007). The wires inserted in the disc were reconstructed by interpolating all the marked points along the wire on both left and right x-ray images (The Matlab code used to reconstruct the 3D images of the x-ray films was supportively provided by J.J. Costi[a,*]).

Each FSU was tested in three cases: in all the three cases disc is inserted with the tantalum wires and lead beads.

Number of tests:	**Case 1:** Left and right images were taken after each degree of freedom	**Case 2:** Left and right images were taken after each degree of freedom	**Case 3:** Left and right images were taken after each degree of freedom
1	Neutral position	Neutral position	Neutral position
2	Left axial rotation (Rz)	Left axial rotation (Rz)	Left axial rotation (Rz)
3	Right lateral bending (Ry)	Right lateral bending (Ry)	Right lateral bending (Ry)
4	Extension (Rx)	Extension (Rx)	Extension (Rx)
5	Flexion (Ry)	Flexion (Ry)	Flexion (Ry)
6	Flexion (Rz) + Rotation (Rz)	Flexion (Rz) + Rotation (Rz)	Flexion (Rz) + Rotation (Rz)
7	Compression (Tz)	Compression (Tz)	Compression (Tz)

Table 4: List of tests after which left and right radiographs are taken

The radiographs digitised for each FSU in this study are listed in Table 4. In total, 42 images of one FSU are digitised to reconstruct 21 images in 3D using the customised code written in MATLAB (Matlab code was supportively provided by J.J. Costi[a,*]). After manually picking the points on the radiograph to digitise, the Matlab code for reconstructing the image is executed, and the 3D reconstructed image of all the points was obtained as an output. Then the obtained outputs are then compared regarding unloaded and loaded files (the unloaded file will be the output file of the neutral position reconstructed image and the loaded file will be the output file of each degree of freedom).

5 Analysis

After the test was completed there are two types of data analysed. One is mechanical data, which gives the mechanical properties of the intervertebral disc regarding stiffness and hysteresis loss coefficient. The second one is x-ray images used to calculate internal strains of the intervertebral disc by RSA. In total five specimens were tested but only four specimen results were considered in this project. The reason to void one specimen was the specimen tilted 22^0 during the process of pre-load which is not acceptable as it is ideal to maintain the specimen straight while pre-loading it and the neutral position of the specimen was taken incorrect.

5.1 Analyzing mechanical properties of the specimens:

The data from the hexapod robot was saved in the computer as Excel files with columns of data using a personalised program written in MATLAB. There were 13 columns in total representing time, three displacements (Tx, Ty, Tz), three rotations (Rx, Ry, Rz), three forces (Fx, Fy, Fz), and three moments (Mx, My, Mz) (Costi et al., 2008). For each DOF first, a sinusoidal graph (Figure 18) was plotted to identify the final cycle of the data. After identifying the final loading cylce (Figure 19) for each DOF of all the specimens, the stiffness of the FSU is calculated for the loading area in the respected degree of freedom. The stiffness is calculated in excel using the slope formula.

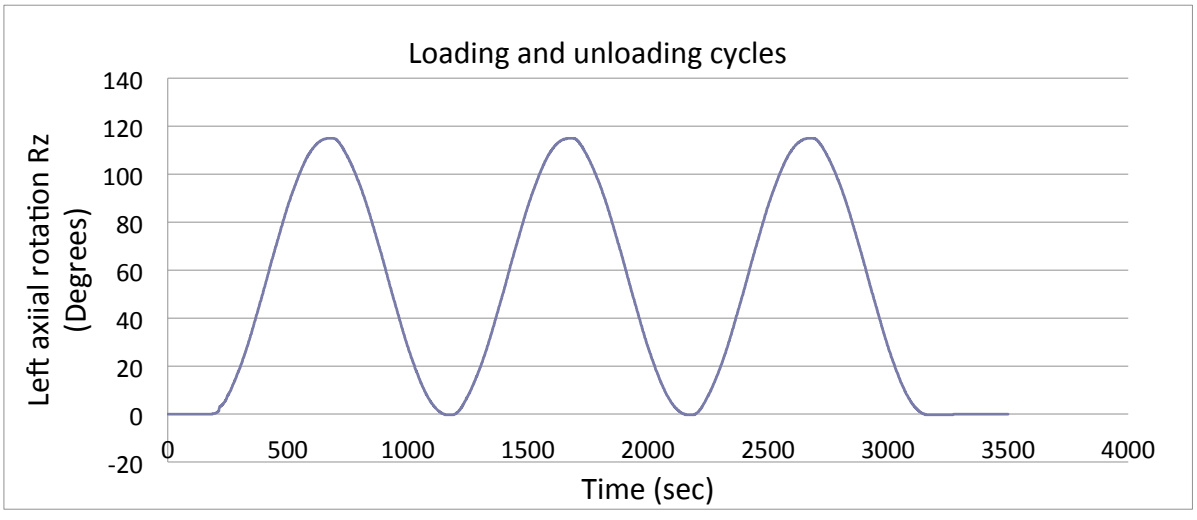

Figure 18: Showing the graph of a sinusoidal waveform with 3 loading and unloading cycles

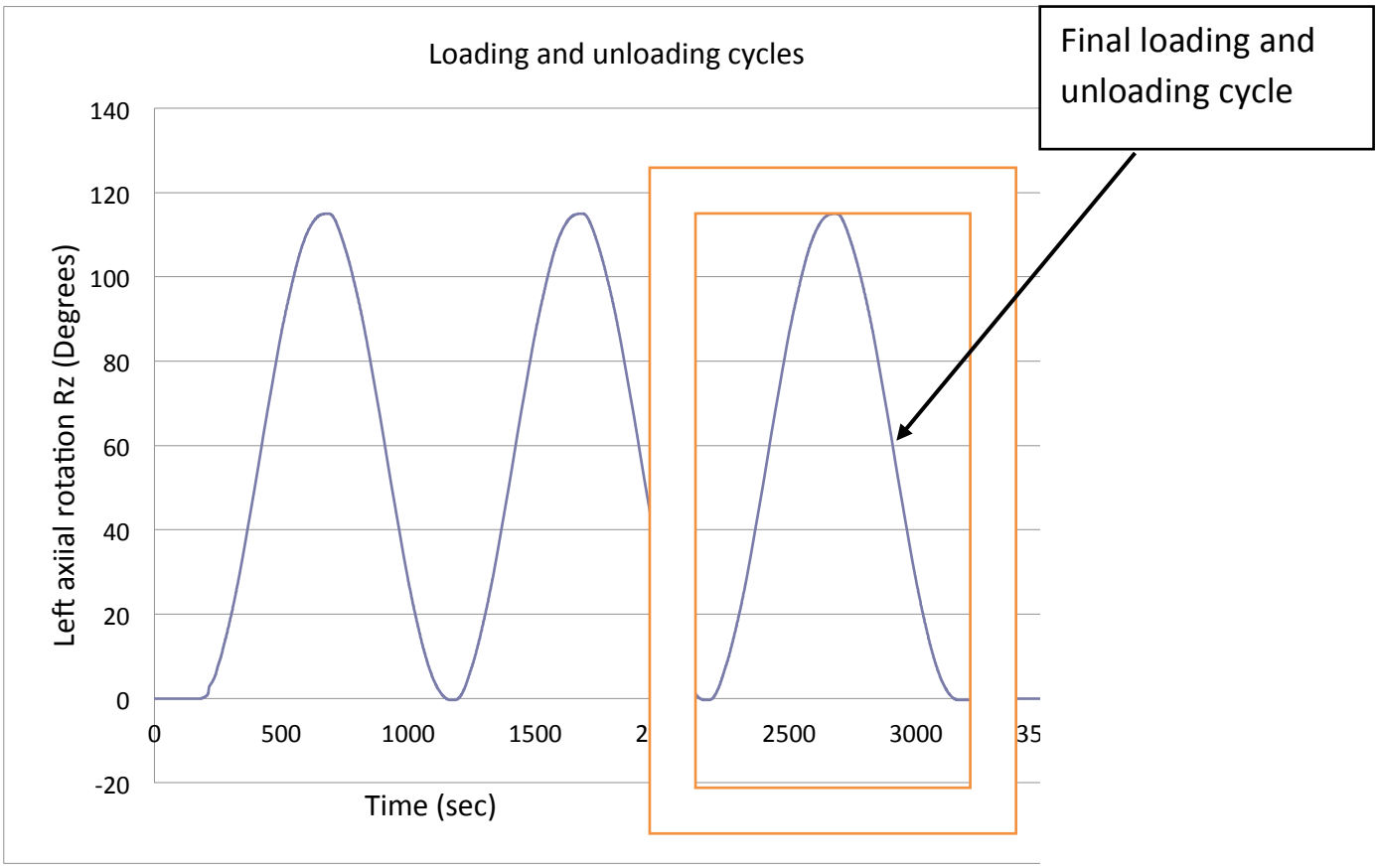

Figure 19: Showing the final cycle

Hysteresis loss coefficient of the final cycle is calculated by dividing the difference between the loading cycle area and unloading cycle area with loading cycle area. The sum of each area under the graph (example: between X_n and X_{n+1}) between the two points gives the total area under the curve (Figure 21). Hence, with the increasing number of data points, the accuracy of the area calculation increases.

$$Hysteresis\ loss\ coefficient = \frac{Hysteresis\ area}{Area\ under\ the\ loading\ curve}$$

Hysteresis area = loading area – unloading area (Figure 20).

Loading area is the area under the loading cure. Unloading area is the area under unloading curve.

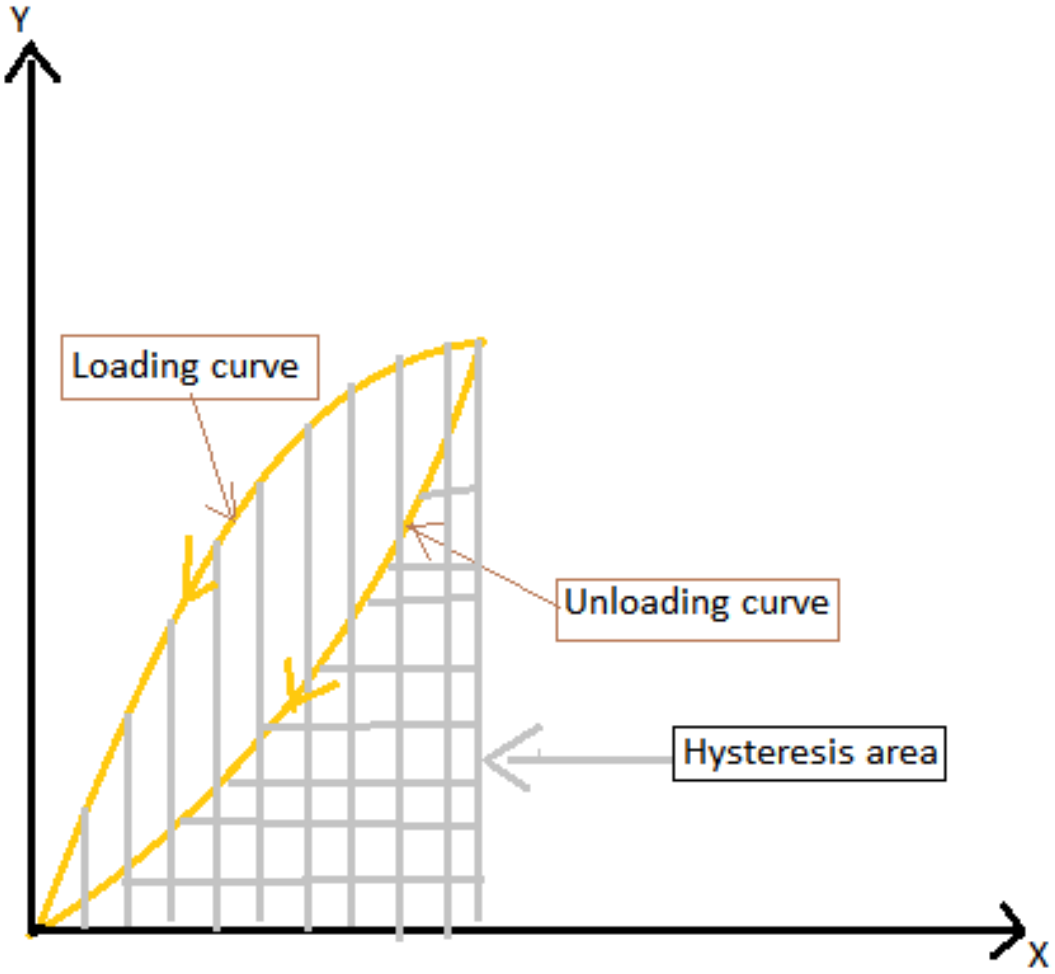

Figure 20: Graphical representation of the hysteresis area

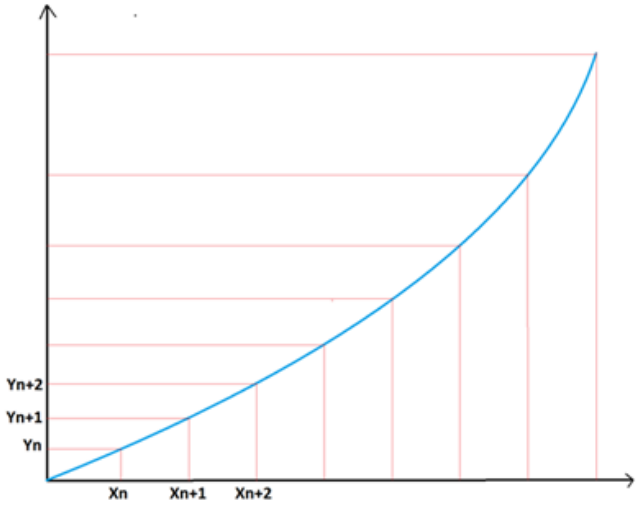

Figure 21: Showing how to calculate the area under the curve

$$\text{Area} = \sum_{n=1}^{\infty} \left(\frac{Y_n + Y_{n+1}}{2}\right) * (X_{n+1} - X_n)$$

Digitizing the x-rays:

The x-ray images are analysed by using the RSA to calculate internal strains of the intervertebral disc (Costi et al., 2007). First, manually picking the points and then reconstructing a 3D image using the Direct Linear Transformation Method digitize the left and right x-ray images of the FSU in each direction. The DLT method is used based on the procedures followed in dltfu.m, and reconfu.m ("ISB Software Resources - Movement Analysis Software", Costi et al., 2007) to reconstruct a point on a stereo-radiograph into a 3D plane point.

Detailed description of the digitizing process:

In total 84, 3D images were obtained by digitizing the left and right images of four specimens after each DOF and at the neutral position. The reconstruction procedure for a specimen in the neutral position is explained below as an example:

Step 1: Obtained the left and right x-ray images taken during the 6 DOF testing of all specimens.

Step 2: The following procedure was followed to obtain the output files that are used to construct a 3D image from left and right x-ray images.

I. Open the digitizing software (Figure 22).
II. Click on the tab named open images to access the required x-ray images. This opens the required left and right x-ray images of the specimen (Figure 23 & 24).
III. Start picking the points that needs to be reconstructed into a 3D image. First the calibration beads are marked on both left and right x-ray films (Figure 25 & 26). Calibration beads are actually present on the anterior, posterior, left lateral, and right lateral sides of the bath. Calibration beads have a particular numbering that needs to be followed to reconstruct the 3D image properly.

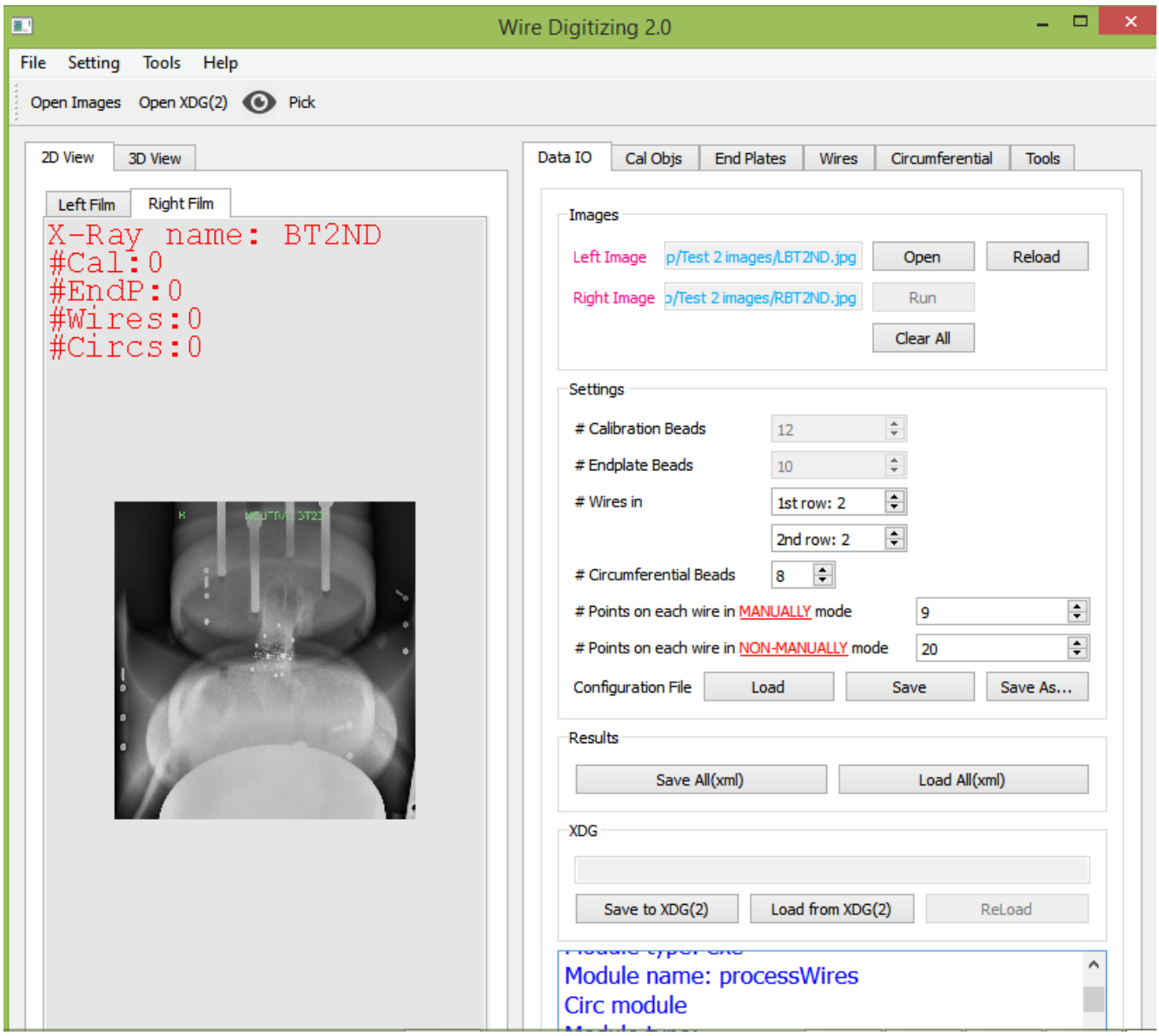

Figure 22: Image showing digitizing software where the required points are picked/identified for 3D reconstruction of the image

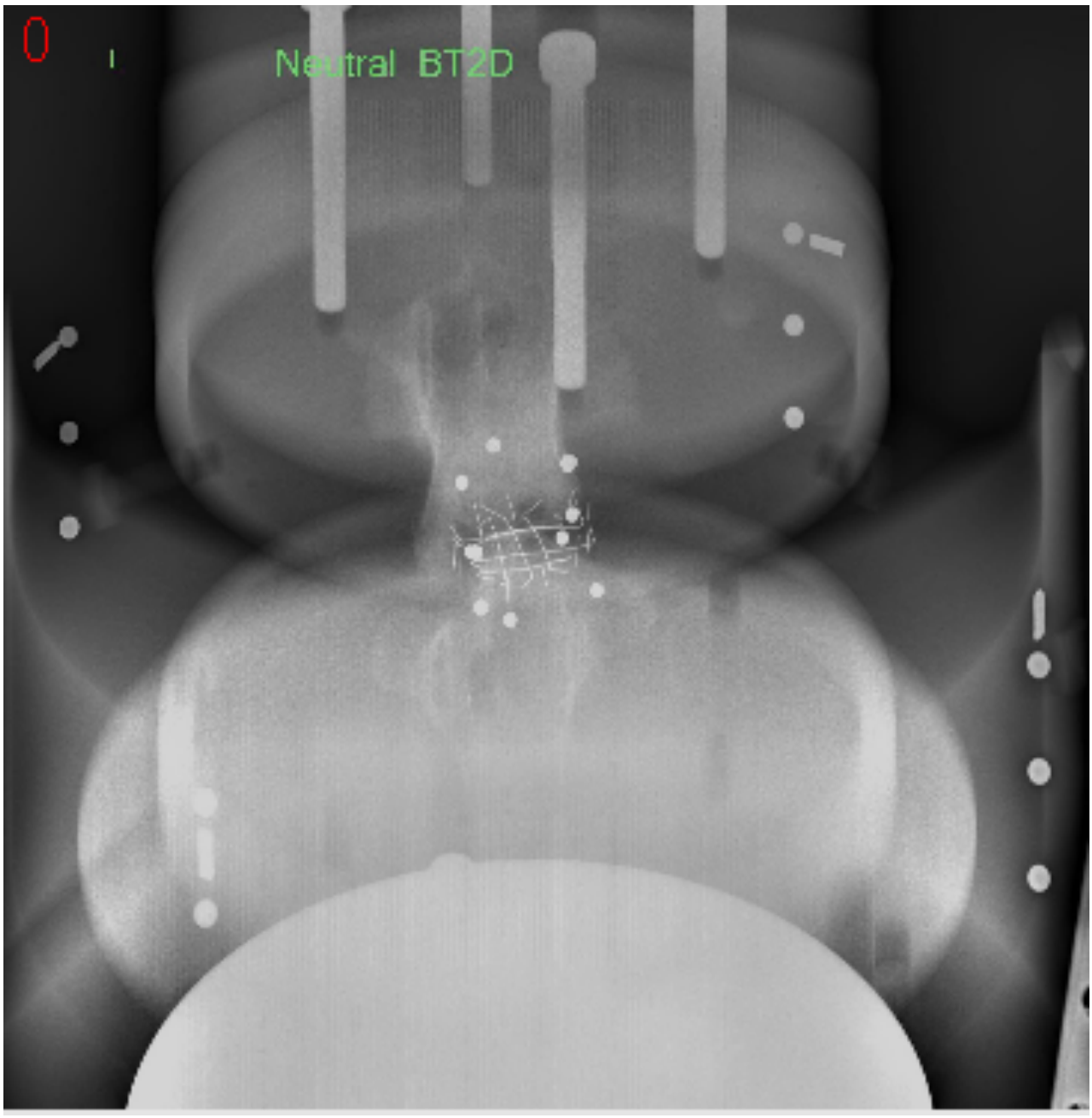

Figure 23: Left x-ray image of a specimen

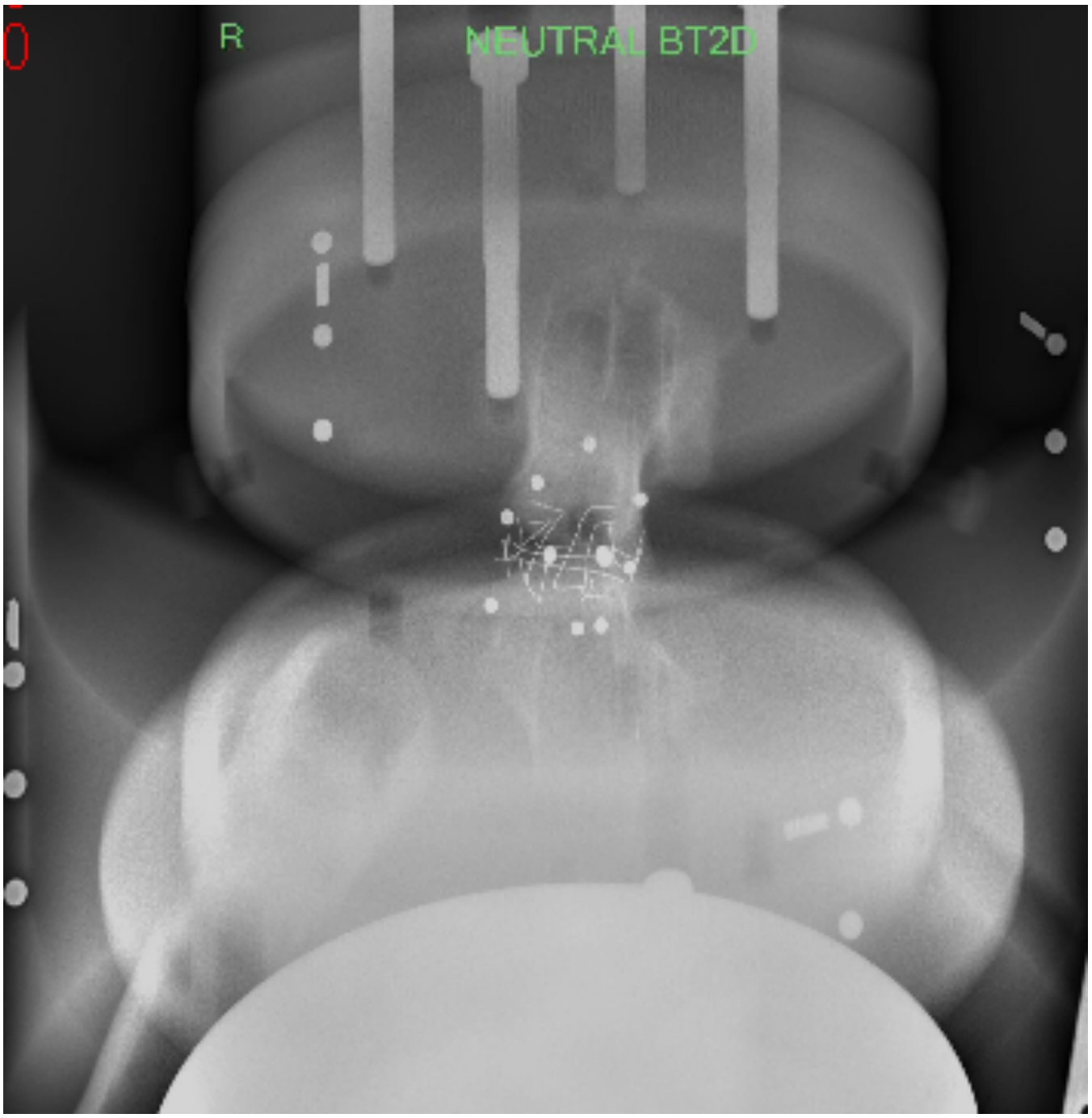

Figure 24: Right x-ray image of a specimen

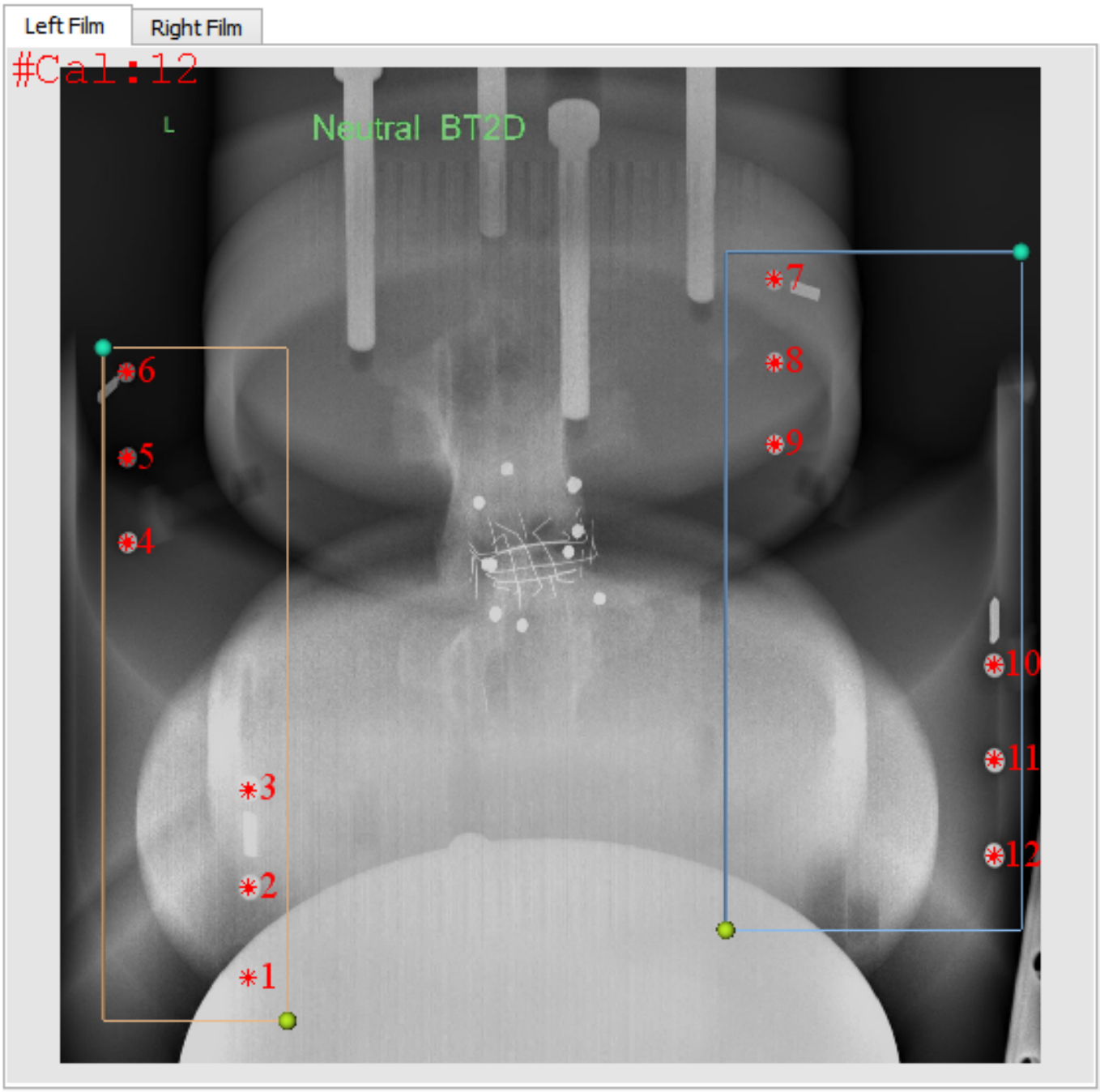

Figure 25: **Calibration beads identified on left x-ray**

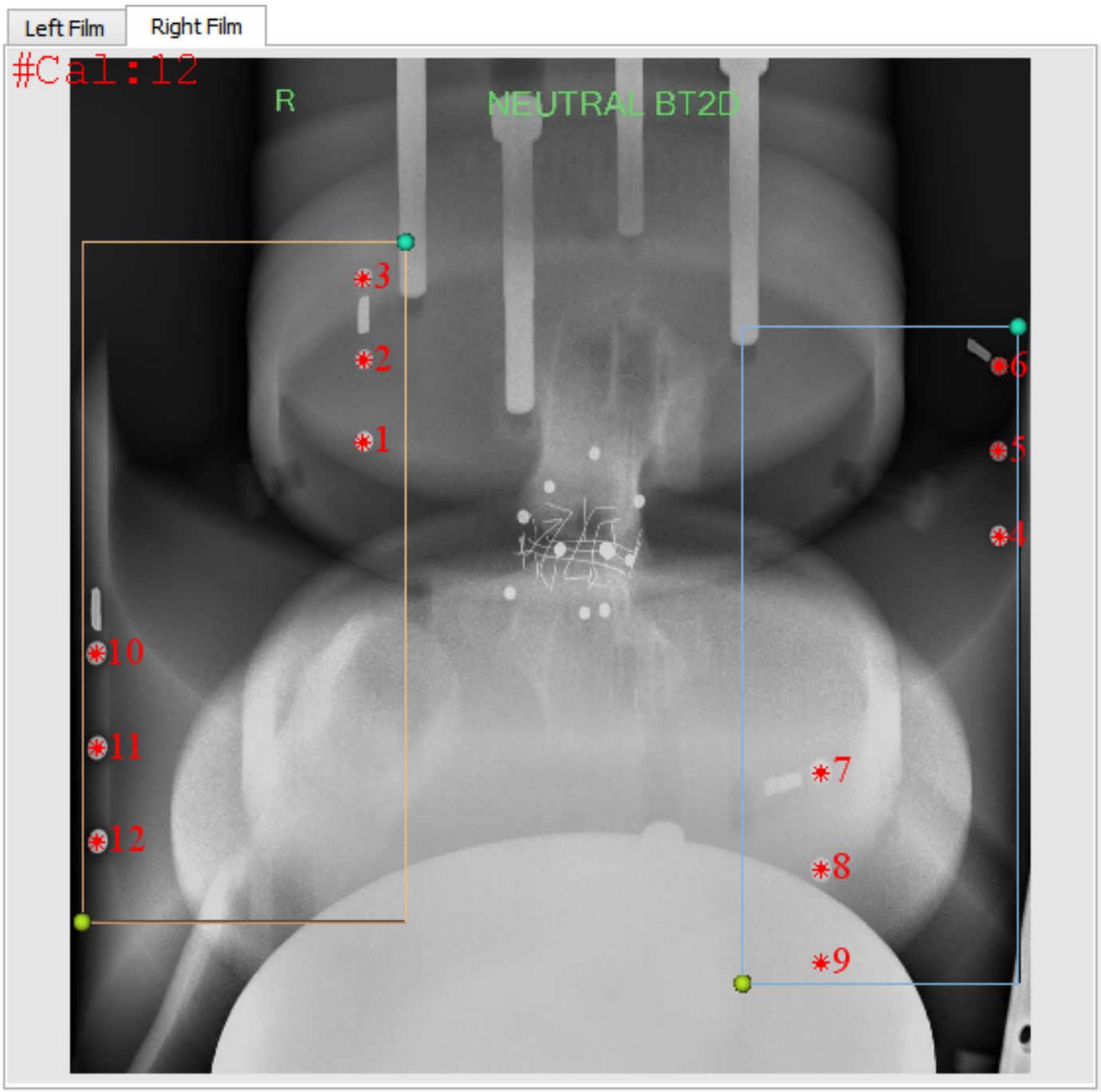

Figure 26: Calibration **beads identified on right x-ray**

IV. After marking the calibration beads, end-plate beads are marked on both left and right x-ray films (Figure 27 & 28).

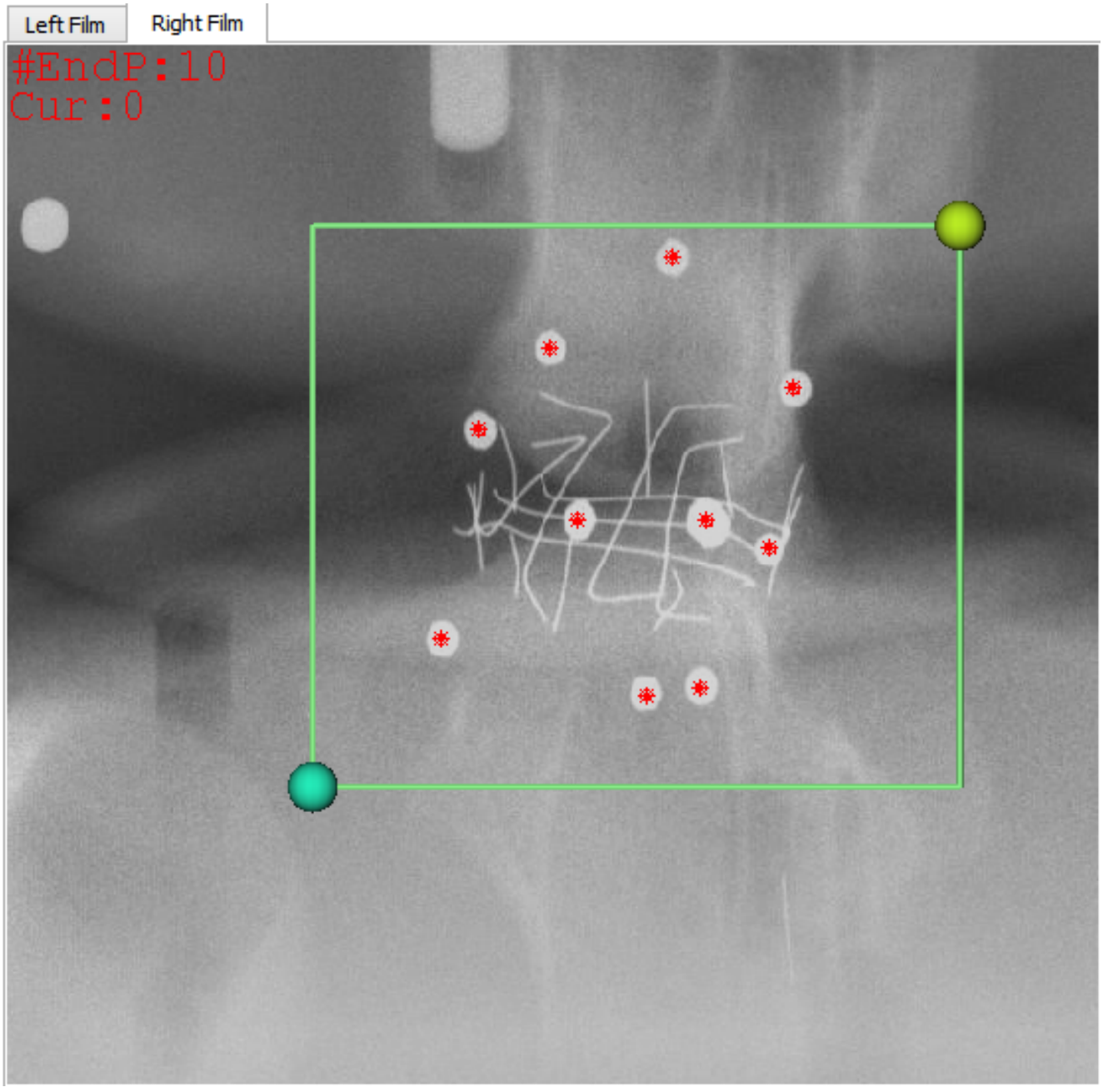

Figure 27: End-plate beads on the right x-ray

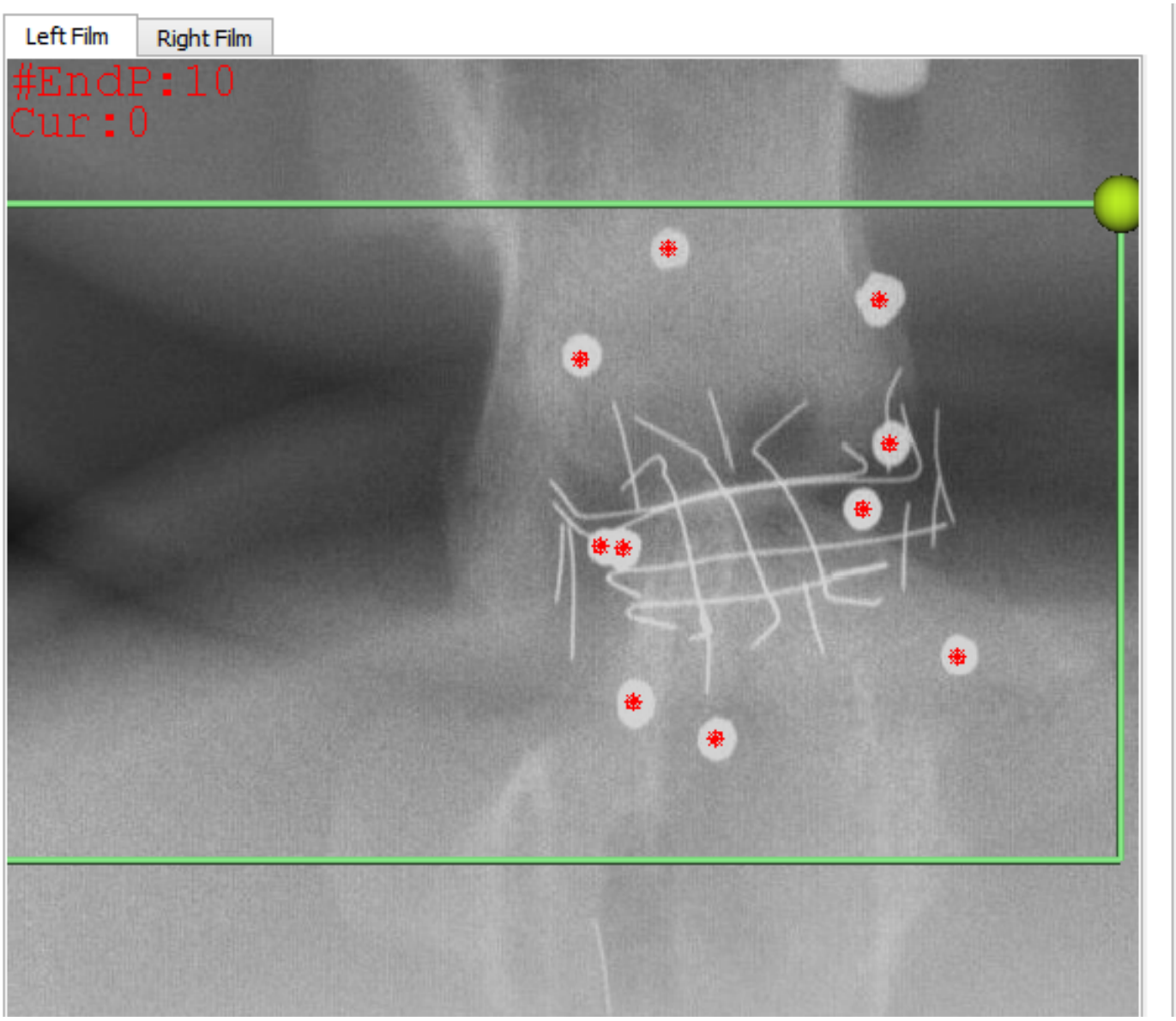

Figure 28: End-plate beads on the **left** x-ray

V. 2X2 wire grid was marked on both left and right x-ray images (Figure 29 & 30).

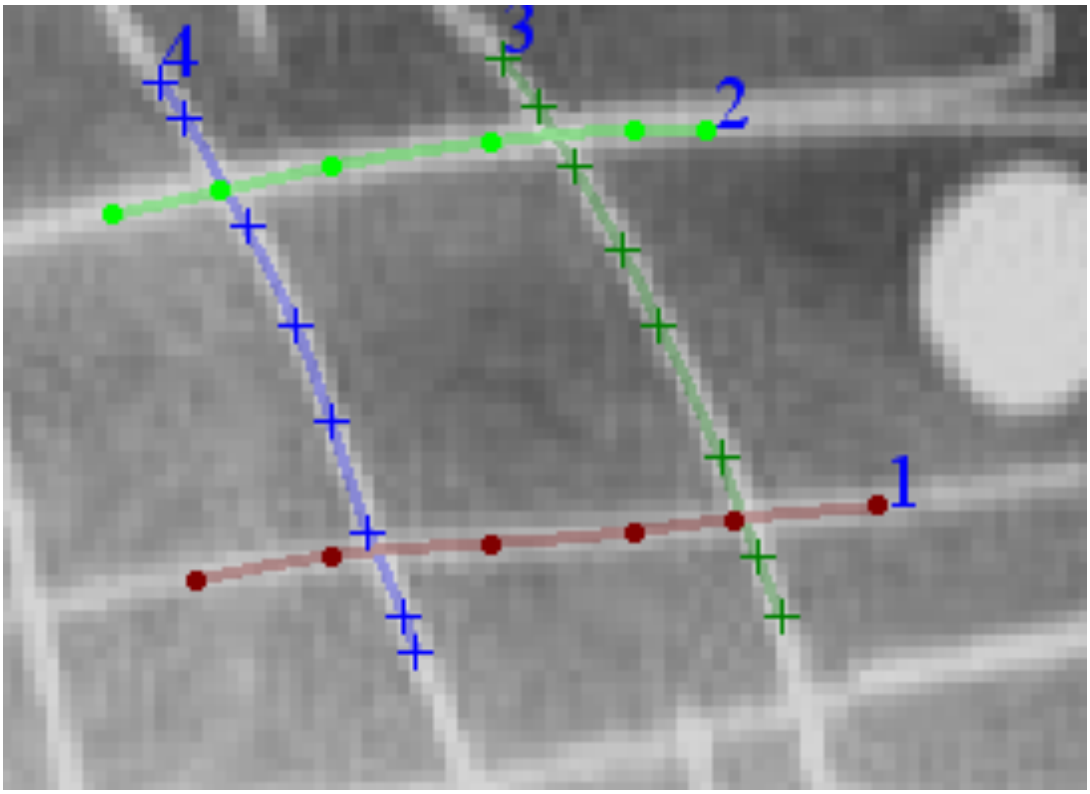

Figure 29: Wire grid on the left x-ray

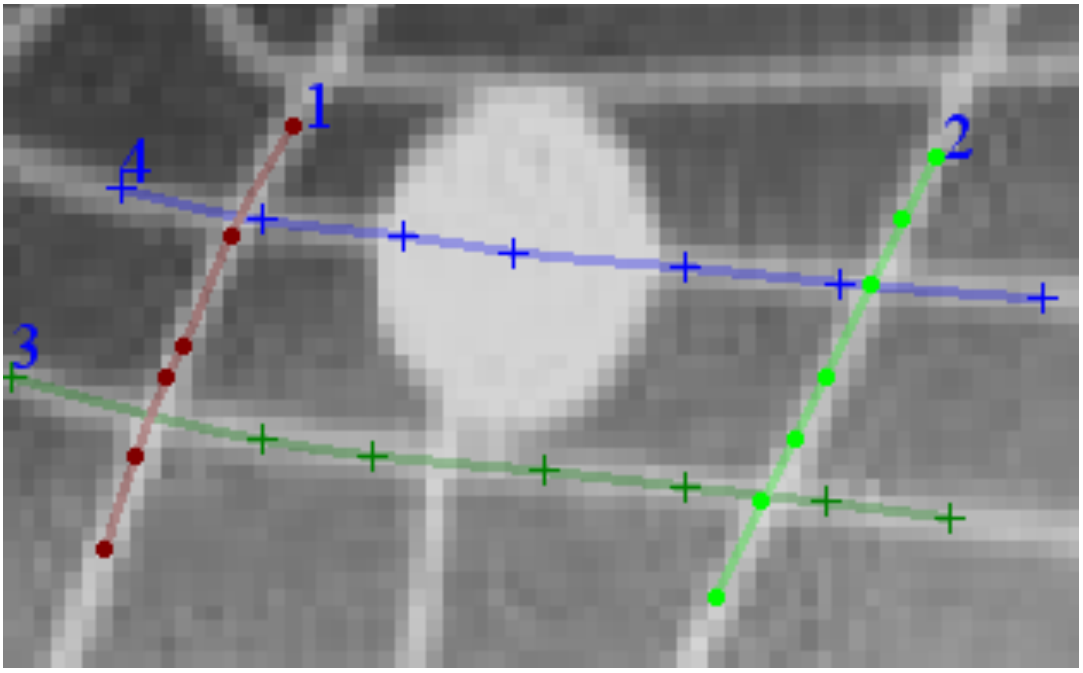

Figure 30: Wire grid on the right x-ray

VI. Circumferential markers, which were placed on the disc periphery, are identified on both left and right x-ray images (Figure 31 & 32).

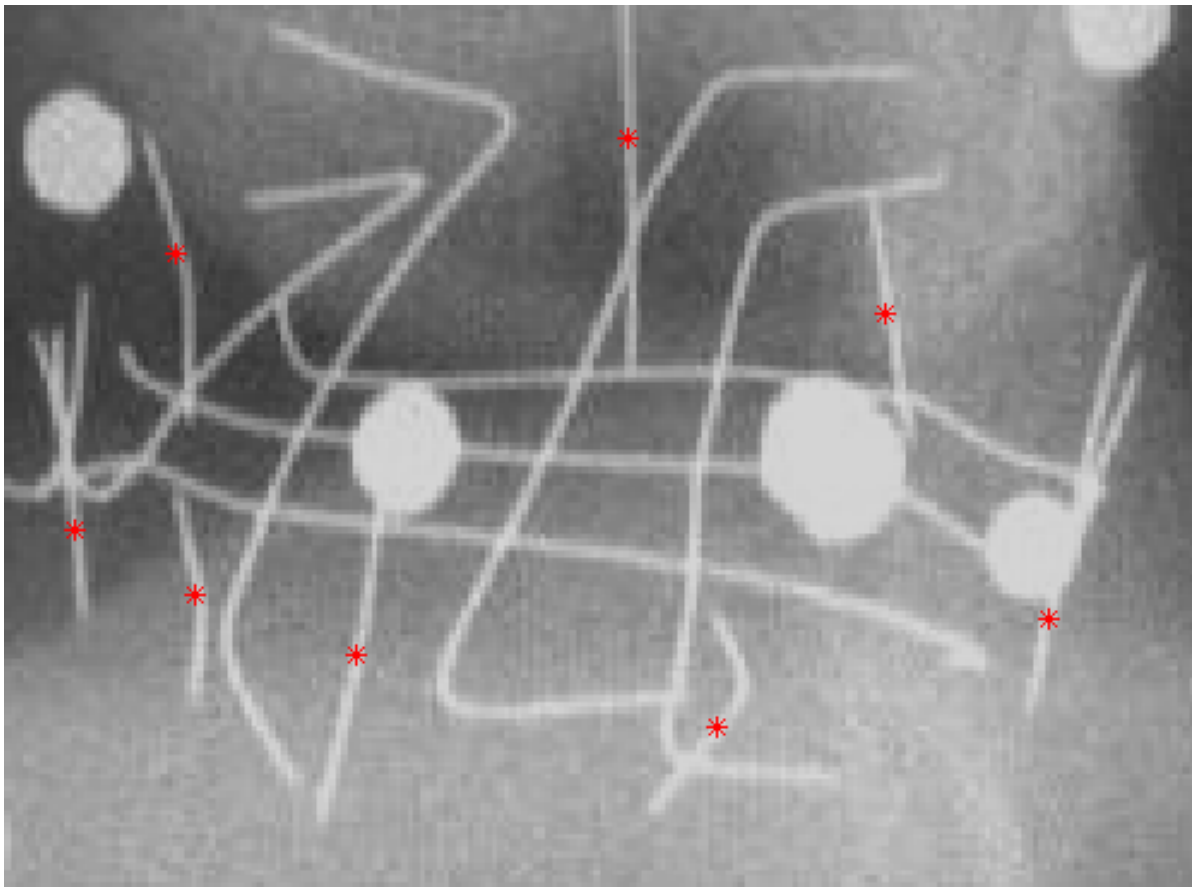

Figure 31: Circumferential markers on the right x-ray image

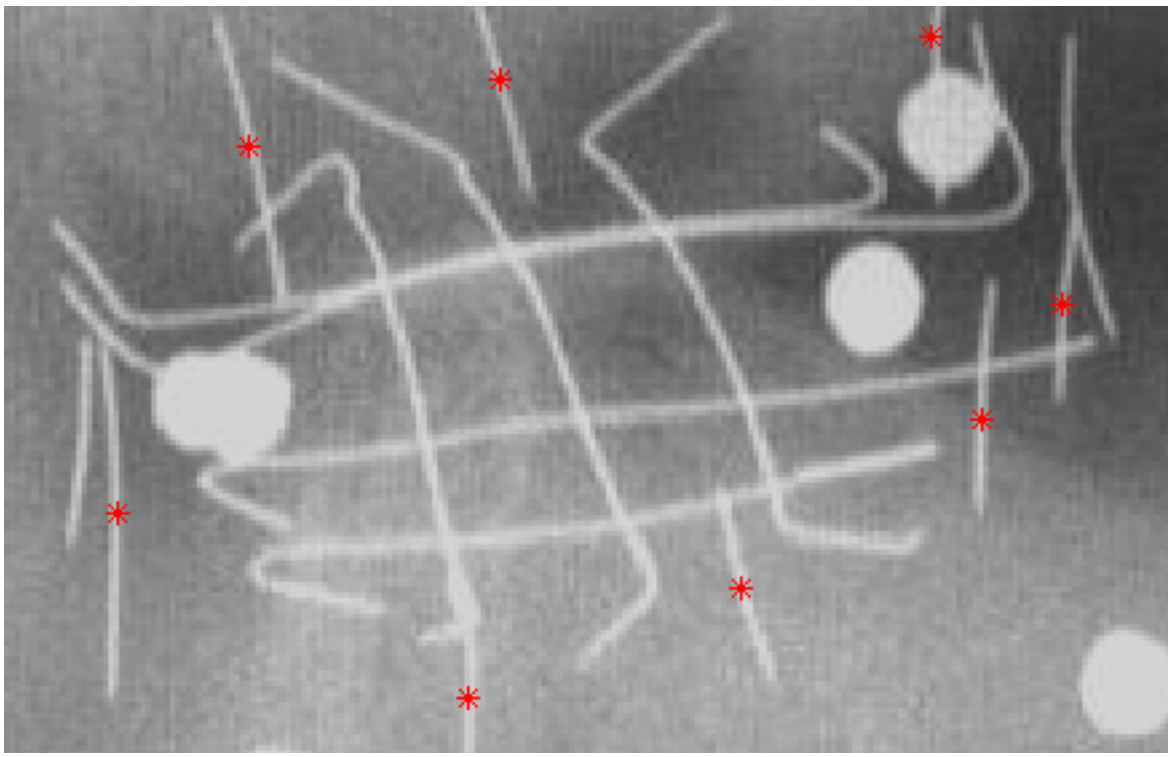

Figure 32: Circumferential markers on the left x-ray image

VII. The data was saved as an xdg2 file.

VIII. Reconstruction code using DLT reconstruction methods written in 'Matlab' was used and obtained the 3D reconstructed image of the points identified.

IX. The 3D coordinates (X, Y, and Z coordinated) of each point are obtained in text file named .out file

Step 3: All the left and right images taken during the testing process are digitized and obtained the 3D images.

Step 4: Changes in the periphery of the IVD and the radial strains of the disc are calculated using a matlab code.

The radial strains in all three cases (refer to section 4.1 point 5 (b)) of the specimen are obtained. Taking the results of case 1 as reference data difference in the radial strains of the specimen in case 2 and case 3 are calculated. The change in the radial strain was observed and analyzed to understand which area on the disc periphery has more strain change. A graphical

representation of the data shown in figure 33 gives a better idea about the radial strain changes of the disc.

	Difference between the radial strains in the direction of left axial rotation with respect to neutral position		
ANGLE	For case 2 (Injured) and case 1(Uninjured)		For case 3 (Injured) and case 1(Uninjured)
(deg)			
-180	0.01234		-0.00566
-170	-0.00072		-0.00433
-160	-0.02106		-0.01002
-150	-0.04091		-0.01842
-140	-0.05569		-0.02585
-130	-0.06321		-0.03002
-120	-0.06148		-0.02887
-110	-0.04839		-0.02107
-100	-0.02839		-0.00908
-90	-0.00635		0.00464
-80	0.0122		0.01728
-70	0.02132		0.02613
-60	0.0206		0.03101
-50	0.01319		0.03229
-40	0.00375		0.03049
-30	-0.00228		0.02625
-20	-0.00468		0.02018
-10	-0.0056		0.01331
0	-0.00755		0.00679
10	-0.01302		0.0015
20	-0.02246		-0.00287
30	-0.03144		-0.00625
40	-0.03547		-0.00787
50	-0.03153		-0.00745
60	-0.02159		-0.00655
70	-0.00988		-0.00583
80	0.00021		-0.00559
90	0.00618		-0.00586
100	0.00743		-0.00728
110	0.00604		-0.00947
120	0.0041		-0.01185
130	0.00355		-0.01393
140	0.00648		-0.01514
150	0.01263		-0.01392
160	0.01923		-0.0097
170	0.02218		-0.00262
180	0.01644		0.00582

Figure 33: Radial strain changes in the specimen periphery in case 2 and case 3 with respect to case 1

Step 5: For each specimen the disc periphery was compared as follows:

First the disc peripheries in each DOF are compared with the neutral position of the disc. After obtaining the results of disc periphery as listed in table 5, the disc periphery in case 1, 2, and 3 are plotted in the same graph to graphically present the change in the displacement of the disc in different cases.

Number of comparisons	Comparing the circumferential displacements in case 1	Comparing the circumferential displacements in case 2	Comparing the circumferential displacements in case 3
1	Neutral position – Left axial rotation	Neutral position – Left axial rotation	Neutral position – Left axial rotation
2	Neutral position – right lateral bending	Neutral position – right lateral bending	Neutral position – right lateral bending
3	Neutral position - extension	Neutral position - extension	Neutral position - extension
4	Neutral position - flexion	Neutral position - flexion	Neutral position - flexion
5	Neutral position – flexion + rotation	Neutral position – flexion + rotation	Neutral position – flexion + rotation
6	Neutral position – compression position	Neutral position – compression position	Neutral position – compression position

Table 5: Comparison of the output data performed to obtain the results of radial strains and the results of change in disc periphery (mm)

Step 6: Graphical representation (Figure 34) of the disc periphery in all the three cases are obtained using a radar plot in excel.

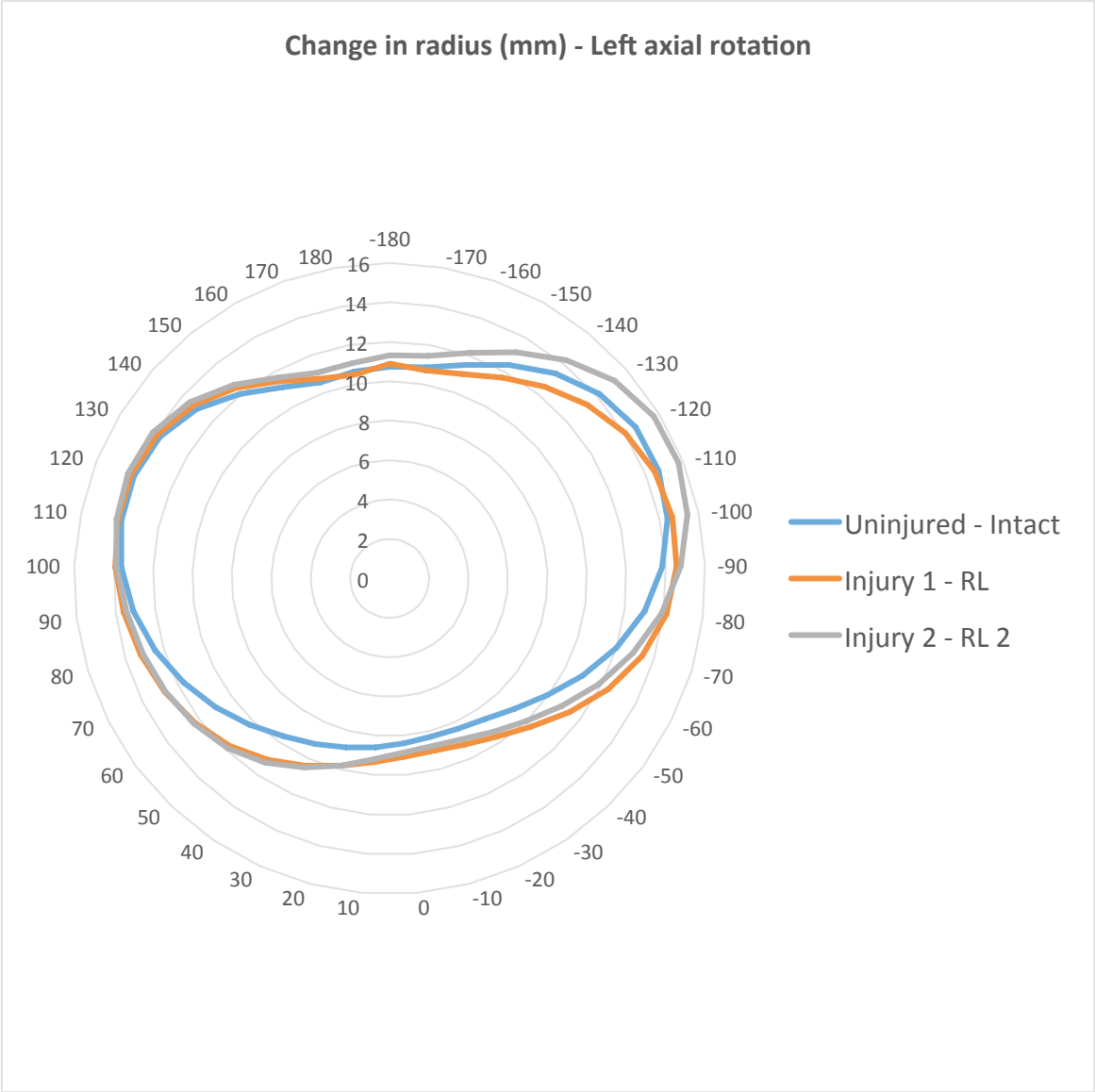

Figure 34: Disc periphery in different cases

Step 7: Change in the x, y, and z coordinates of the wire intersection points are calculated to analyze the difference in the displacement of wires that were inserted in the disc. This helps to calculate the internal strains of the disc in future.

Repeatability study analysis:

An intra-observer repeatability study was conducted in this project to exclude the user error in the output data. Left and right x-ray images of a specimen in its neutral position were chosen to conduct the intra-observer repeatability study. The same left and right images of specimen are digitized three times and saved the all the three outputs of the digitized images. Then the x, y, and z coordinates of the wire intersection points were compared between the three-output data. The comparison of the data was performed by importing the output data into excel sheet and taking the difference in the values compared to each other and then by taking an average of all the compared data the average value of the user error is calculated.

6 Results

6.1 Results obtained from the radio-stereometric analysis

FSU 1: Results of specimen 1

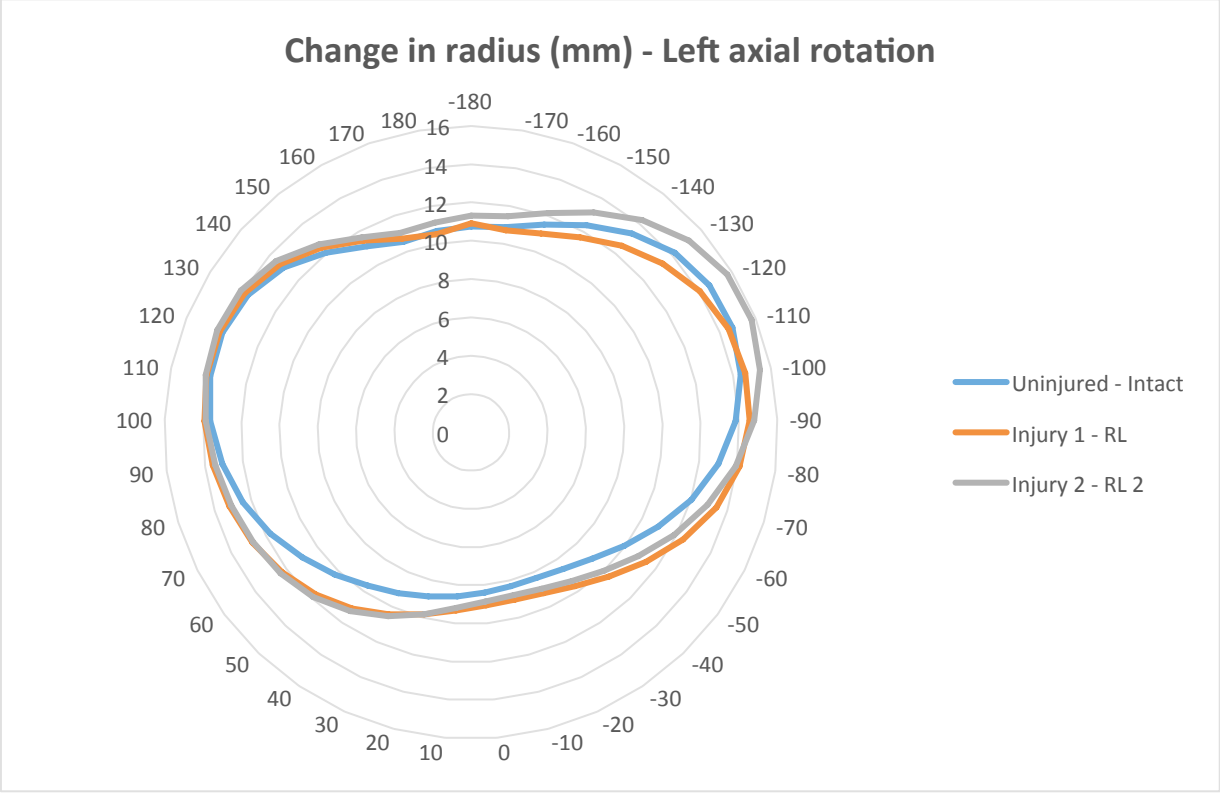

Figure 35: FSU 1 Disc periphery of the specimen in the direction of left axial rotation for different test conditions (Uninjured represents case 1, injury 1 represents case 2, injury 2 represents case 3)

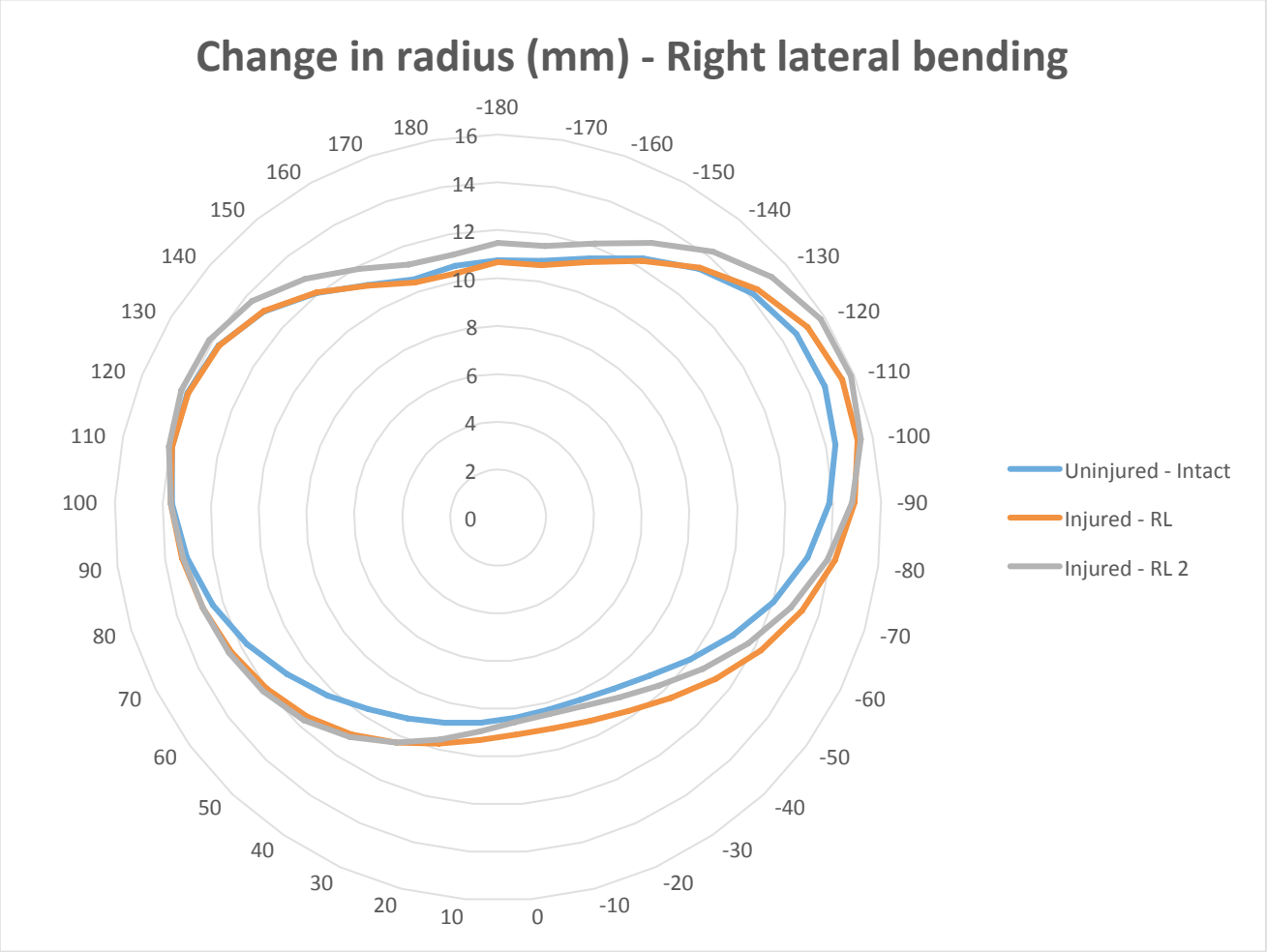

Figure 36: FSU 1 Disc periphery of the specimen in the direction of right lateral bending for different test conditions (Uninjured represents case 1, injury 1 represents case 2, injury 2 represents case 3)

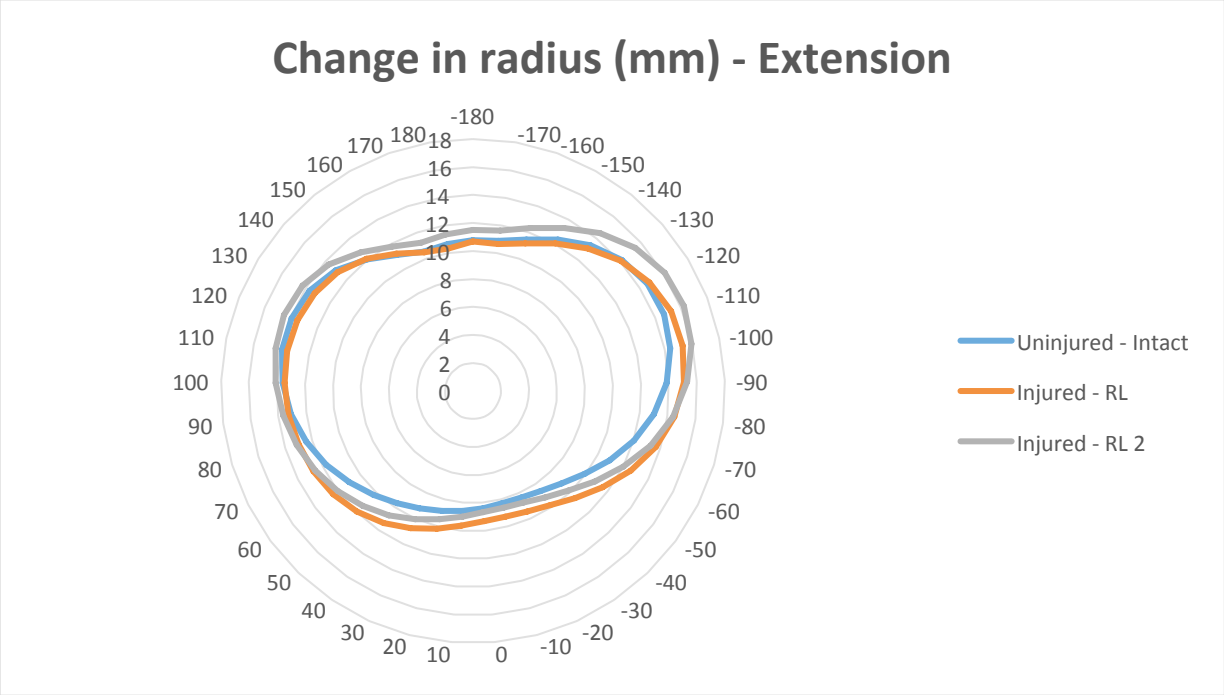

Figure 37: FSU 1 Disc periphery of the specimen in the direction of extension for different test conditions. Uninjured represents case 1, injury 1 represents case 2, injury 2 represents case 3

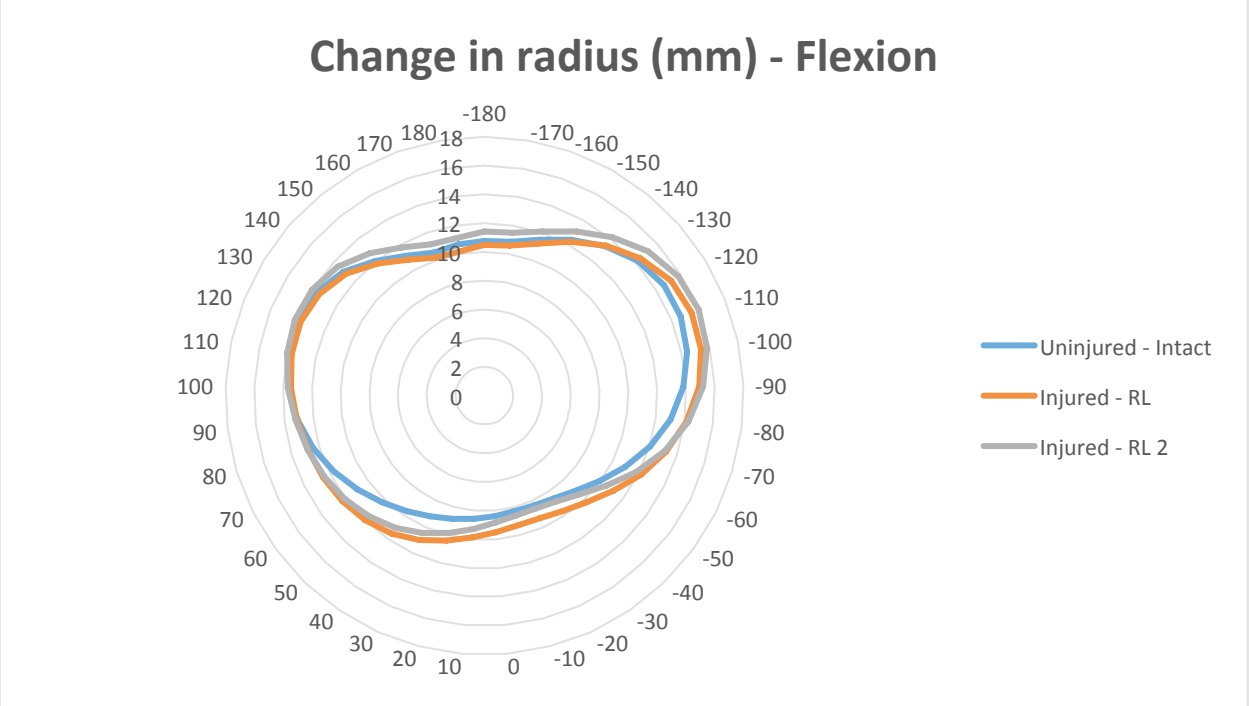

Figure 38: FSU 1 Disc periphery of the specimen in the direction of flexion for different test conditions (Uninjured represents case 1, injury 1 represents case 2, injury 2 represents case 3)

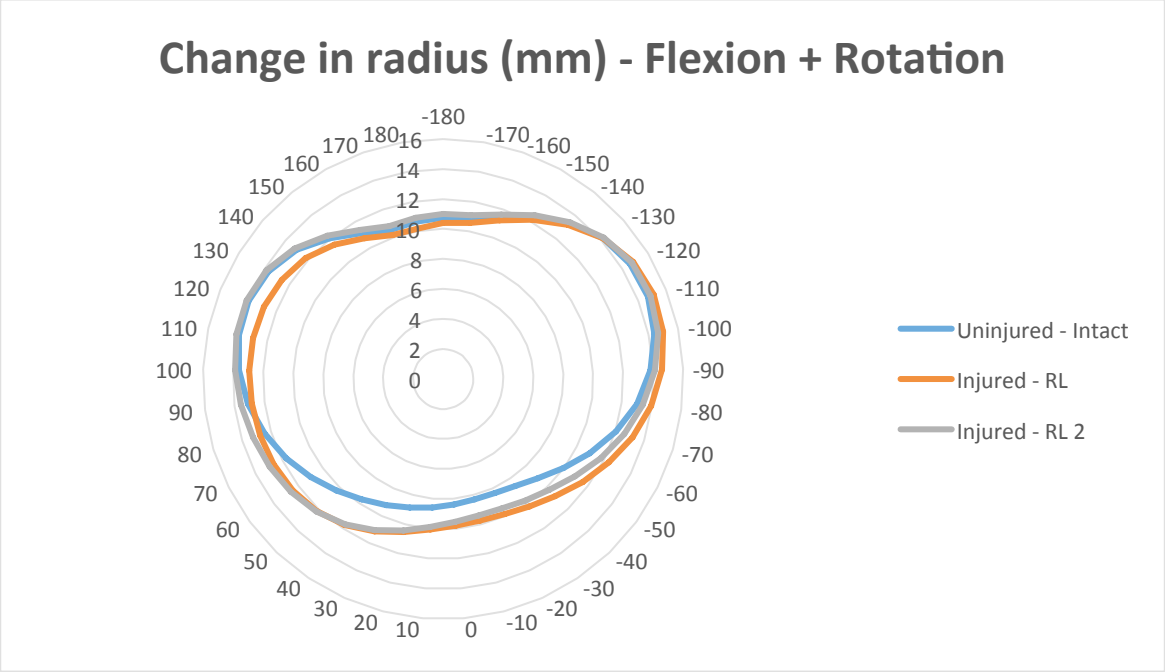

Figure 39: FSU 1 Disc periphery of the specimen in the direction of flexion + rotation for different test conditions (Uninjured represents case 1, injury 1 represents case 2, injury 2 represents case 3)

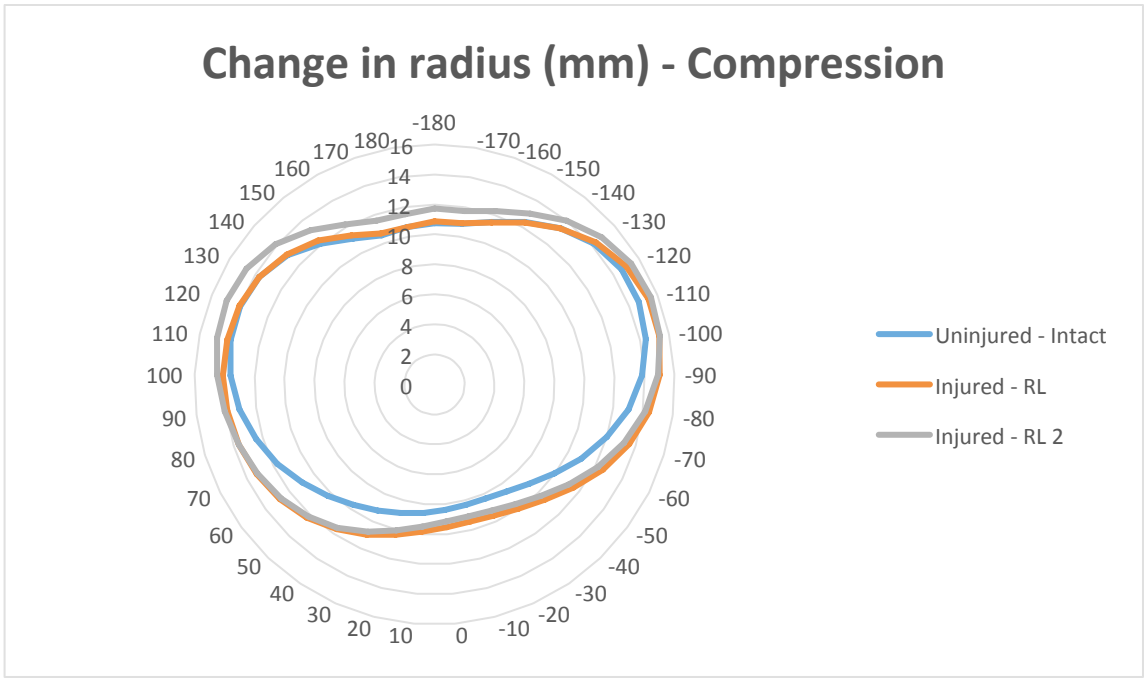

Figure 40: FSU 1 Disc periphery of the specimen in the direction of compression for different test conditions (Uninjured represents case 1, injury 1 represents case 2, injury 2 represents case 3)

The RSA results give the radial strains of the disc in all three testing cases (refer section 4.1 point 5(b)). The annular tear was made on the antero-right lateral side and inferior to the upper endplate of the intervertebral disc. Change in radius of the intervertebral disc in three different cases (refer to section 4.1 point 5(b)) after performing a DOF test is represented graphically. The graphical representation is shown in the figure 35 to figure 40. In the graphical representation, one half of the disc is marked from 0^0 to 180^0 and the other half is marked from 0^0 to -180^0. The side 0^0 pointing is the anterior side of the disc, the side pointing 180^0 and -180^0 is the posterior side of the disc, 90^0 and -90^0 sides will be right lateral and left lateral sides of the disc respectively (Figure 35 to Figure 40). The annular tear is on the antero-right lateral side of the disc, which is approximately in the range of 40^0 to 90^0. To look if there is any changes in the disc radius due to the induced annular tear the area of the disc from 40^0 to 90^0 on the graph is taken into consideration. In FSU 1 results (Figure 35 to figure 40), there is a change in the radius of the disc in injury 1 and injury 2 states when compared with the radius of the disc in uninjured state. In case of the FSU 2 results (Figure 71 to figure 77), there is a change in the radius of the disc in injury 1 and injury 2 states when compared with the radius of the disc in uninjured state. In case of the FSU 3 results (Figure 78 to figure 82), there is no visible change noticed in the radius of the disc when compared the disc radius in injury 1 and injury 2 to uninjured disc radius. In case of FSU 4 results (Figure 83 to figure 88), there is no visible change in the area where the annular tear is induced on the disc when compared the disc radius in injury 1 and injury 2 states to uninjured state of the disc.

The radial strains of the IVD in each 6 DOF compared to the neutral position are calculated successfully in this study.

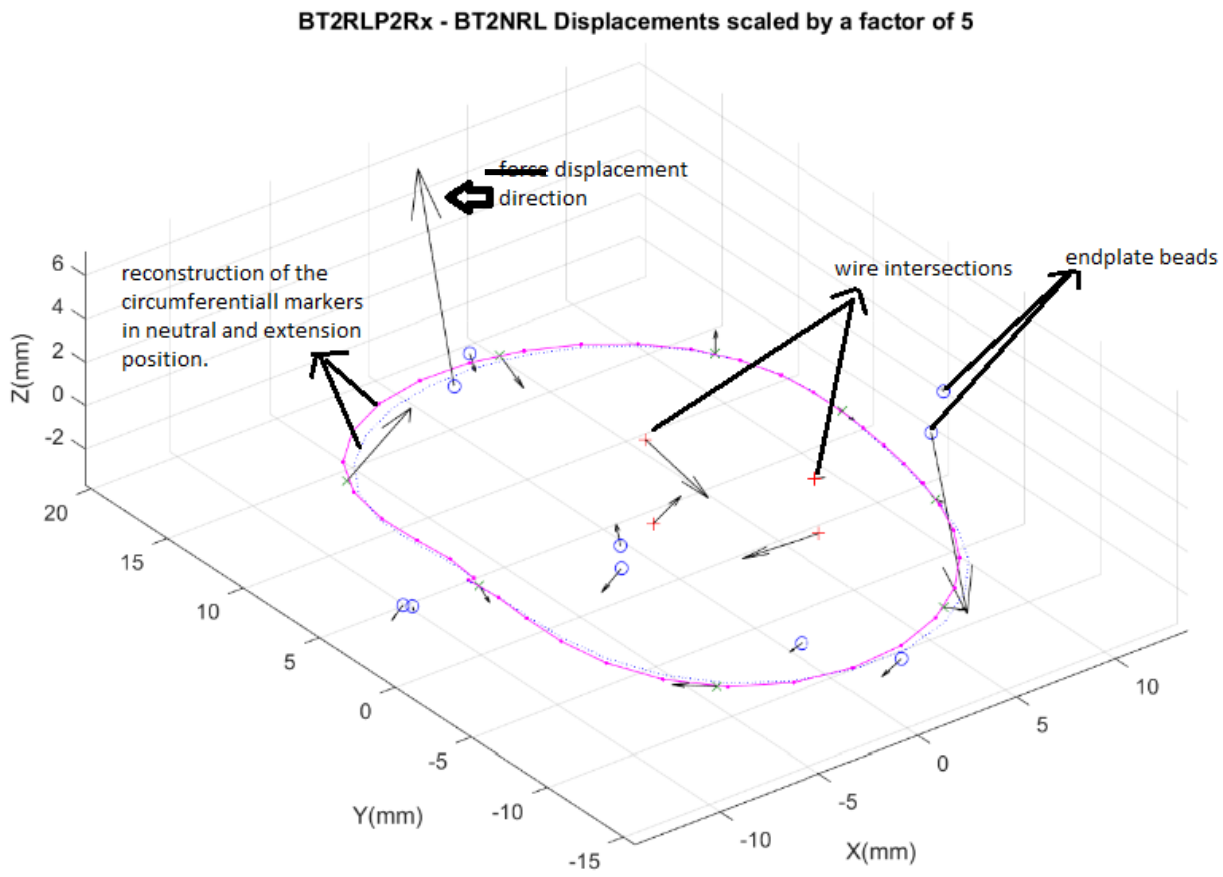

Figure 41: Reconstructed image of the IVD in the direction of extension compared with neutral position

6.2 Repeatability study results

The average value of the difference in the output data, after performing tests on the same FSU for three times is shown in figure 42.

Taking the average of the intra-observer repeatability study the maximum user error that can be caused is about 0.29 mm. When we look at the displacements of the x, y, and z coordinates of the wire intersection points (presented in the section of appendix B) there was a change observed in the x, y, and z coordinated of the wire intersection points in the disc when the comparisons were between the three testing cases of the study.

1	REPEATABILITY STUDY CONDUCTED ON					
2	THE LEFT AND RIGHT X-RAY IMAGES IN THE NEUTRAL POSITION OF ONE SPECIMEN					
3						
4		FIRST DIGITISED OUTPUT				
5		ROW 1	ROW 2	X Dis (mm)	Y Dis (mm)	Z Dis (mm)
6		Wire 1	Wire 3	5.23	-0.85	8.64
7		Wire 1	Wire 4	2.5	-3.55	8.53
8		Wire 2	Wire 3	1	3.42	9.13
9		Wire 2	Wire 4	-2.07	0.61	9.04
10						
11						
12		SECOND DIGITISED OUTPUT				
13		ROW 1	ROW 2	X Dis (mm)	Y Dis (mm)	Z Dis (mm)
14		Wire 1	Wire 3	5.24	-0.85	8.64
15		Wire 1	Wire 4	2.47	-3.57	8.53
16		Wire 2	Wire 3	1.01	3.42	9.14
17		Wire 2	Wire 4	-1.93	0.55	9.07
18						
19						
20		THIRD DIGITISED OUTPUT				
21		ROW 1	ROW 2	X Dis (mm)	Y Dis (mm)	Z Dis (mm)
22		Wire 1	Wire 3	5.26	-0.85	8.64
23		Wire 1	Wire 4	2.27	-3.47	8.49
24		Wire 2	Wire 3	1.01	3.42	9.14
25		Wire 2	Wire 4	-1.79	0.66	9.09

DIFFERENCE BETWEEN THE THREE DIGITISED OUTPUTS

ROW 1	ROW 2	X Dis (mm)	Y Dis (mm)	Z Dis (mm)		X Dis (mm)	Y Dis (mm)	Z Dis (mm)
Wire 1	Wire 3	0.03	0	0		0.02	0	0
Wire 1	Wire 4	-0.23	0.08	-0.04		-0.2	0.1	-0.04
Wire 2	Wire 3	0.01	0	0.01		0	0	0
Wire 2	Wire 4	0.28	0.05	0.05		0.14	0.11	0.02

AVERAGE OF ALL THE DIFFERENCES IN X, Y, AND Z COORDINATES
AFTER DIGITISING LEFT AND RIGHT X-RAY IMAGES OF A SPECIMEN IN NEUTRAL POSITION

X Dis (mm)	Y Dis (mm)	Z Dis (mm)
0.025	0	0
-0.215	0.09	-0.04
0.005	0	0.005
0.21	0.08	0.035

Figure 42: Results obtained from intra-observer repeatability study

6.3 Mechanical properties of bovine intervertebral disc

Stiffness and hysteresis loss coefficient of the bovine intervertebral disc are calculated.

6.3.1 Results of stiffness

The mean of all the FSU stiffness values in each direction are calculated (Appendix B) and plotted graphically as shown below:

Intact = uninjured disc

Injured - RL = injured disc with 5mm width and depth rim lesion

Injured - RL 2 = injured disc with 5mm depth and 10mm width rim lesion

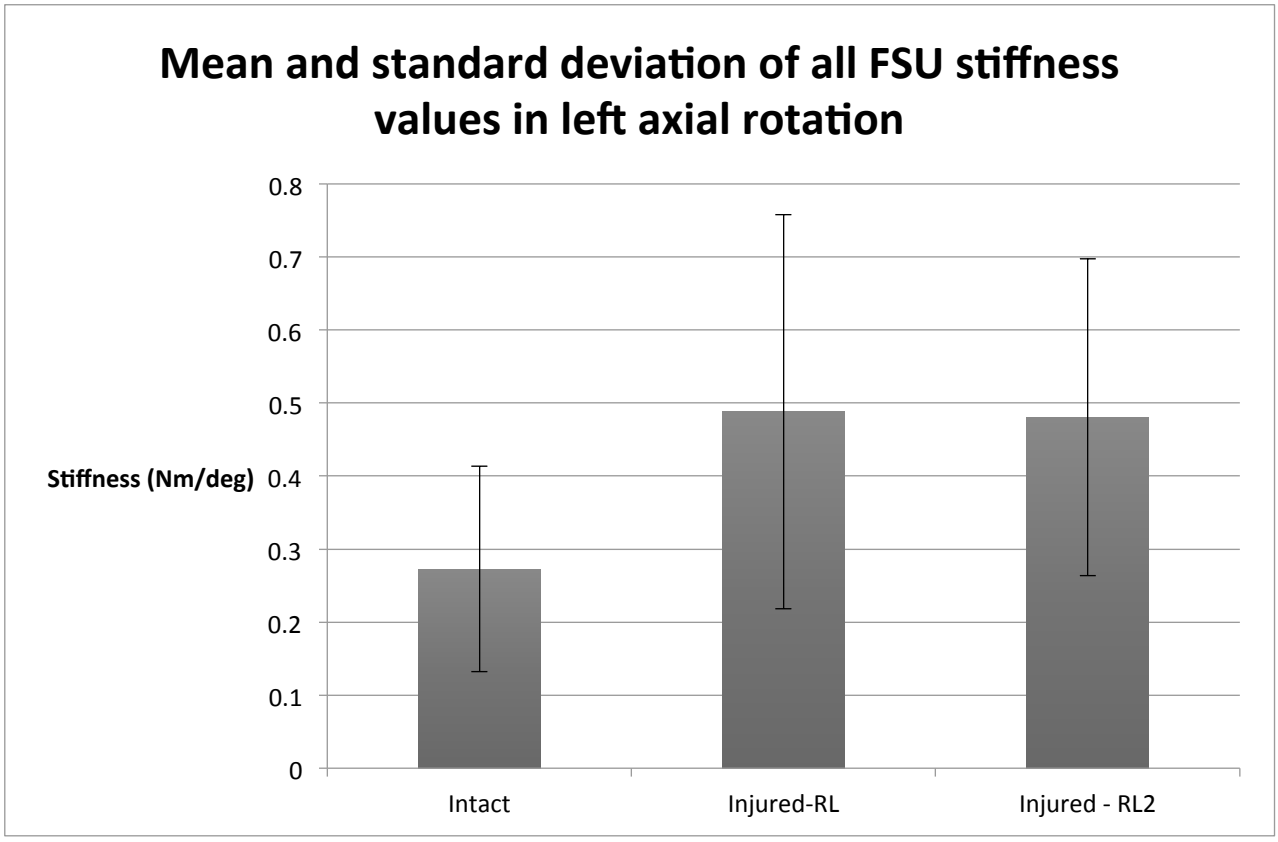

Figure 43: Mean and standard deviation of the stiffness values of the intervertebral disc in left axial rotation

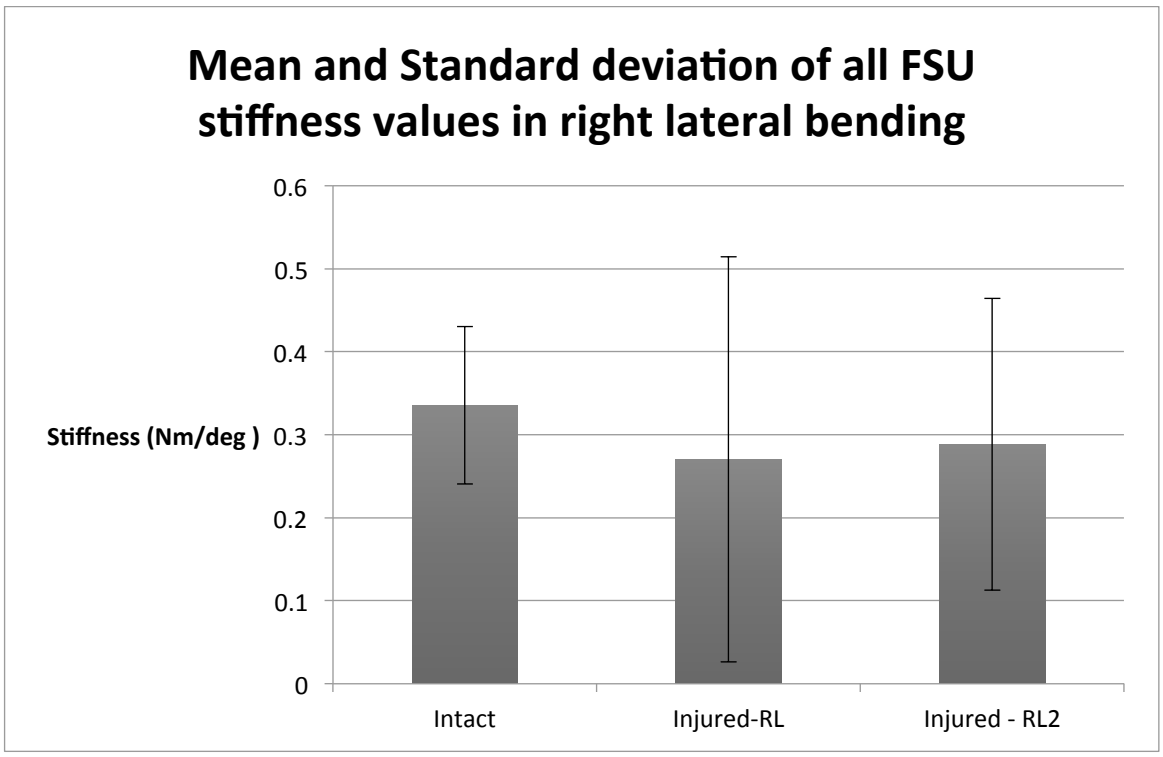

Figure 44: Mean and standard deviation of the stiffness values in right lateral bending

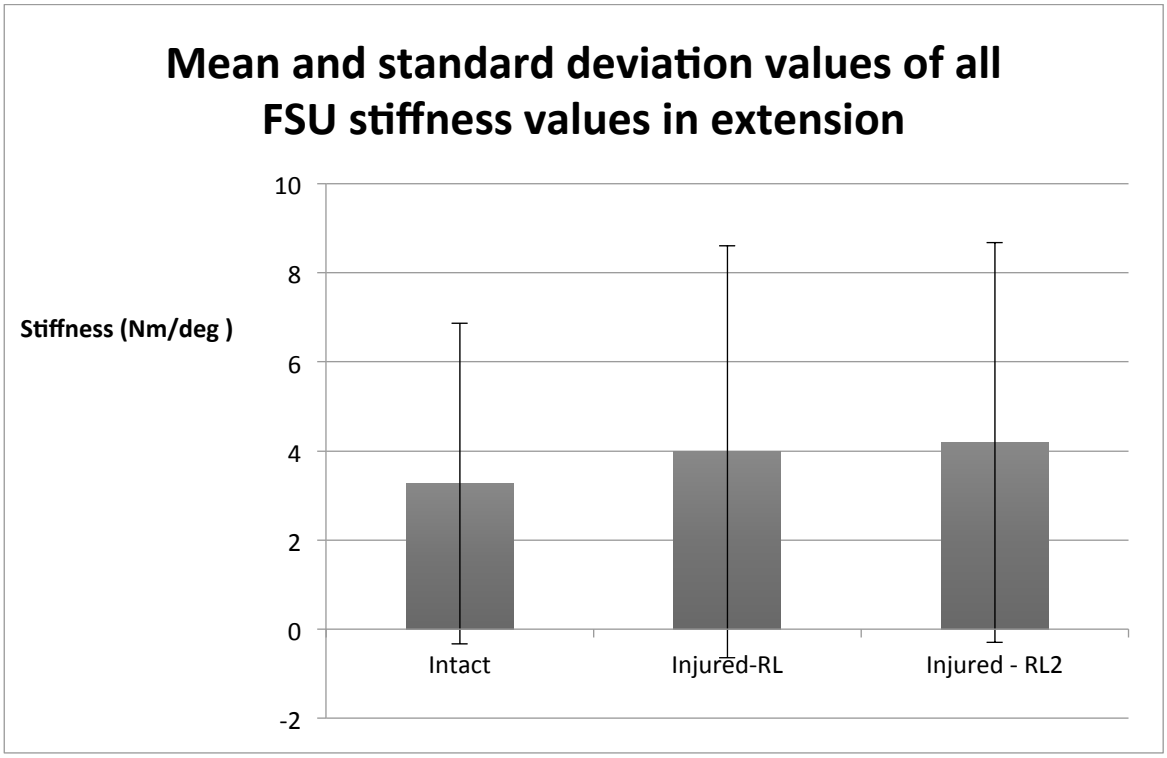

Figure 45: Mean and standard deviation of the stiffness values in extension

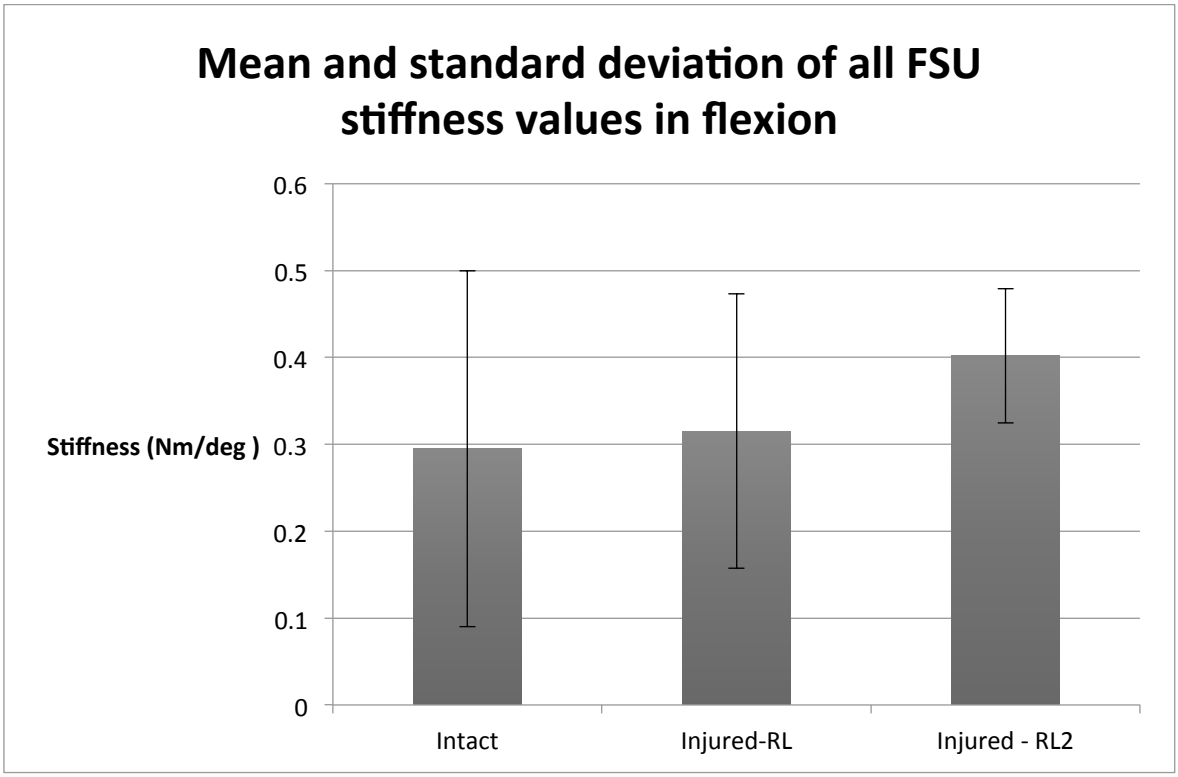

Figure 46: Mean and standard deviation of the stiffness values in flexion

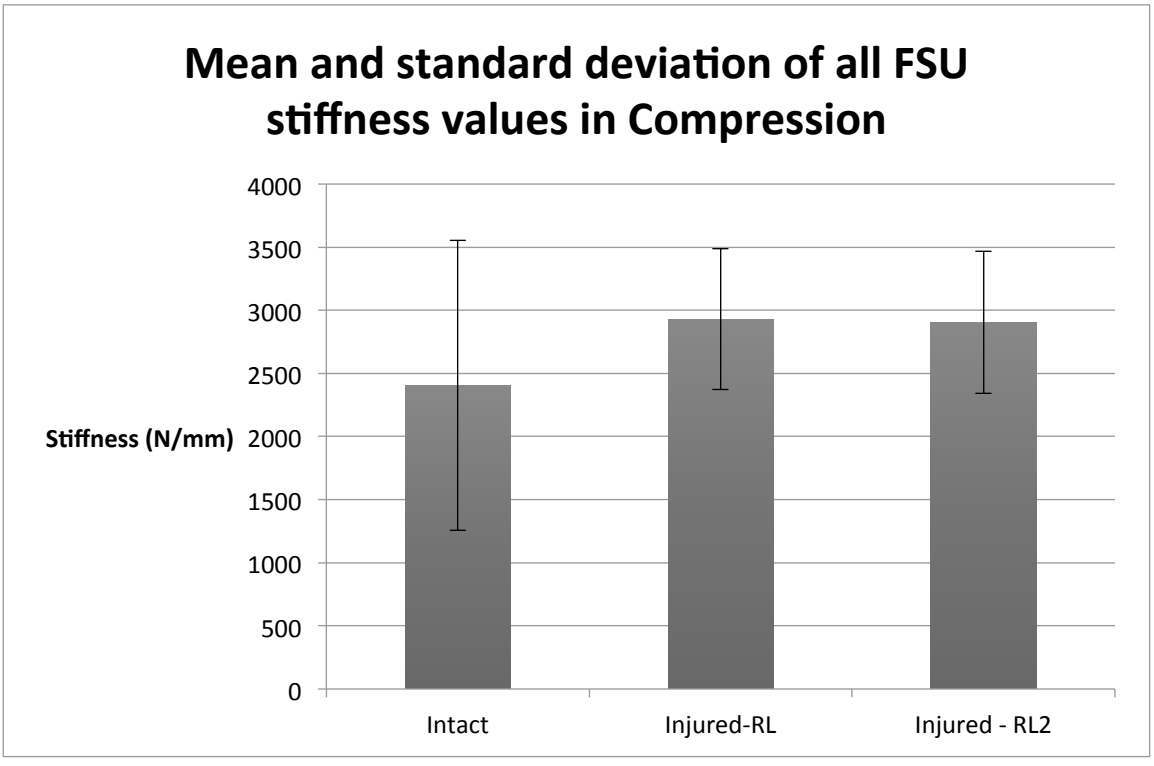

Figure 47: Mean and standard deviation of the stiffness values in compression

6.3.2 Results of hysteresis loss coefficient

The mean of all the FSU hysteresis loss coefficient values in each direction are calculated and plotted graphically as shown below:

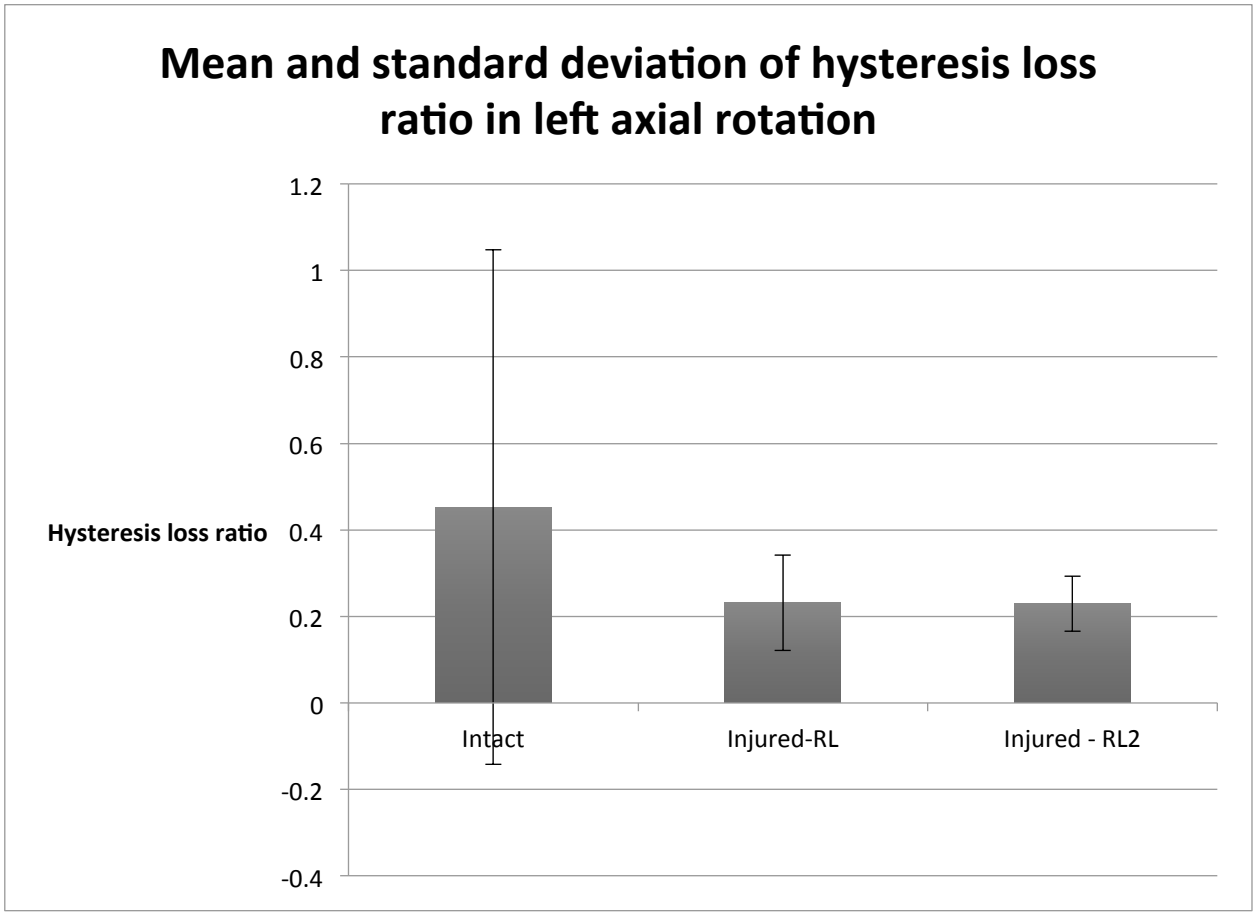

Figure 48: Mean and standard deviation of the hysteresis loss ratio values in left axial rotation

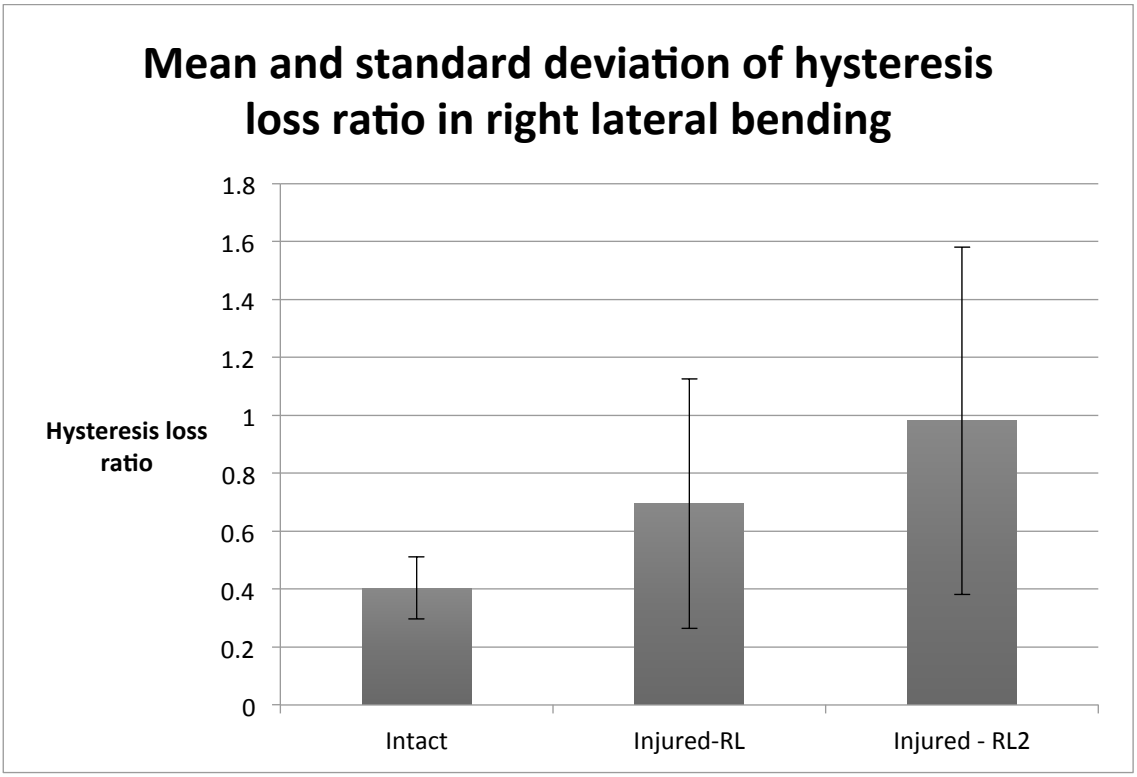

Figure 49: Mean and standard deviation of the hysteresis loss ratio values in right lateral bending

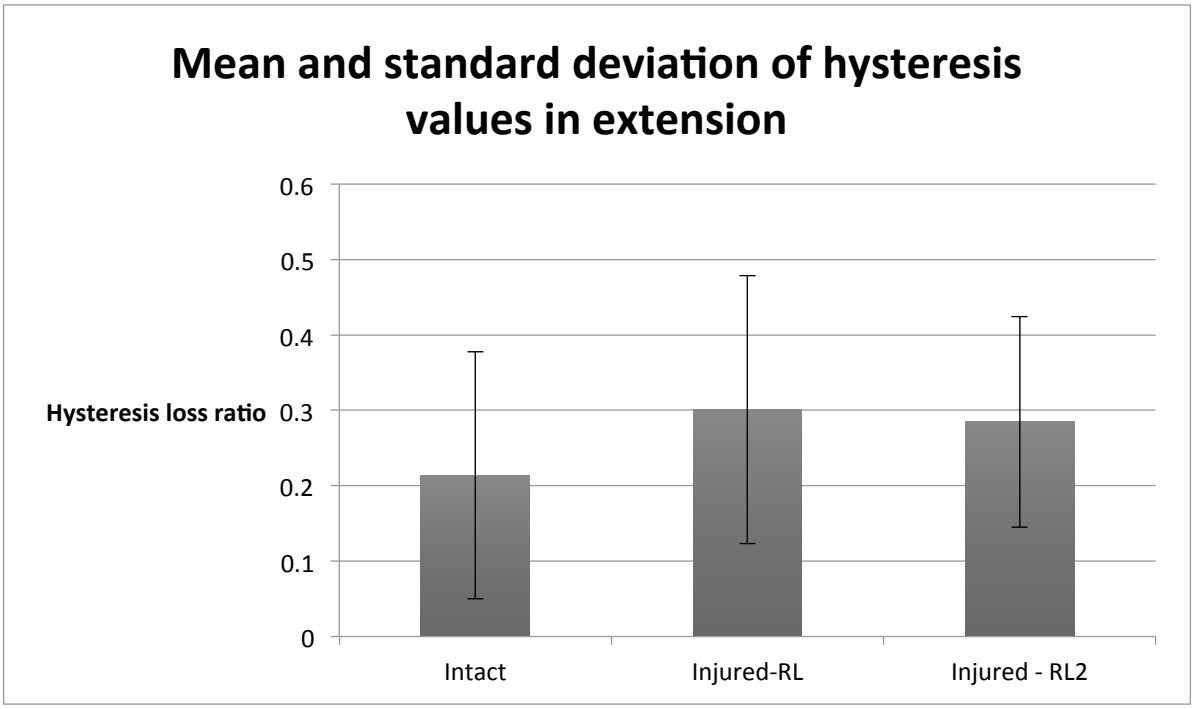

Figure 50: Mean and standard deviation of the hysteresis loss ratio values in extension

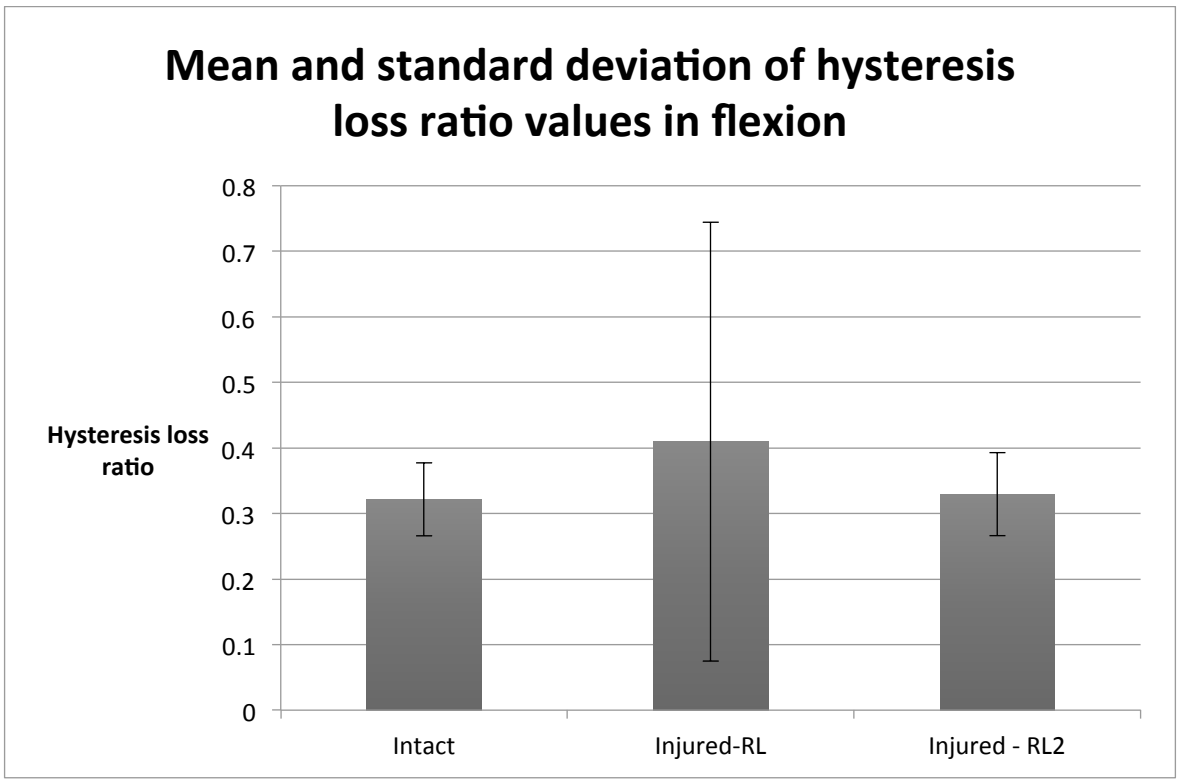

Figure 51: Mean and standard deviation of the hysteresis loss ratio values in flexion

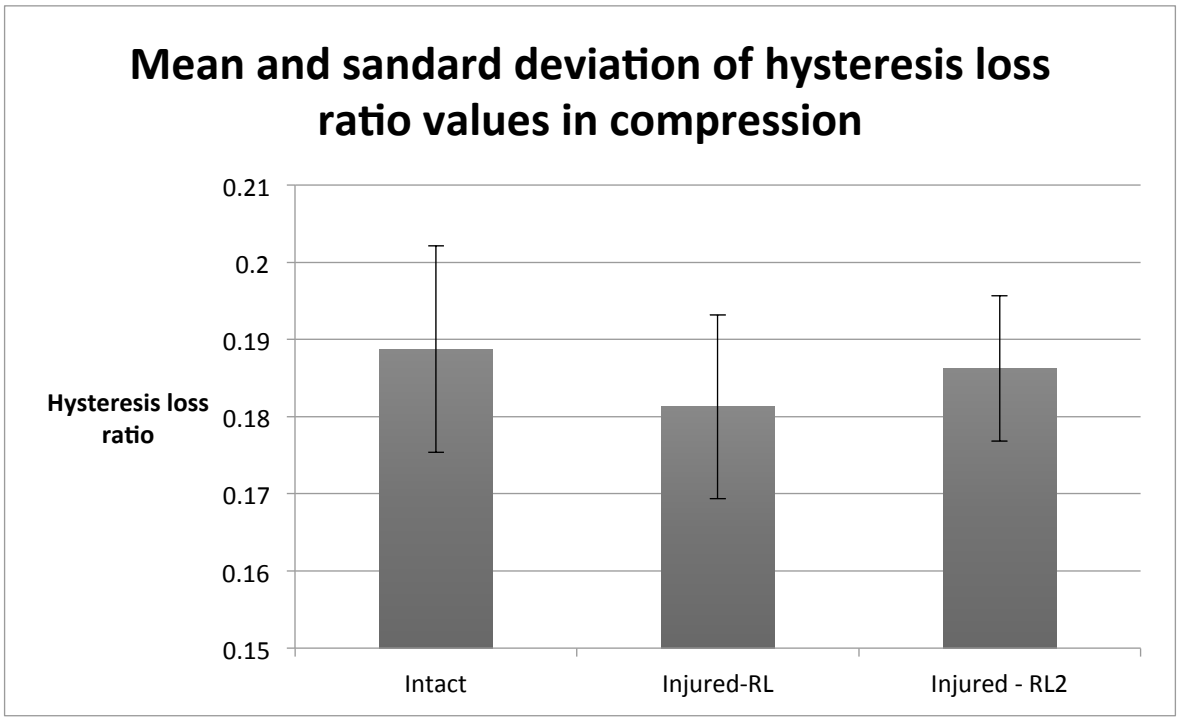

Figure 52: Mean and standard deviation of the hysteresis loss ratio values in compression

	A	B	C
1		Test results of within-subjects effects	
2	DOF	Stiffness *p*=	Hysteresis loss ratio *p* =
3	Left axial rotation	0.195	0.287
4	Right lateral bending	0.586	0.346
5	Extension	0.251	0.365
6	Flexion	0.537	0.655
7	Compression	0.25	0.121

Table 6: Statistical results of stiffness and hysteresis loss ratio values of all FSU in 6DOF

The mechanical data results obtained from the specimen does not show any significant within-subject effects in terms of stiffness ($p > 0.05$) and hysteresis loss ratio ($p > 0.05$) of the intervertebral disc (Table 6), when comparison was done between case1, case2, and case3 (refer section 4.1 point 5(b)) testing states of the disc.

7 Discussion

The aims of this study were to determine the sensitivity of the internal strain measurement using RSA in detecting disc injury, to determine repeatability/precision of the digitizing technique, and to determine mechanical properties of the disc. The mechanical properties and radial strains of the IVD were obtained. Result of the intra-observer repeatability study was obtained.

7.1 Limitations

In total a 4x4 wire grid was inserted in the disc, but only 2x2 grid was considered in the project. That is due to improper insertion of the wire grid. There were no intersection points of the grid on the x-ray films and could not get proper reconstructed image of the IVD. Considering 2X2 grid reduces the periphery of the wire grid inside the disc and limits the internal strain calculation to the grid area. Total internal strains of the disc can be calculated when the grid is inserted properly covering all the disc area.

There was high level of difficulty obtaining bovine tails for testing, as the butchers were not ready to provide or sell the bovine tails. It took a very long time (almost a year) to obtain bovine tails for testing. Due to which the testing was delayed and lead to time constraint.

There was leakage of water from the water heater, which caused shut down of the hexapod. The other reasons that delayed the process are hexapod shutting down caused by entering wrong input values. Due to which the testing had to be done from the start causing delay. Problems were faced with the software, while calculating the strains of the disc.

At first the overnight preload was applied by the hexapod for FSU, specimen was rotated when checked before starting the test. Which means that the specimen did not stay straight and was preloaded overnight in the rotated state and had to void the testing of that specimen. The rotation might be normal as the specimen is from a bovine tail, which does not stay straight normally.

7.2 Results discussion

Disc periphery changes were observed from the RSA results. Comparing the disc periphery radius (mm) in case1 (uninjured disc) with the disc periphery radius (mm) in case2 and case 3 (induced a rim lesion into the disc) gives the changes in the disc periphery. The data was graphically represented in section 6.1 to present a visual difference to the viewer. Figure 93 shows the average values of all the FSUs radial strains in three different cases (refer section 4.1 point 5(b)) after performing each DOF. Case 2 has the highest radial strain when compared to case 1 and 3 after performing left axial rotation, and right lateral bending. The radial strains are highest in case 3 when compared to case 1 and 2 after performing flexion, and flexion+rotation. It is observed that case 1 has highest amount of radial strains after performing compression and extension. The basic idea was that the strain rate increases from a healthy disc to injured disc based on a study conducted by Amin et al., 2016. In flexion the significant increase in the stiffness observed between mild and severely degenerated disc. In axial the stiffness increased in between moderate and severe degeneration of the disc. In lateral shear the stiffness is higher in the moderately degenerated disc compared to mild degeneration (Amin et al., 2016).

In this project it is interesting that the change in the radial strains in not consistent with the rate of injury to the disc. Inconsistence in the increase of radial strains could be due to improper fixing of the beads and markers, specimen being a bovine tail disc could also be one of the reasons, as it does not stay still. Figure 35 to figure 40 and figure 71 to figure 88 shows the graphical representation of the disc periphery in the three cases after performing each DOF, in which FSU1 and FSU2 there is visual change in the disc periphery and there is no visual change in the disc periphery for FSU3 and FSU4.

Mechanical properties of the disc were calculated to analyze if there is any effect of the induced injury on the stiffness and hysteresis loss ratio of the IVD. The statistics were done using ANOVA and there was no significant change in the stiffness (p>0.05) and hysteresis loss ratio (p>0.05) of the disc was observed (Table 6).

In this study it was observed that there is change in the radial strains but not accordingly with the severity of the injury. Fixing the tantalum beads and markers properly and conducting the study on more number of specimens could obtain precise results.

7.3 Reasons for using Bovine discs in this study

Based on the experimental studies of comparing different animals' intervertebral discs to human intervertebral disc, it is said that the animal species intervertebral discs have similar geometry and anatomy to the human intervertebral disc (Showalter et al., 2012; O'Connell et al., 2007). As this experiment is to test the sensitivity of the intervertebral disc strain measurement technique, bovine tail discs serve the purpose well. A wire grid insertion is required to calculate the internal strains, and this can be done only if the disc has reasonable height and this requirement is met by the bovine tail disc.

The most important reasons for using cow discs for this project was because cow discs have a similar anatomy as human discs and are less expensive. Using human discs for the project is not a very feasible option because of its rare availability and high cost. One of the reasons for using cow discs for the project is that lots of samples can be obtained and studied under a controlled environment. In the case of using human discs, we won't have the luxury to use multiple samples if human discs because of the rare and expensive availability of human discs. Due to lack of samples, we won't be able to prove our findings. But in the case of using cow discs in the project, we can easily get multiple samples and can prove our findings with their help.

Human discs can only be used in these projects if someone willingly donates his body to science. But it is a very lengthy process to acquire a body like that, and sometimes the human body is not in a very good condition to be examined. Cow meat is widely consumed all over the world, so there won't be a problem in acquiring cow discs from the slaughter house, and different samples can be examined in different ways to study the problems related to intervertebral discs.

Although there is a possibility of not using cows or about animals in researches and doing this work with the help of computer models to determine the outcomes of an experiment. But sometimes there is no specific data available against a certain disease and the only way to

retrieve this data is by using real organs. Now as said earlier that using human organs or in general using human intervertebral discs is not very feasible options due to its expensiveness. So, what choice do we have left? We only have one choice that we use the vertebral disc of the next best match to the human intervertebral disc and the intervertebral disc of the cow is very similar in structure and functioning that it can be used to study the behavior of the human intervertebral disc.

Using Cow specimens have several advantages over human specimens. First of all healthy bovine specimens are easily available, and there are no complexities of IVD degeneration which is very common in old specimens of humans (Newell et al., 2017)

Specimens from animals are widely used in the study of intervertebral disc degeneration and to find disc treatment methods that can be helpful for finding the cure for human disc degeneration disease. As the samples are very easily available, therefore there is less variability in the tissue samples of different cow subjects as compared to humans (O'connell et al., 2007). A great deal of interest exists currently in developing new therapies, which can address the degeneration of an intervertebral disc in humans. In some of which a synthetic nucleus replacement is injected while other techniques involve biological approaches like cell therapy (Roberts et al., 2008)

The bovine disc has been used as a model in many in vitro studies of the intervertebral disc because of its similar physical and chemical properties of the human disc. However, there is a drawback that these discs have a very high swelling pressure that it is almost impossible to insert any substantial amount of volume into them and therefore cannot be used for nuclear replacements testing unless and until they are modified. We will describe a technique for the development of an explant model; for understanding the disc degeneration using bovine disc through which we will be able to inject the nucleus pulposus. (Roberts et al., 2008)

Figure 53 shows the graphical representation of the intervertebral disc area of different species. Figure 54 shows the graphical representation of the intervertebral disc height of different species in comparison with the human intervertebral disc. From the measurements shown in the figure 53 and 54, Bovine T meets the required specifications regarding the intervertebral

disc are and height in comparison with the human intervertebral disc area and height for this experiment.

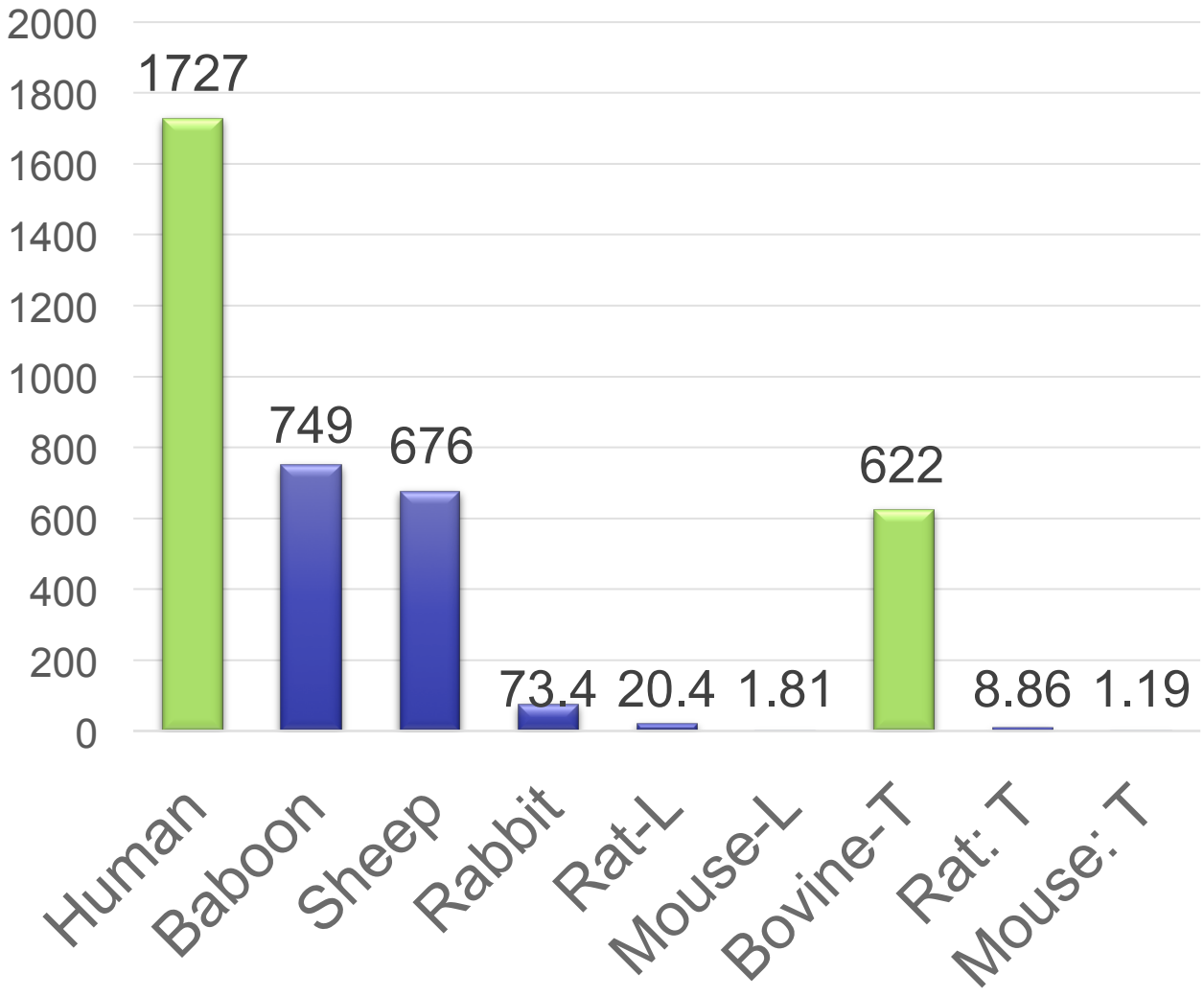

Figure 53: Showing disc area (mm2) of different species in comparison to human disc (Showalter et al., 2012; O'Connell et al., 2007).

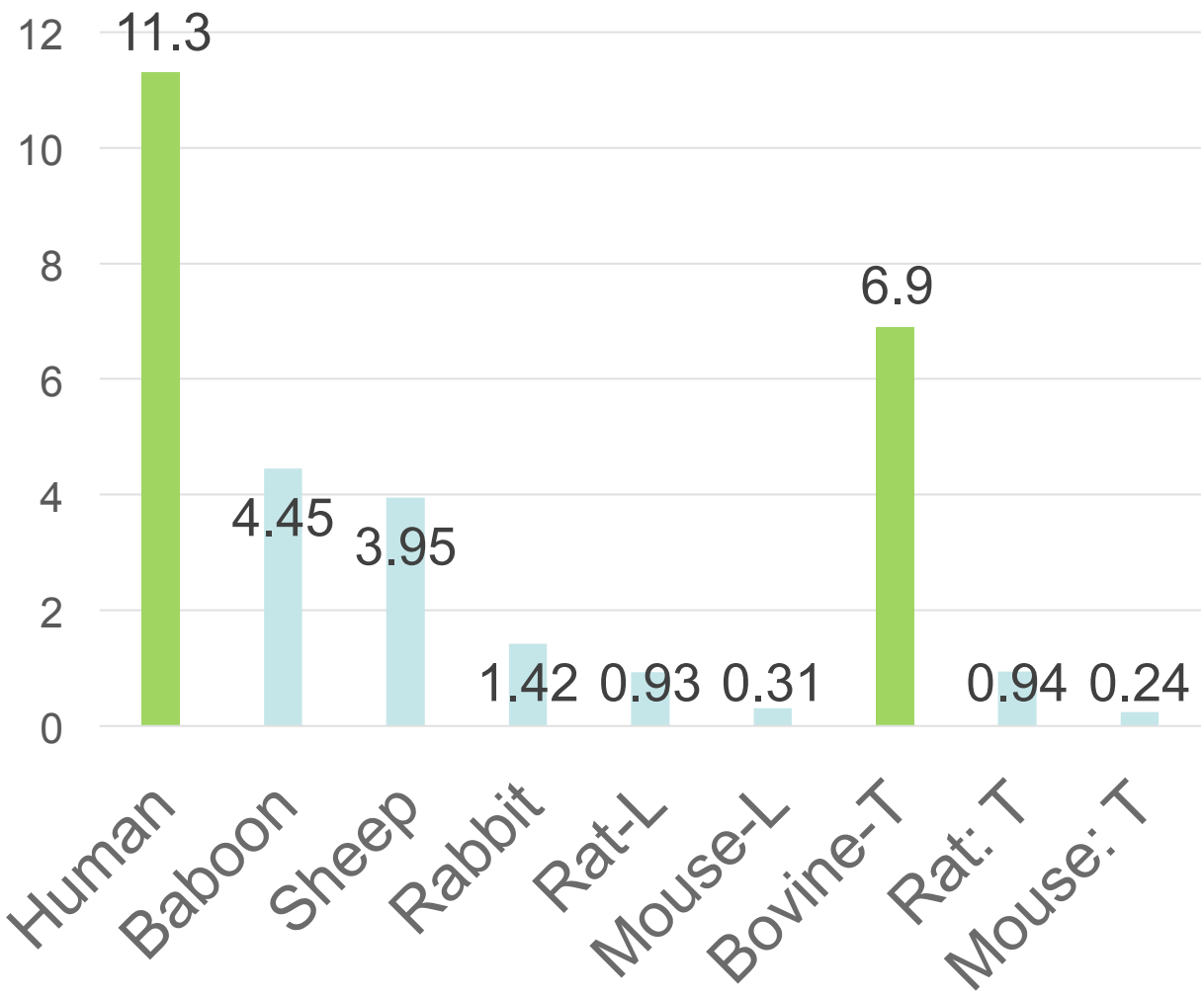

Figure 54: **Showing disc height (mm) of different species in comparison to human disc (Showalter et al., 2012; O'Connell et al., 2007).**

7.4 Importance of hydrating the disc and applying pre-load before testing

Hydrating the specimen is important as it helps the intervertebral disc to maintain the mechanical properties of the disc. But when the disc is kept hydrated for a long time without any load it tends to swell about 20% (McMillan et al., 1996). To get back the disc to its normal physiological range of mechanical behavior a compressive pre-load depending on area of the disc is applied on the disc for 12 hours (Adams 1995). Applying the pre-load and follower pre-load on the cadaveric intervertebral disc is very important as it affects the mechanical properties of the disc, and applying the proper amount of load is must (Patwardhan et al., 2003, Janevic, Ashton-Miller and Schultz 1991, Stanley et al., 2004). The intradiscal pressure of the human intervertebral disc in the lying supine position is 0.1MPa and 0.5MPa at relaxed standing position (Wilke et al., 1999).

The pre-load and the follower pre-load to apply on intervertebral disc is calculated as follows:

$$nucleus\ pulposus\ pressure\ (0.1MPa) = 1.5 * external\ pressure\ (MPa)$$

$$convert\ pressure\ (MPa) into\ force\ \left(\frac{N}{mm^2}\right)$$

$$calculating\ the\ pre-load\ for\ bovine\ intervertebral\ disc\ testing:$$

$$pre-load = \frac{0.1}{1.5} * area\ of\ the\ bovine\ intervertebral\ disc\ (N) \ldots\ldots..eq\ 1$$

$$calculating\ the\ follower\ pre-load\ for\ bive\ intervertebral\ disc\ testing:$$

$$follower\ pre-load = \frac{0.5}{1.5} * area\ of\ the\ bovine\ intervertebral\ disc\ (N) \ldots\ldots\ldots eq\ 2$$

8 Conclusion

The main aim of the project was to determine the sensitivity of the strain measurement technique to detect disc injury using RSA method. The results show that there is visual difference in the periphery of the disc when tested in three different states of the disc (i.e. uninjured state where there is no known damage done to the disc, injured state is where the disc is injured with an induced rim lesion of 5mm width and depth, and then by increasing the length of the rim lesion by 5mm and maintaining the same depth of 5mm). There was no significant difference observed in the stiffness and hysteresis loss ratio values of the disc when compared in its different stages of injury.

8.1 Future development

The internal strain experienced by the disc can be calculated using a customised 'MATLAB' code and get potential outputs to determine the sensitivity of the strain measurement technique in detecting disc injury using RSA. Conducting the tests on more number of specimens might give a better understanding and support to the results obtained.

9 Reference

1) "ISB Software Resources - Movement Analysis Software". Isbweb.org. N.p., 2017. Web. 9 March 2017.
2) Adams, M. A. "Spine Update Mechanical Testing of The Spine an Appraisal of Methodology, Results, And Conclusions". *Spine* 20.19 (1995): 2151-2156. Web.
3) Adams, M.A. and Roughley, P.J., (2006). What is intervertebral disc degeneration, and what causes it? *Spine*, *31*(18), pp.2151-2161.
4) ALLAN, D. B. & WADDELL, G. 1989. An historical perspective on low back pain and disability. *Acta Orthopaedica Scandinavica,* 60**,** 1-23.
5) Amin, D., Sommerfeld, D., Lawless, I., Stanley, R., Ding, B. and Costi, J. (2016). Effect of degeneration on the six degree of freedom mechanical properties of human lumbar spine segments. *Journal of Orthopaedic Research*, 34(8), pp.1399-1409.
6) Beckstein, Jesse C. et al. "Comparison Of Animal Discs Used In Disc Research To Human Lumbar Disc". *Spine* 33.6 (2008): E166-E173. Web.
7) Bland, J.M. and Altman, D.G., (2010). Statistical methods for assessing agreement between two methods of clinical measurement. *International Journal of Nursing Studies*, *47*(8), pp.931-936.
8) BODEN, S. D., DAVIS, D., DINA, T., PATRONAS, N. & WIESEL, S. 1990. Abnormal magnetic-resonance scans of the lumbar spine in asymptomatic subjects. A prospective investigation. *J Bone Joint Surg Am,* 72**,** 403-408
9) BOGDUK, N., TYNAN, W. & WILSON, A. 1981. The nerve supply to the human lumbar intervertebral discs. *Journal of Anatomy,* 132**,** 39.
10) Bojan, A.J., Bragdon, C., Jönsson, A., Ekholm, C. and Kärrholm, J. (2015). Three-dimensional bone-implant movements in trochanteric hip fractures: Precision and accuracy of radiostereometric analysis in a phantom model. *Journal of Orthopaedic Research*, *33*(5), pp.705-711.
11) BOOS, N., WEISSBACH, S., ROHRBACH, H., WEILER, C., SPRATT, K. F. & NERLICH, A. G. 2002. Classification of age-related changes in lumbar intervertebral discs: 2002 Volvo Award in basic science. *Spine,* 27**,** 2631-2644

12) BORENSTEIN, D. G., O'MARA, J. W., BODEN, S. D., LAUERMAN, W. C., JACOBSON, A., PLATENBERG, C., SCHELLINGER, D. & WIESEL, S. W. 2001. The value of magnetic resonance imaging of the lumbar spine to predict low-back pain in asymptomatic subjects. *J Bone Joint Surg Am,* 83**,** 1306-1311.

13) Bottner, F., Su, E., Nestor, B., Azzis, B., Sculco, T. and Bostrom, M. (2005). *Radiostereometric Analysis: The Hip. HSS Journal,* 1(1), pp.94-99.

14) BRINCKMANN, P. and GROOTENBOER, H. (1991). Change of Disc Height, Radial Disc Bulge, and Intradiscal Pressure from Discectomy An In vitro Investigation on Human Lumbar Discs. *Spine*, 16(6), pp.641-646.

15) CHAN, S. C. & GANTENBEIN-RITTER, B. 2012. Preparation of intact bovine tail intervertebral discs for organ culture. *JoVE (Journal of Visualized Experiments)***,** e3490-e3490.

16) COSTI, J. J., STOKES, I. A., GARDNER-MORSE, M., LAIBLE, J., SCOFFONE, H. M. & IATRIDIS, J. 2007. Direct measurement of intervertebral disc maximum shear strain in six degrees of freedom: motions that place disc tissue at risk of injury. *Journal of biomechanics,* 40**,** 2457-2466.

17) Costi, John J, Trevor C Hearn, and Nicola L Fazzalari. "The Effect of Hydration on the Stiffness of Intervertebral Discs in an Ovine Model". *Clinical Biomechanics* 17.6 (2002): 446-455. Web.

18) Costi, John J. et al. "Frequency-Dependent Behavior Of the Intervertebral Disc in Response to Each of Six Degree Of Freedom Dynamic Loading". *Spine* 33.16 (2008): 1731-1738. Web.

19) De Carvalho, D.E., Soave, D., Ross, K. and Callaghan, J.P., (2010). Lumbar spine and pelvic posture between standing and sitting: a radiologic investigation including reliability and repeatability of the lumbar lordosis measure. *Journal of manipulative and physiological therapeutics*, *33*(1), pp.48-55.

20) DE PALMA, A. F. & ROTHMAN, R. H. 1970. *The intervertebral disc*, Saunders Limited.

21) Ebara, Sohei et al. "Tensile Properties of Nondegenerate Human Lumbar Anulus Fibrosus". *Spine* 21.4 (1996): 452-461. Web.

22) ECK, J., HUMPHREYS, S. & HODGES, S. 1999. Adjacent-segment degeneration after lumbar fusion: a review of clinical, biomechanical, and radiologic studies. *American journal of orthopedics (Belle Mead, NJ),* 28**,** 336-340.

23) EXPERIMENTAL INVESTIGATIONS INTO THE PHYSICAL PROPERTIES OF THE INTERVERTEBRAL DISC. (1951). *The Bone & Joint Journal*, [online] vol 33(4), pp.607-611.

24) FAIRBANK, J. 2002. Clinical importance of the intervertebral disc, or back pain for biochemists. Portland Press Limited.

25) FRAYSSE, FRANÇOIS ET AL. "A NOVEL METHOD TO REPLICATE THE KINEMATICS OF THE CARPUS USING A SIX DEGREE-OF-FREEDOM ROBOT". *JOURNAL OF BIOMECHANICS* 47.5 (2014): 1091-1098. WEB.

26) Galbusera, F., Van Rijsbergen, M., Ito, K., Huyghe, J.M., Brayda-Bruno, M. and Wilke, H.J., (2014). Ageing and degenerative changes of the intervertebral disc and their impact on spinal flexibility. *European spine journal*, *23*(3), pp.324-332.

27) GALIS, F. 1999. Why do almost all mammals have seven cervical vertebrae? Developmental constraints, Hox genes, and cancer. *Journal of Experimental Zoology,* 285**,** 19-26.

28) Gallucci, M., Anselmi, M., Di Sibio, A. and Gregori, L.M., (2011). Annular tears, fissures or HIZ?. *Neuroradiology*, *53*(1), p.161.

29) GIANAKOS, A. L., YASUI, Y., FRASER, E. J., ROSS, K. A., PRADO, M. P., FORTIER, L. A. & KENNEDY, J. G. 2016. The Effect of Different Bone Marrow Stimulation Techniques on Human Talar Subchondral Bone: A Micro–Computed Tomography Evaluation. *Arthroscopy: The Journal of Arthroscopic & Related Surgery,* 32**,** 2110-2117.

30) Guerin, H.L. and Elliott, D.M. (2007). Quantifying the contributions of structure to annulus fibrosus mechanical function using a nonlinear, anisotropic, hyperelastic model. *Journal of Orthopaedic Research*, *25*(4), pp.508-516.

31) Guterl, C.C., See, E.Y., Blanquer, S.B., Pandit, A., Ferguson, S.J., Benneker, L.M., Grijpma, D.W., Sakai, D., Eglin, D., Alini, M. and Iatridis, J.C., (2013). Challenges and strategies in the repair of ruptured annulus fibrosus. *European cells & materials*, *25*, p.1-3.

32) Humzah, M. and Soames, R. (1988). Human intervertebral disc: Structure and function. *The Anatomical Record*, 220(4), pp.337-356.

33) Iatridis, J.C. (2016). Structural and Functional Repair of the Annulus Fibrosus. *Global Spine Journal*, *6*(S 01), p.WIN001.

34) Inoue, N. and Orías, A.A.E., (2011). Biomechanics of intervertebral disk degeneration. *Orthopedic Clinics of North America*, *42*(4), pp.487-499.

35) Iorio, J., Jakoi, A. and Singla, A. (2016). Biomechanics of Degenerative Spinal Disorders. *Asian Spine Journal*, 10(2), p.377.

36) Janevic, J., J.A. Ashton-Miller, and A.B. Schultz. "Large Compressive Preloads Decrease Lumbar Motion Segment Flexibility". *Journal of Biomechanics* 23.7 (1990): 722. Web.

37) JAY LIPSON, S. & MUIR, H. 1981. Experimental intervertebral disc degeneration. Morphologic and proteoglycan changes over time. *Arthritis & Rheumatism,* 24**,** 12-21.

38) KANEOKA, K., ONO, K., INAMI, S. & HAYASHI, K. 1999. Motion analysis of cervical vertebrae during whiplash loading. *Spine,* 24**,** 763-769.

39) KELSEY, J. L. & WHITE III, A. A. 1980. Epidemiology and impact of low-back pain. *Spine,* 5**,** 133-142.

40) Kepler, C.K., Ponnappan, R.K., Tannoury, C.A., Risbud, M.V. and Anderson, D.G., (2013). The molecular basis of intervertebral disc degeneration. *The Spine Journal*, *13*(3), pp.318-330.

41) KERTTULA, L. I., SERLO, W. S., TERVONEN, O. A., PÄÄKKÖ, E. L. & VANHARANTA, H. V. 2000. Post-traumatic findings of the spine after earlier vertebral fracture in young patients: clinical and MRI study. *Spine,* 25**,** 1104-1108.

42) Key, J. and LOUIS, S. (1945). INTERVERTEBRAL DISC LESIONS ARE THE MOST COMMON CAUSE OF LOW BACK PAIN WITH OR WITHOUT SCIATICA. *Annals of Surgery,* 121(4), p.534.

43) KRAG, MARTIN H. et al. "Internal Displacement Distribution From In Vitro Loading of Human Thoracic and Lumbar Spinal Motion Segments: Experimental Results and Theoretical Predictions". *Spine* 12.10 (1987): 1001-1007. Web.

44) Kwon3d.com. (2017). DLT Method. [online] Available at: http://www.kwon3d.com/theory/dlt/dlt.html [Accessed 9 March 2017].

45) Lin, P.S., Chiou, B., Abrahamson, N., Walling, M., Lee, C.T. and Cheng, C.T. (2011). Repeatable source, site, and path effects on the standard deviation for empirical ground-motion prediction models. *Bulletin of the Seismological Society of America*, *101*(5), pp.2281-2295.

46) Lin, S.C., Huang, C.H., Hsu, C.P., Chang, S.S., Hsieh, P.H., Shih, H.N., Chang, Y.H. and Chan, Y.S. (2017). Pose-induced effects of femur and tibia on accuracy of model-based radiostereometric analysis. *Computer Methods in Biomechanics and Biomedical Engineering: Imaging & Visualisation*, pp.1-8.

47) LOTZ, J. C., COLLIOU, O. K., CHIN, J. R., DUNCAN, N. A. & LIEBENBERG, E. 1998. Compression-induced degeneration of the intervertebral disc: an in vivo mouse model and finite-element study. *Spine,* 23**,** 2493-2506.

48) Lu, W., Luk, K., Holmes, A., Cheung, K. and Leong, J. (2005). Pure Shear Properties of Lumbar Spinal Joints and the Effect of Tissue Sectioning on Load Sharing. *Spine*, 30(8), pp.E204-E209.

49) LUOMA, K., RIIHIMÄKI, H., LUUKKONEN, R., RAININKO, R., VIIKARI-JUNTURA, E. & LAMMINEN, A. 2000. Low back pain in relation to lumbar disc degeneration. *Spine,* 25**,** 487-492.

50) MAETZEL, A. & LI, L. 2002. The economic burden of low back pain: a review of studies published between 1996 and 2001. *Best Practice & Research Clinical Rheumatology,* 16**,** 23-30.

51) MANIADAKIS, N. & GRAY, A. 2000. The economic burden of back pain in the UK. *Pain,* 84**,** 95-103.

52) Marchand, F. and Ahmed, A.M. (1990). Investigation of the laminate structure of lumbar disc anulus fibrosus. *Spine*, *15*(5), pp.402-410.

53) Masuoka, K., Michalek, A., MacLean, J., Stokes, I. and Iatridis, J. (2007). Different Effects of Static Versus Cyclic Compressive Loading on Rat Intervertebral Disc Height and Water Loss In Vitro. *Spine*, 32(18), pp.1974-1979.

54) Maxfield, B.A. (2010). Sports-related injury of the pediatric spine. *Radiologic Clinics of North America*, *48*(6), pp.1237-1248.

55) MAYNARD, F. M., BRACKEN, M. B., CREASEY, G., DITUNNO, J. F., DONOVAN, W. H., DUCKER, T. B., GARBER, S. L., MARINO, R. J., STOVER, S. L. & TATOR, C. H. 1997. International standards for neurological and functional classification of spinal cord injury. *Spinal cord,* 35**,** 266-274.

56) MCLAIN, R. F. 1994. Mechanoreceptor endings in human cervical facet joints. *Spine,* 19**,** 495-501.

57) McMillan, D W, G Garbutt, and M A Adams. "Effect Of Sustained Loading On The Water Content Of Intervertebral Discs: Implications For Disc Metabolism.". *Annals of the Rheumatic Diseases* 55.12 (1996): 880-887. Web.

58) MILLER, J., SCHMATZ, C. & SCHULTZ, A. 1988. Lumbar disc degeneration: correlation with age, sex, and spine level in 600 autopsy specimens. *Spine,* 13**,** 173-178.

59) NACHEMSON, A. L. 1976. The Lumbar Spine An Orthopaedic Challenge. *Spine,* 1**,** 59-71.

60) NEWELL, N., GRIGORIADIS, G., CHRISTOU, A., CARPANEN, D. & MASOUROS, S. D. 2017. Material properties of bovine intervertebral discs across strain rates. *Journal of the Mechanical Behavior of Biomedical Materials,* 65**,** 824-830.

61) Newell, N., Little, J., Christou, A., Adams, M., Adam, C. and Masouros, S. (2017). Biomechanics of the human intervertebral disc: A review of testing techniques and results. *Journal of the Mechanical Behavior of Biomedical Materials*, 69, pp.420-434.

62) Nonsteroidal anti-inflammatory drugs. *Cancer,* 115**,** 5662-5671.

63) O'CONNELL, G. D., VRESILOVIC, E. J. & ELLIOTT, D. M. 2007. Comparison of animals used in disc research to human lumbar disc geometry. *Spine,* 32**,** 328-333.

64) OSTI, O L, B VERNON-ROBERTS, and R D FRASER. "1990 Volvo Award In Experimental Studies: Anulus Tears And Intervertebral Disc Degeneration". *Spine* 15.8 (1990): 762-767. Web.

65) Osti, O., Vernon-Roberts, B., Moore, R. and Fraser, R. (1992). Annular tears and disc degeneration in the lumbar spine. A post-mortem study of 135 discs. *The Journal of Bone and Joint Surgery. British volume*, 74-B(5), pp.678-682.

66) PAGET, J. 1877. On a form of chronic inflammation of bones (osteitis deformans). *Medico-chirurgical transactions,* 60**,** 37.

67) Patwardhan, Avinash G. et al. "Effect Of Compressive Follower Preload On The Flexion–Extension Response Of The Human Lumbar Spine". *Journal of Orthopaedic Research* 21.3 (2003): 540-546. Web.

68) Pearcy, M. and Tibrewal, S. (1984). Axial Rotation and Lateral Bending in the Normal Lumbar Spine Measured by Three-Dimensional Radiography. *Spine*, 9(6), pp.582-587.

69) Peng, B. (2013). Pathophysiology, diagnosis, and treatment of discogenic low back pain. *World Journal of Orthopedics*, 4(2), p.42.

70) Pineau, V., Lebel, B., Gouzy, S., Dutheil, J.J. and Vielpeau, C. (2010). Dual mobility hip arthroplasty wear measurement: Experimental accuracy assessment using radiostereometric analysis (RSA). *Orthopaedics & Traumatology: Surgery & Research*, *96*(6), pp.609-615.

71) PUUSTJÄRVI, K., LAMMI, M., HELMINEN, H., INKINEN, R. & TAMMI, M. 1994. Proteoglycans in the intervertebral disc of young dogs following strenuous running exercise. *Connective tissue research,* 30**,** 225-240.

72) Raj, P. P. (2008), Intervertebral Disc: Anatomy-Physiology-Pathophysiology-Treatment. Pain Practice, 8: 18–44. doi:10.1111/j.1533-2500.2007.00171.x

73) Reinschmidt, C. et al. "Effect of Skin Movement On The Analysis Of Skeletal Knee Joint Motion During Running". *Journal of Biomechanics* 30.7 (1997): 729-732. Web.

74) ROBERTS, S., MENAGE, J., SIVAN, S. & URBAN, J. P. 2008. Bovine explant model of degeneration of the intervertebral disc. *BMC musculoskeletal disorders,* 9**,** 24.

75) Saad, A., Saab, M. and Gatinel, D. (2010). Repeatability of measurements with a double-pass system. *Journal of Cataract & Refractive Surgery*, *36*(1), pp.28-33.

76) SACHS, B., VANHARANTA, H., SPIVEY, M., GUYER, R., VIDEMAN, T., RASHBAUM, R., JOHNSON, R., HOCHSCHULER, S. and MOONEY, V. (1987). Dallas Discogram Description A New Classification of CT/Discography in Low-back Disorders. *Spine,* 12(3), pp.287-294.

77) Solomon, L.B., Stevenson, A.W., Callary, S.A., Sullivan, T.R., Howie, D.W. and Chehade, M.J. (2010). The accuracy and precision of radiostereometric analysis in monitoring tibial plateau fractures. *Acta orthopaedica*, *81*(4), pp.487-494.

78) Stanley, Scott K. et al. "Flexion–Extension Response Of The Thoracolumbar Spine Under Compressive Follower Preload". *Spine* 29.22 (2004): E510-514. Web.

79) Stefanakis, M., Luo, J., Pollintine, P., Dolan, P. and Adams, M. (2014). ISSLS Prize Winner. *Spine,* 39(17), pp.1365-1372.

80) Stilling, M., Kold, S., de Raedt, S., Andersen, N.T., Rahbek, O. and Søballe, K. (2012). Superior accuracy of model-based radiostereometric analysis for measurement of polyethylene wear. *Bone and Joint Research*, *1*(8), pp.180-191.

81) STOKES, I. and FRYMOYER, J. (1987). Segmental Motion and Instability. *Spine*, 12(7), pp.688-691.

82) Stokes, Ian A. et al. "Measurement of A Spinal Motion Segment Stiffness Matrix". *Journal of Biomechanics* 35.4 (2002): 517-521. Web.

83) Tavakoli, J., Elliott, D.M. and Costi, J.J., (2016). Structure and mechanical function of the inter-lamellar matrix of the annulus fibrosus in the disc. *Journal of Orthopaedic Research*, *34*(8), pp.1307-1315.

84) Ten Brinke, B., Beumer, A., Koenraadt, K.L., Eygendaal, D., Kraan, G.A. and Mathijssen, N.M. (2017). The accuracy and precision of radiostereometric analysis in upper limb arthroplasty: A systematic review of 23 RSA studies. *Acta orthopaedica*, *88*(3), pp.320-325.

85) THOMPSON, J., PEARCE, R., SCHECHTER, M., ADAMS, M., TSANG, I. and BISHOP, P. (1990). Preliminary Evaluation of a Scheme for Grading the Gross Morphology of the Human Intervertebral Disc. *Spine*, 15(5), pp.411-415.

86) Tsantrizos, Anthony et al. "Internal Strains in Healthy and Degenerated Lumbar Intervertebral Discs". *Spine* 30.19 (2005): 2129-2137. Web.

87) TWOMEY, L. & TAYLOR, J. 1987. Age changes in lumbar vertebrae and intervertebral discs. *Clinical orthopaedics and related research,* 224**,** 97-104.

88) Urban, J.P. and Roberts, S., (2003). Degeneration of the intervertebral disc. *Arthritis Res Ther*, *5*(3), p.120.

89) VACCARO, A. R., RIZZOLO, S. J., ALLARDYCE, T. J., RAMSEY, M., SALVO, J., BALDERSTON, R. A. & COTLER, J. M. 1995a. Placement of pedicle screws in the thoracic spine. Part I: Morphometric analysis of the thoracic vertebrae. *J Bone Joint Surg Am,* 77**,** 1193-1199.

90) VACCARO, A. R., RIZZOLO, S. J., BALDERSTON, R. A., ALLARDYCE, T. J., GARFIN, S. R., DOLINSKAS, C. & AN, H. S. 1995b. Placement of pedicle screws in the thoracic spine. Part II: An anatomical and radiographic assessment. *J Bone Joint Surg Am,* 77**,** 1200-1206.

91) Vergroesen, P., Kingma, I., Emanuel, K., Hoogendoorn, R., Welting, T., van Royen, B., van Dieën, J. and Smit, T. (2015). Mechanics and biology in intervertebral disc degeneration: a vicious circle. *Osteoarthritis and Cartilage*, 23(7), pp.1057-1070.

92) Wang, Y., Videman, T. and Battié, M.C., (2012). Lumbar vertebral endplate lesions: prevalence, classification, and association with age. *Spine*, *37*(17), pp.1432-1439.

93) Weiner, B. (2010). Treatment of lumbar disc herniation: Evidence-based practice. *International Journal of General Medicine*, p.209.

94) WHITE, A. A. & PANJABI, M. M. 1978. *Clinical biomechanics of the spine*, Lippincott Williams & Wilkins.ZELL, J. A., ZIOGAS, A., BERNSTEIN, L., CLARKE, C. A., DEAPEN, D., LARGENT, J. A., NEUHAUSEN, S. L., STRAM, D. O., URSIN, G. & ANTON-CULVER, H. 2009.

95) Wilke, Hans–Joachim et al. "New In Vivo Measurements Of Pressures In The Intervertebral Disc In Daily Life". *Spine* 24.8 (1999): 755-762. Web.

96) Youssef, G., Lopez, C. and Kabo, J.M., (2017). Composite mechanics of the multilayer structure of the annulus fibrosus. *Journal of Mechanical Engineering*, *1*(5), pp.126-134.

97) Zhou, Y. and Abdi, S. (2006). Diagnosis and Minimally Invasive Treatment of Lumbar Discogenic Pain ??? A Review of the Literature. The Clinical Journal of Pain, 22(5), pp.468-481.

10 Appendix:

10.1 Appendix A

The results of the displacements observed in the x, y, and z coordinates of the wire intersection points inside the disc are presented below. First the results of the specimen in all three testing cases are obtained; the results of case2 and case3 are compared with the results of case1. Case1 was the reference point to measure the difference in the x, y, and z coordinates of the wire intersection points in the disc. As case1 is the state in which no injury is induced into the disc, case2 and case3 state of disc consists an injury of controlled width, depth, and position of the injury (rim lesion). The coordinates displacement is calculated in 6 DOF.

FSU 1: Wire intersection coordinates for specimen 1.

Wire intersection point coordinates difference between 'RL and Intact'				
ROW 1 AND 2	X DIS	Y DIS	Z DIS	
1 3	-0.21	-0.11	-0.12	
1 4	-0.74	1.22	-0.28	
2 3	0.8	0.15	-0.3	
2 4	-2.44	0.54	1.42	
Wire intersection point coordinates difference between 'RL2 and Intact'				
ROW 1 AND 2	X DIS	Y DIS	Z DIS	
1 3	0.37	-0.17	-0.22	
1 4	0.28	0.39	0.15	
2 3	1.63	-0.36	-0.27	
2 4	-0.49	-0.97	-0.65	

Figure 55: Difference in the displacement of x, y, and z coordinates of the wire intersection points when the results of the specimen tested in case1 (Intact/uninjured) are compared to results of case2 (RL/injured) and case3 (RL2/injured) in the direction of left axial rotation – FSU1

Wire intersection point coordinates difference between 'RL and Intact'			
ROW 1 AND 2	X DIS	Y DIS	Z DIS
1 3	-0.38	-0.02	-0.37
1 4	0.01	0.45	-0.29
2 3	-0.44	-0.1	-0.32
2 4	-0.31	-0.3	-0.17
Wire intersection point coordinates difference between 'RL2 and Intact'			
ROW 1 AND 2	X DIS	Y DIS	Z DIS
1 3	1.72	2.86	1.12
1 4	-0.33	0.34	0.09
2 3	0.52	-0.22	0.06
2 4	0.33	0	0.14

Figure 56: Difference in the displacement of x, y, and z coordinates of the wire intersection points when the results of the specimen tested in case1 (Intact/uninjured) are compared to results of case2 (RL/injured) and case3 (RL2/injured) in the direction of right lateral bending – FSU1

Wire intersection point coordinates difference between 'RL and Intact'			
ROW 1 AND 2	X DIS	Y DIS	Z DIS
1 3	-0.1	-0.58	-0.43
1 4	-2.58	-0.63	-0.73
2 3	-0.37	-0.65	-0.08
2 4	0.58	-0.65	-1.71
Wire intersection point coordinates difference between 'RL2 and Intact'			
ROW 1 AND 2	X DIS	Y DIS	Z DIS
1 3	0.13	-0.75	-0.02
1 4	1.17	0.03	0.45
2 3	0.59	-0.43	0.05
2 4	0.5	-0.86	-1.52

Figure 57: Difference in the displacement of x, y, and z coordinates of the wire intersection points when the results of the specimen tested in case1 (Intact/uninjured) are compared to results of case2 (RL/injured) and case3 (RL2/injured) in the direction of extension-FSU1

Wire intersection point coordinates difference between 'RL and Intact'			
ROW 1 AND 2	X DIS	Y DIS	Z DIS
1 3	-0.09	-0.21	-0.04
1 4	0.48	0	0.06
2 3	0.42	1.74	0.12
2 4	-0.08	0.29	0.16
Wire intersection point coordinates difference between 'RL2 and Intact'			
ROW 1 AND 2	X DIS	Y DIS	Z DIS
1 3	-1.75	1.41	-0.57
1 4	0.45	0.45	0.11
2 3	0.12	0.06	0.02
2 4	-0.51	0.2	0.08

Figure 58: Difference in the displacement of x, y, and z coordinates of the wire intersection points when the results of the specimen tested in case1 (Intact/uninjured) are compared to results of case2 (RL/injured) and case3 (RL2/injured) in the direction of flexion-FSU1

Wire intersection point coordinates difference between 'RL and Intact'			
ROW 1 AND 2	X DIS	Y DIS	Z DIS
1 3	-0.04	-0.01	-0.3
1 4	0.13	0.12	-0.25
2 3	0.08	0.26	-0.25
2 4	-0.34	0.57	-0.02
Wire intersection point coordinates difference between 'RL2 and Intact'			
ROW 1 AND 2	X DIS	Y DIS	Z DIS
1 3	0.05	0.11	-0.3
1 4	0.54	0.23	-0.12
2 3	0.12	0.27	-0.27
2 4	-1.18	0.77	-0.34

Figure 59: Difference in the displacement of x, y, and z coordinates of the wire intersection points when the results of the specimen tested in case1 (Intact/uninjured) are compared to results of case2 (RL/injured) and case3 (RL2/injured) in the direction of flexion + rotation-FSU1

Wire intersection point coordinates difference between 'RL and Intact'					
ROW 1 AND 2	X DIS	Y DIS	Z DIS		
1 3	-11.19	-18.69	-6.29		
1 4	4.82	-0.19	-1.12		
2 3	3.68	-2.82	-1.38		
2 4	1.52	-3.15	-2.29		
Wire intersection point coordinates difference between 'RL2 and Intact'					
ROW 1 AND 2	X DIS	Y DIS	Z DIS		
1 3	-10.85	-17.49	-6.71		
1 4	8.35	1.1	0.04		
2 3	4.45	0.08	-2.46		
2 4	0.93	-1.94	-2.38		

Figure 60: Difference in the displacement of x, y, and z coordinates of the wire intersection points when the results of the specimen tested in case1 (Intact/uninjured) are compared to results of case2 (RL/injured) and case3 (RL2/injured) in the direction of compression-FSU1

FSU 2: Wire intersection point coordinates of specimen 2

Wire intersection point coordinates difference between 'RL and Intact'					
ROW 1 AND	X DIS	Y DIS	Z DIS		
1 3	-5.62	0.68	-0.31		
1 4	7.58	4.98	3.33		
2 3	0.21	1.17	-0.64		
2 4	-8.82	6.99	-2.23		
Wire intersection point coordinates difference between 'RL2 and Intact'					
ROW 1 AND	X DIS	Y DIS	Z DIS		
1 3	-4.26	-0.01	-0.47		
1 4	7.18	5.2	2.92		
2 3	-1.32	-3.47	-0.7		
2 4	-4.1	-6.66	-0.37		

Figure 61: Difference in the displacement of x, y, and z coordinates of the wire intersection points when the results of the specimen tested in case1 (Intact/uninjured) are compared to results of case2 (RL/injured) and case3 (RL2/injured) in the direction of left axial rotation- FSU2

Wire intersection point coordinates difference between 'RL and Intact'			
ROW 1 AND 2	X DIS	Y DIS	Z DIS
1 3	-6.66	-1.71	1.38
1 4	-0.22	-0.37	0.12
2 3	0.66	2.19	-0.2
2 4	-3.18	3.59	-1.31
Wire intersection point coordinates difference between 'RL2 and Intact'			
ROW 1 AND 2	X DIS	Y DIS	Z DIS
1 3	-14.3	-7.54	-1.4
1 4	0.05	-0.09	-0.15
2 3	1.26	-0.87	-0.17
2 4	1.15	-1.95	0.79

Figure 62: Difference in the displacement of x, y, and z coordinates of the wire intersection points when the results of the specimen tested in case1 (Intact/uninjured) are compared to results of case2 (RL/injured) and case3 (RL2/injured) in the direction of right lateral bending – FSU 2

Wire intersection point coordinates difference between 'RL and Intact'			
ROW 1 AND 2	X DIS	Y DIS	Z DIS
1 3	-10.23	-4.97	-1.52
1 4	-11.3	-6.06	-4.43
2 3	1.73	-0.22	-0.55
2 4	-8.35	3.35	-2.77
Wire intersection point coordinates difference between 'RL2 and Intact'			
ROW 1 AND 2	X DIS	Y DIS	Z DIS
1 3	-8.18	-2.88	-1.23
1 4	-0.58	-1.23	0.46
2 3	-0.03	-4.47	-0.48
2 4	1.18	-4.17	1.64

Figure 63: Difference in the displacement of x, y, and z coordinates of the wire intersection points when the results of the specimen tested in case1 (Intact/uninjured) are compared to results of case2 (RL/injured) and case3 (RL2/injured) in the direction of extension – FSU2

Wire intersection point coordinates difference between 'RL and Intact'				
ROW 1 AND 2	X DIS	Y DIS	Z DIS	
1 3	-4.27	-1.07	-0.47	
1 4	-0.73	-0.01	0.16	
2 3	-2.96	2.3	-0.57	
2 4	-2.81	1.72	-0.61	
Wire intersection point coordinates difference between 'RL2 and Intact'				
ROW 1 AND 2	X DIS	Y DIS	Z DIS	
1 3	-6.8	-2.96	-1.22	
1 4	-4.17	-0.99	-0.53	
2 3	-1.25	0.19	-0.39	
2 4	-0.44	-2.66	0.46	

Figure 64: Difference in the displacement of x, y, and z coordinates of the wire intersection points when the results of the specimen tested in case1 (Intact/uninjured) are compared to results of case2 (RL/injured) and case3 (RL2/injured) in the direction of flexion – FSU2

Wire intersection point coordinates difference between 'RL and Intact'				
ROW 1 AND 2	X DIS	Y DIS	Z DIS	
1 3	-29.29	-9.41	-5	
1 4	-0.46	-1.29	1	
2 3	5.35	9.59	-1	
2 4	-17.16	17.43	-6.16	
Wire intersection point coordinates difference between 'RL2 and Intact'				
ROW 1 AND 2	X DIS	Y DIS	Z DIS	
1 3	-20.73	-11.21	-4.71	
1 4	-2.91	0.57	1.04	
2 3	24.91	-28.94	5.46	
2 4	4.84	-13.53	4.96	

Figure 65: Difference in the displacement of x, y, and z coordinates of the wire intersection points when the results of the specimen tested in case1 (Intact/uninjured) are compared to results of case2 (RL/injured) and case3 (RL2/injured) in the direction of compression – FSU2

FSU 3: Wire intersection point coordinates of specimen 3

Wire intersection point coordinates difference between 'RL and Intact'			
ROW 1 AND 2	X DIS	Y DIS	Z DIS
1 3	-0.22	-0.1	-0.23
1 4	-0.79	1.63	1.78
2 3	0.75	-3.01	0.56
2 4	-0.83	0.41	0.45
Wire intersection point coordinates difference between 'RL2 and Intact'			
ROW 1 AND 2	X DIS	Y DIS	Z DIS
1 3	0.18	0.78	-0.09
1 4	-3.3	-0.55	5.39
2 3	-0.32	0.34	-0.43
2 4	-1.17	1.28	-0.09

Figure 66: Difference in the displacement of x, y, and z coordinates of the wire intersection points when the results of the specimen tested in case1 (Intact/uninjured) are compared to results of case2 (RL/injured) and case3 (RL2/injured) in the direction of left axial rotation- FSU3

Wire intersection point coordinates difference between 'RL and Intact'			
ROW 1 AND 2	X DIS	Y DIS	Z DIS
1 3	4.08	5.63	2.01
1 4	2.62	0.69	-5.27
2 3	-0.59	3.28	0.57
2 4	-0.78	1.47	-0.02
Wire intersection point coordinates difference between 'RL2 and Intact'			
ROW 1 AND 2	X DIS	Y DIS	Z DIS
1 3	4.09	5.54	1.62
1 4	0.31	-0.84	-0.09
2 3	-0.08	2.3	0.77
2 4	-1.19	1.9	-0.45

Figure 67: Difference in the displacement of x, y, and z coordinates of the wire intersection points when the results of the specimen tested in case1 (Intact/uninjured) are compared to results of case2 (RL/injured) and case3 (RL2/injured) in the direction of right lateral bending- FSU3

Wire intersection point coordinates difference between 'RL and Intact'					
ROW 1 AND 2	X DIS	Y DIS	Z DIS		
1 3	0.36	-1.45	0.41		
1 4	3.87	-1.29	-3.97		
2 3	1.45	-0.12	0.21		
2 4	-0.38	-0.47	1.96		
Wire intersection point coordinates difference between 'RL2 and Intact'					
ROW 1 AND 2	X DIS	Y DIS	Z DIS		
1 3	-0.92	-1.35	-0.41		
1 4	3.8	1.23	1.34		
2 3	-0.27	0.46	-0.42		
2 4	0.42	2.65	0.46		

Figure 68: Difference in the displacement of x, y, and z coordinates of the wire intersection points when the results of the specimen tested in case1 (Intact/uninjured) are compared to results of case2 (RL/injured) and case3 (RL2/injured) in the direction of extension-FSU3

Wire intersection point coordinates difference between 'RL and Intact'					
ROW 1 AND 2	X DIS	Y DIS	Z DIS		
1 3	2.85	3.89	1.29		
1 4	0.78	-0.1	-1.75		
2 3	-0.56	0.95	0.25		
2 4	-0.36	-0.33	0.08		
Wire intersection point coordinates difference between 'RL2 and Intact'					
ROW 1 AND 2	X DIS	Y DIS	Z DIS		
1 3	2.81	3.37	1.38		
1 4	-0.24	-0.57	0.08		
2 3	-0.22	0.64	0.24		
2 4	-0.42	-0.26	-0.08		

Figure 69 Difference in the displacement of x, y, and z coordinates of the wire intersection points when the results of the specimen tested in case1 (Intact/uninjured) are compared to results of case2 (RL/injured) and case3 (RL2/injured) in the direction of flexion-FSU3

Wire intersection point coordinates difference between 'RL and Intact'			
ROW 1 AND 2	X DIS	Y DIS	Z DIS
1 3	-0.1	-0.01	-0.03
1 4	0.13	-0.07	-0.51
2 3	0.03	-0.04	-0.01
2 4	0.09	-0.35	-0.02

Wire intersection point coordinates difference between 'RL2 and Intact'			
ROW 1 AND 2	X DIS	Y DIS	Z DIS
1 3	-0.16	-0.01	-0.11
1 4	0.04	-0.26	-0.16
2 3	0.58	-0.57	0.09
2 4	0.07	-0.19	-0.16

Figure 70: Difference in the displacement of x, y, and z coordinates of the wire intersection points when the results of the specimen tested in case1 (Intact/uninjured) are compared to results of case2 (RL/injured) and case3 (RL2/injured) in the direction of flexion + rotation-FSU3

Wire intersection point coordinates difference between 'RL and Intact'			
ROW 1 AND 2	X DIS	Y DIS	Z DIS
1 3	-1.61	-0.72	0.83
1 4	5.66	6.05	-12.92
2 3	-1.7	0.9	0.25
2 4	0.62	-6.49	2.92

Wire intersection point coordinates difference between 'RL2 and Intact'			
ROW 1 AND 2	X DIS	Y DIS	Z DIS
1 3	-2.23	-1	0.5
1 4	-1.73	-4.56	0.75
2 3	-0.22	-2	0
2 4	-1.13	0.7	0.67

Figure 71: Difference in the displacement of x, y, and z coordinates of the wire intersection points when the results of the specimen tested in case1 (Intact/uninjured) are compared to results of case2 (RL/injured) and case3 (RL2/injured) in the direction of compression-FSU3

10.2 Appendix B

Stiffness and hysteresis loss ratio values of the FSUs:

	A	B	C	D
1	Stiffness values			
2	Left Axial Rotation (Nm/deg)	Intact	Injured-RL	Injured - RL2
3	FSU 1:	0.25	0.238	0.26
4	FSU 2:	0.089	0.581	0.571
5	FSU 3:	0.42	0.826	0.74
6	FSU 4:	0.331	0.307	0.35
7				
8	Mean:	0.2725	0.488	0.48025
9	Standard Deviation:	0.1406615	0.2696628	0.2169337
10				
11	Right lateral bending (Nm/deg)	Intact	Injured-RL	Injured - RL2
12	FSU 1:	0.375	0.049	0.167
13	FSU 2:	0.4	0.599	0.535
14	FSU 3:	0.373	0.305	0.294
15	FSU 4:	0.194	0.128	0.158
16				
17	Mean:	0.3355	0.27025	0.2885
18	Standard deviation:	0.0951297	0.2439062	0.1756749
19				
20	Extension (Nm/deg)	Intact	Injured-RL	Injured - RL2
21	FSU 1:	0.339	0.585	0.364
22	FSU 2:	7.83	10.31	9.674
23	FSU 3:	4.49	4.532	6.024
24	FSU 4:	0.43	0.492	0.691
25				
26	Mean:	3.27225	3.97975	4.18825
27	Standard deviation:	3.6026999	4.6211749	4.4840115

28				
29	Flexion (Nm/deg)	Intact	Injured-RL	Injured - RL2
30	FSU 1:	0.356	0.235	0.363
31	FSU 2:	0.475	0.397	0.491
32	FSU 3:	0	0.49	0.436
33	FSU 4:	0.348	0.139	0.317
34				
35	Mean:	0.29475	0.31525	0.40175
36	Standard deviation:	0.2049022	0.1578235	0.0770773
37				
38	Compression (N/mm)	Intact	Injured-RL	Injured - RL2
39	FSU 1:	771.51	2228.96	2081.69
40	FSU 2:	3358.97	3577.92	3069.72
41	FSU 3:	3024.41	3045.75	3100
42	FSU 4:	2463.33	2864.12	3368.38
43				
44	Mean:	2404.555	2929.1875	2904.9475
45	Standard deviation:	1149.6983	556.47492	565.0127

47	Hysteresis loss ratio			
48	Left axial rotaion	Intact	Injured-RL	Injured - RL2
49	FSU 1	1.3435	0.1745	0.2362
50	FSU 2	0.123	0.3878	0.312
51	FSU 3	0.1505	0.2246	0.2076
52	FSU 4	0.194	0.1386	0.161
53				
54	Mean of hysteresis loss ratio:	0.45275	0.231375	0.2292
55	Standard deviation:	0.5945523	0.1100858	0.0633052
56				
57	Right lateral bending	Intact	Injured-RL	Injured - RL2
58	FSU 1	0.535	1.2602	1.5684
59	FSU 2	0.28	0.281	0.336
60	FSU 3	0.428	0.7872	1.4065
61	FSU 4	0.372	0.454	0.613
62	Hysteresis loss ratoi mean:	0.40375	0.6956	0.980975
63	Standard deviation:	0.106672	0.4310559	0.5993157
64				
65	Extension:	Intact	Injured-RL	Injured - RL2
66	FSU 1	0.0841	0.413	0.3211
67	FSU 2	0.234	0.224	0.197
68	FSU 3	0.099	0.089	0.155
69	FSU 4	0.4382	0.4779	0.4654
70	Hysteresis loss ratio mean:	0.213825	0.300975	0.284625
71	Standard deviation:	0.1640778	0.1776801	0.1396314

73	Flexion:	Intact	Injured-RL	Injured - RL2
74	FSU 1	0.31	0.8126	0.356
75	FSU 2	0.4	0.5199	0.3355
76	FSU 3	0.269	0.275	0.387
77	FSU 4	0.307	0.031	0.24
78	Hysteresis loss ratio mean:	0.3215	0.409625	0.329625
79	Standard deviatoin	0.0555608	0.3346791	0.0633895
80				
81	Compression:	Intact	Injured-RL	Injured - RL2
82	FSU 1	0.192	0.177	0.185
83	FSU 2	0.185	0.175	0.187
84	FSU 3	0.173	0.174	0.175
85	FSU 4	0.205	0.199	0.198
86	Hysteresis loss ratio mean:	0.18875	0.18125	0.18625
87	Standard deviation:	0.013376	0.0118989	0.0094296

10.3 Appendix C

FSU 2: Results of specimen 2

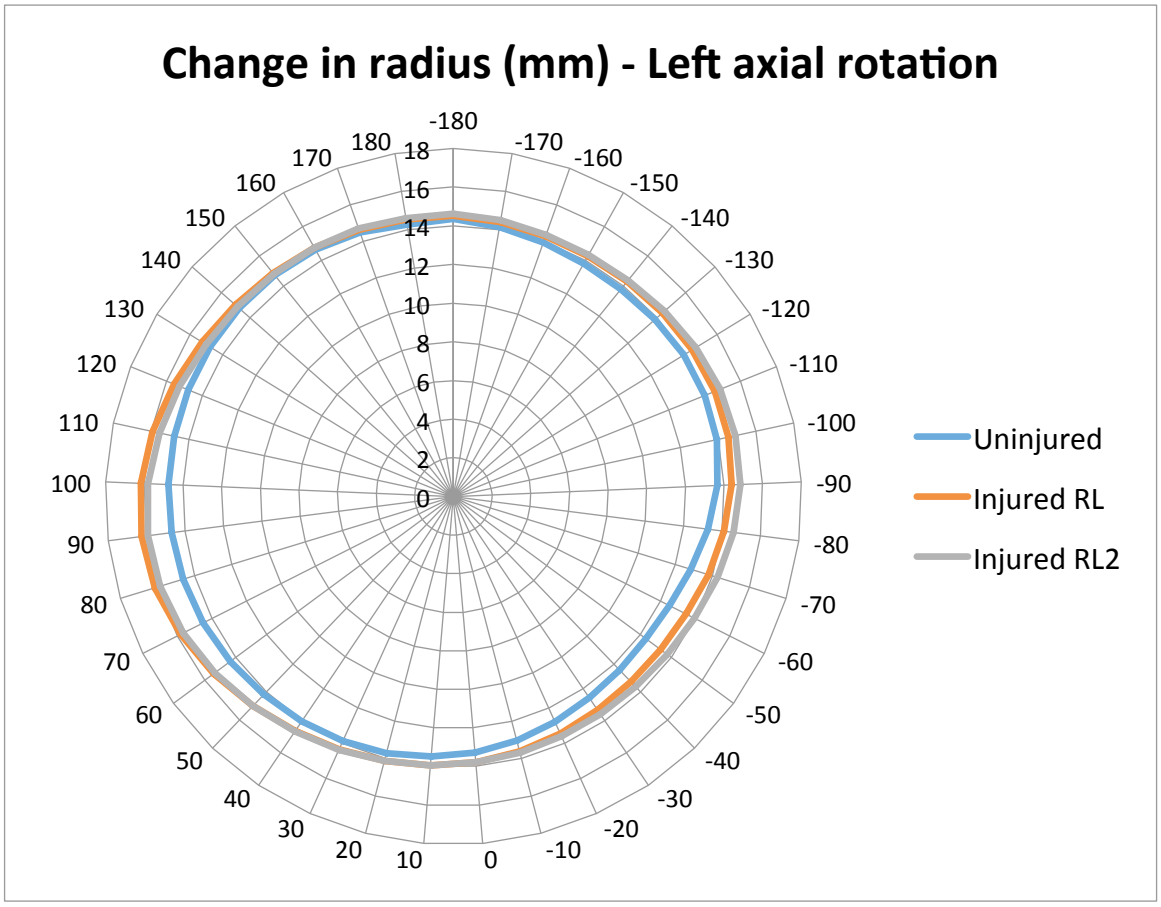

Figure 72: Disc periphery of the specimen in the direction of left axial rotation for different test conditions (Uninjured represents case 1, injury 1 represents case 2, injury 2 represents case 3)-FSU2

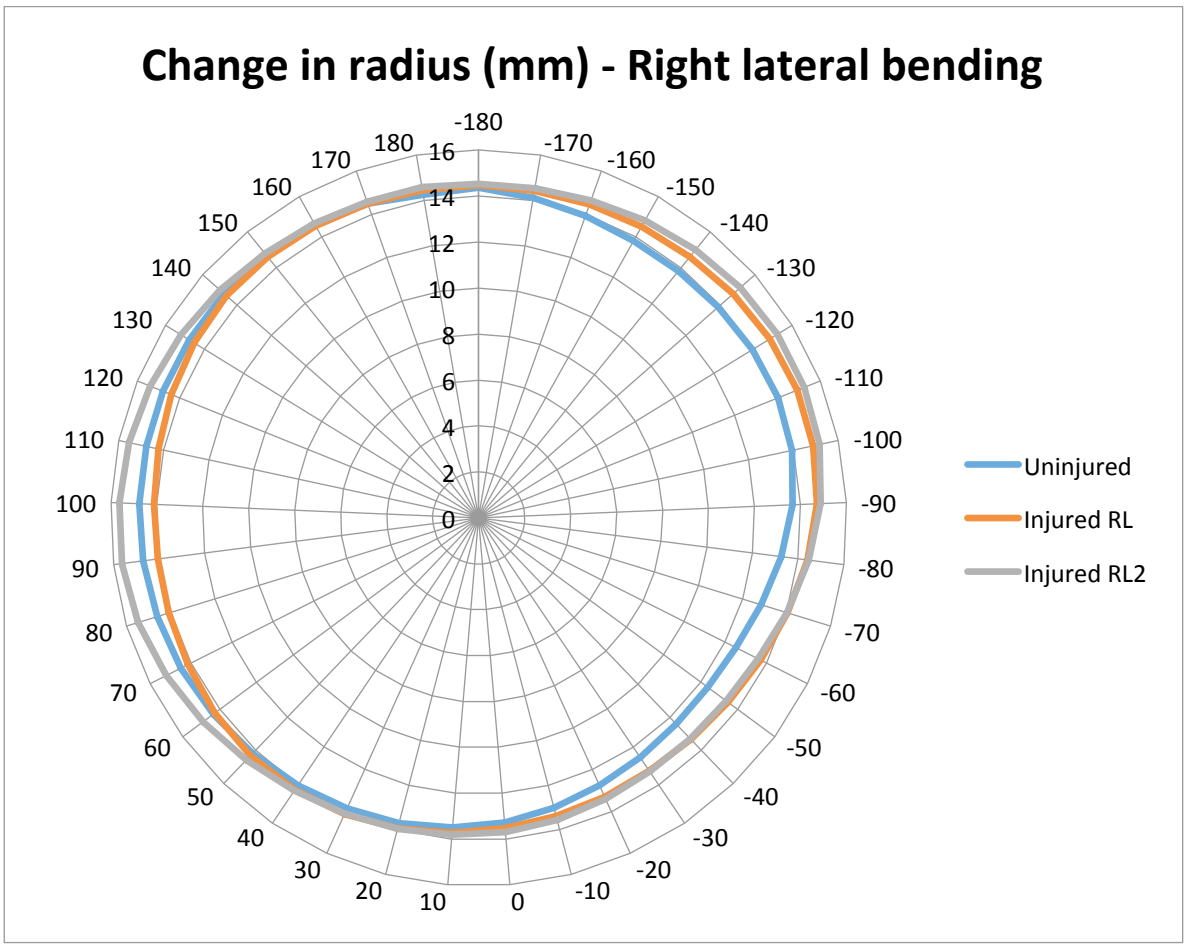

Figure 73: Disc periphery of the specimen in the direction of right lateral bending for different test conditions (Uninjured represents case 1, injury 1 represents case 2, injury 2 represents case 3)-FSU2

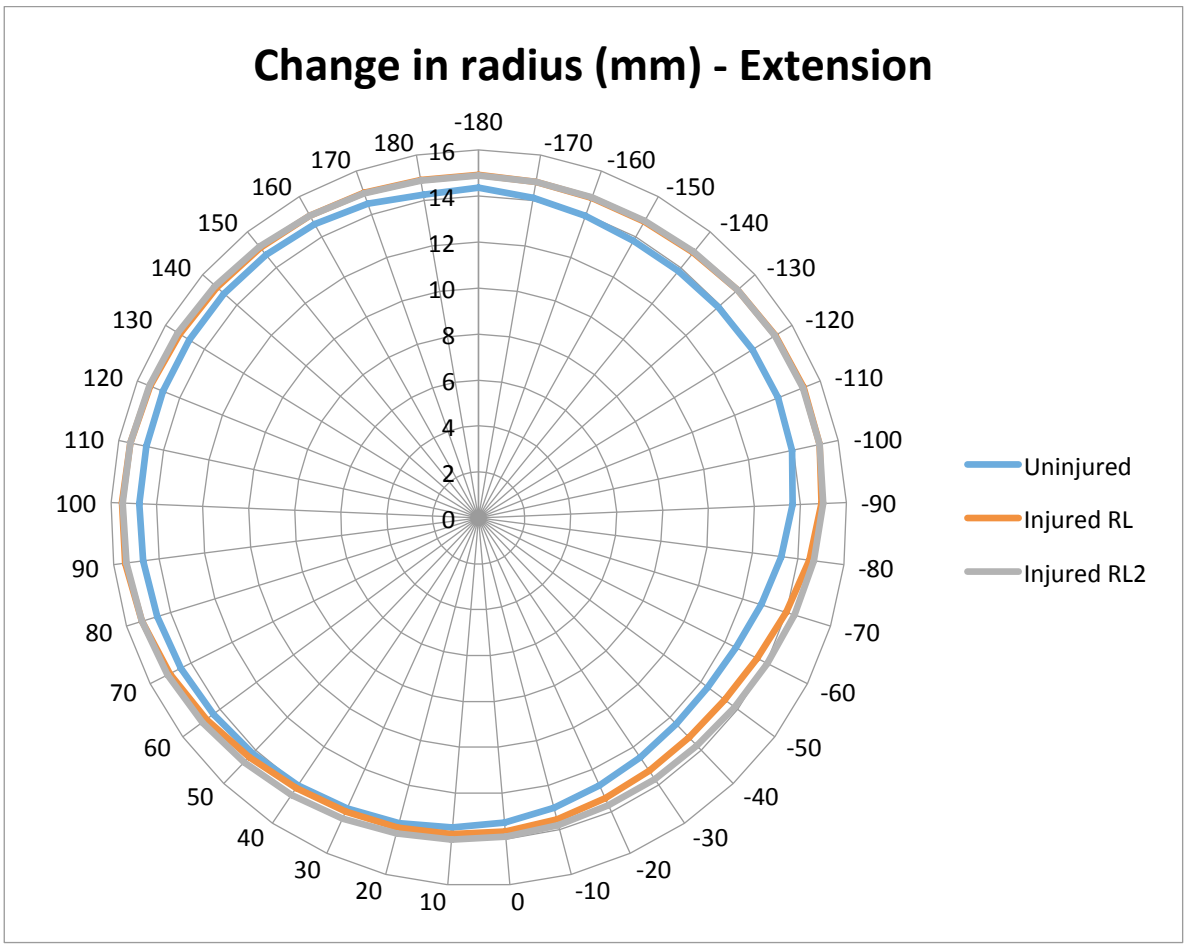

Figure 74: Disc periphery of the specimen in the direction of extension for different test conditions. Uninjured represents case 1, injury 1 represents case 2, injury 2 represents case 3-FSU2

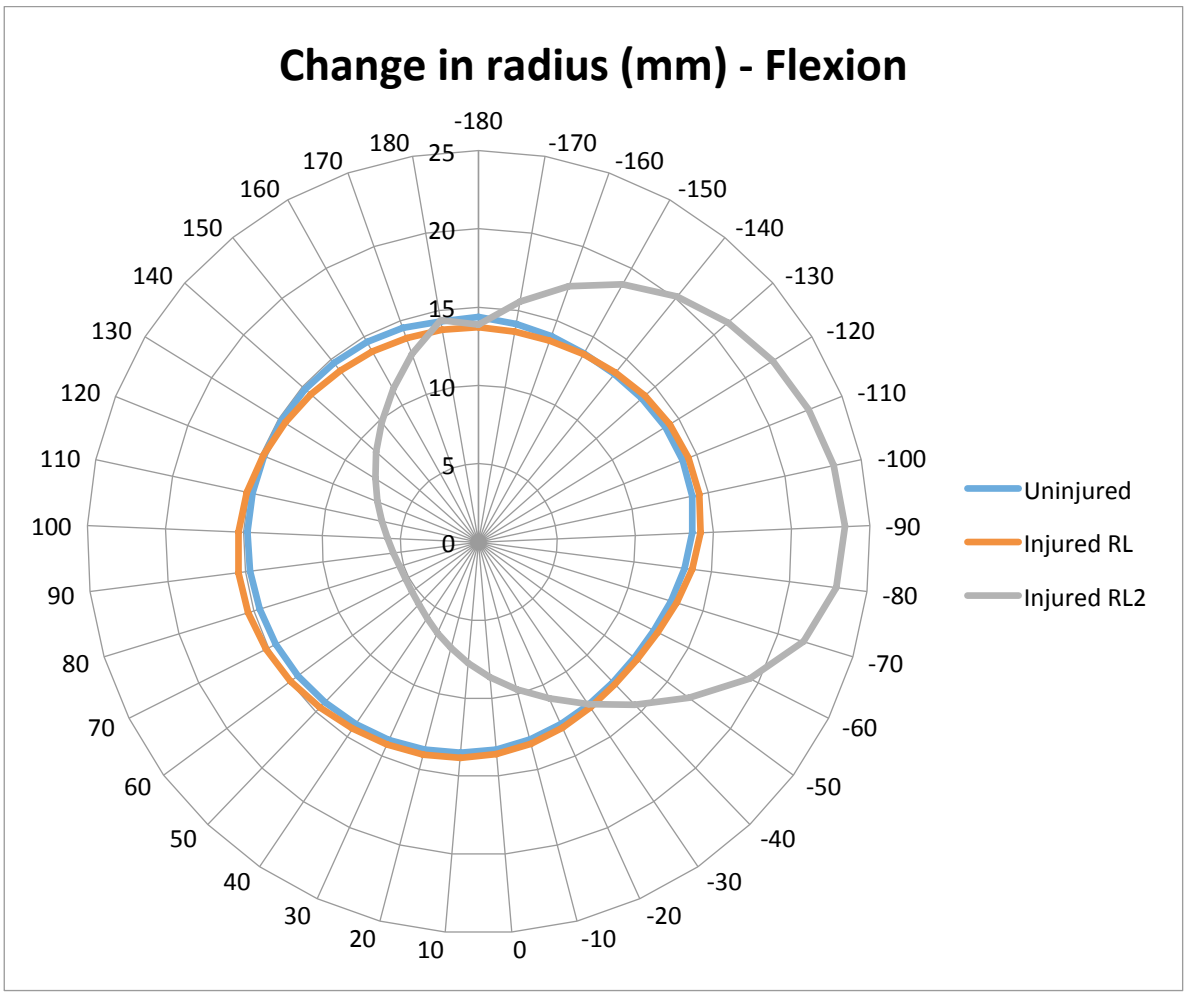

Figure 75: Disc periphery of the specimen in the direction of flexion for different test conditions (Uninjured represents case 1, injury 1 represents case 2, injury 2 represents case 3-FSU2

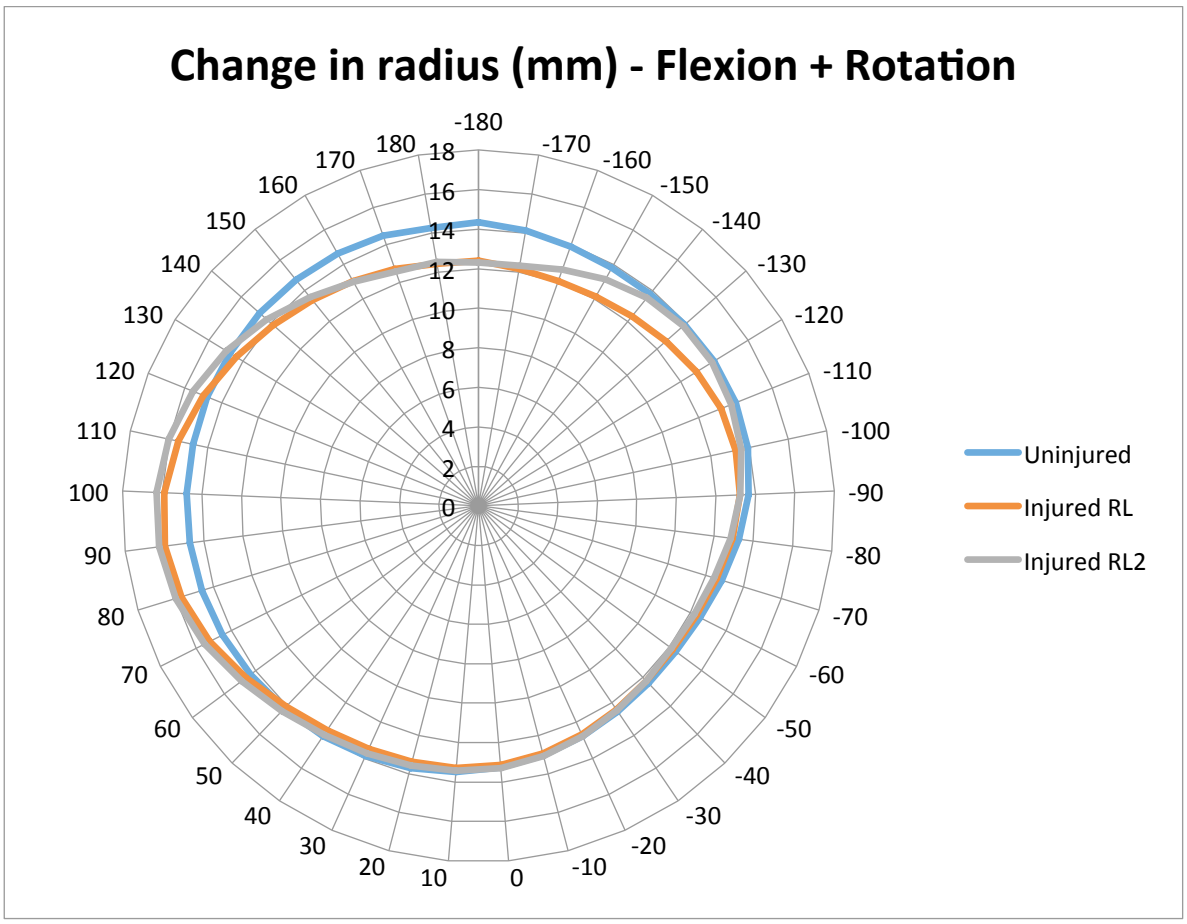

Figure 76: Disc periphery of the specimen in the direction of flexion + rotation for different test conditions (Uninjured represents case 1, injury 1 represents case 2, injury 2 represents case 3)-FSU2

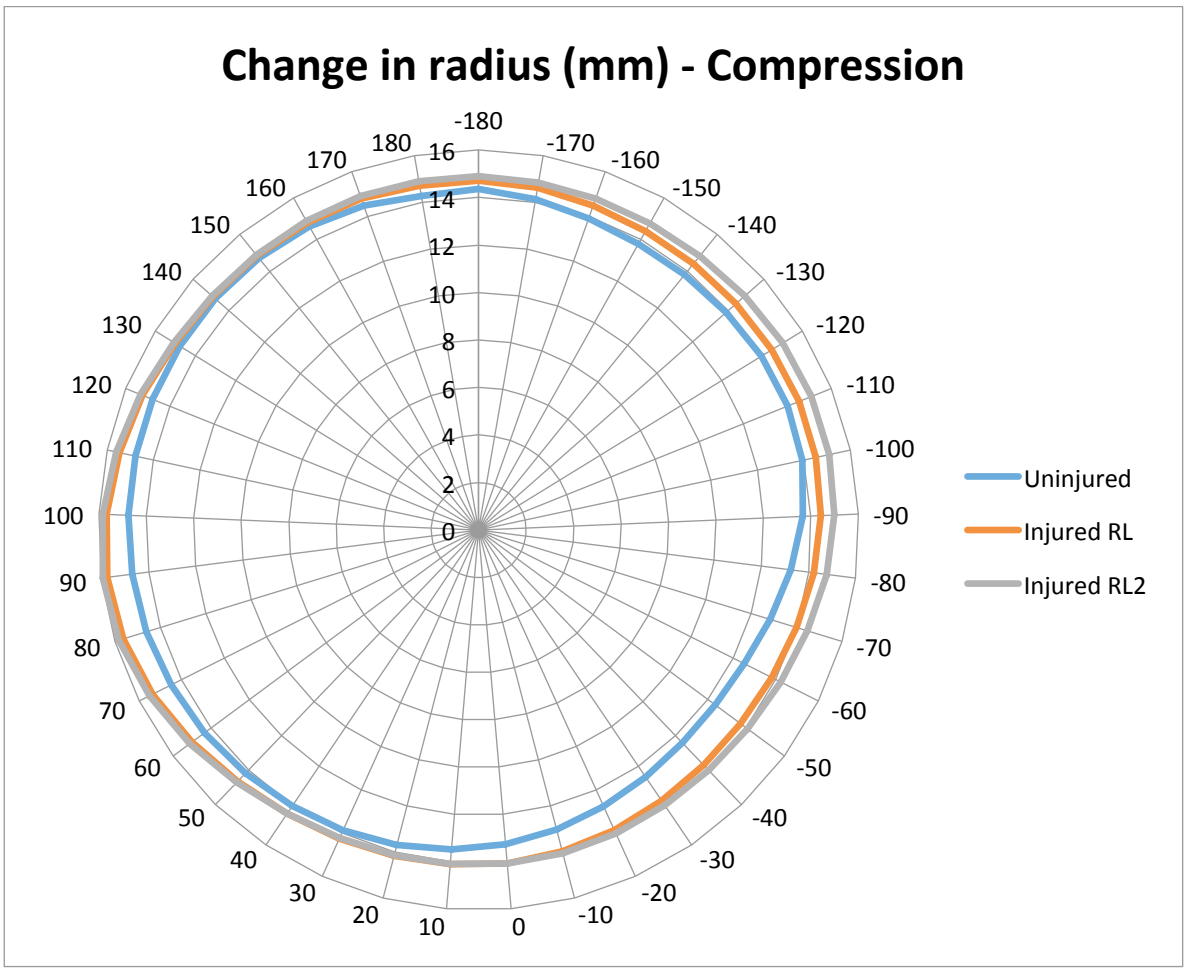

Figure 77: Disc periphery of the specimen in the direction of compression for different test conditions (Uninjured represents case 1, injury 1 represents case 2, injury 2 represents case 3)-FSU2

FSU 3: Results of specimen 3

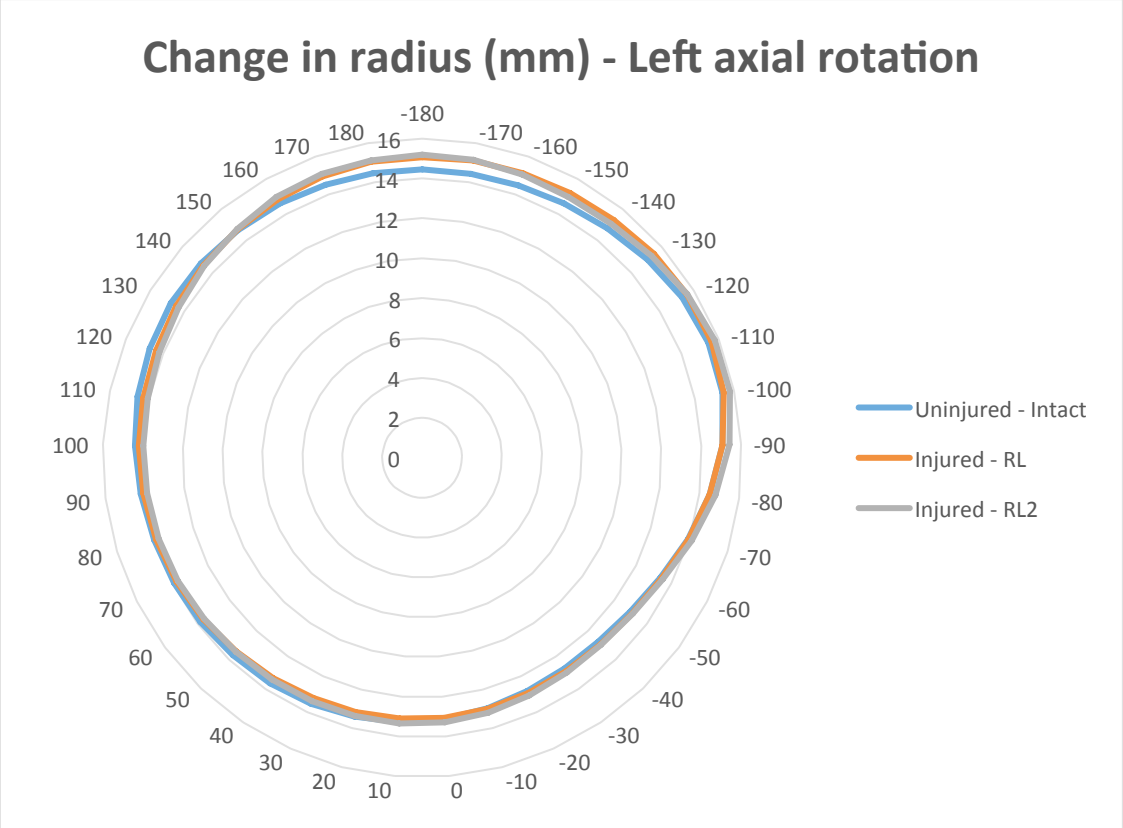

Figure 78: Disc periphery of the specimen in the direction of left axial rotation for different test conditions (Uninjured represents case 1, injury 1 represents case 2, injury 2 represents case 3)-FSU3

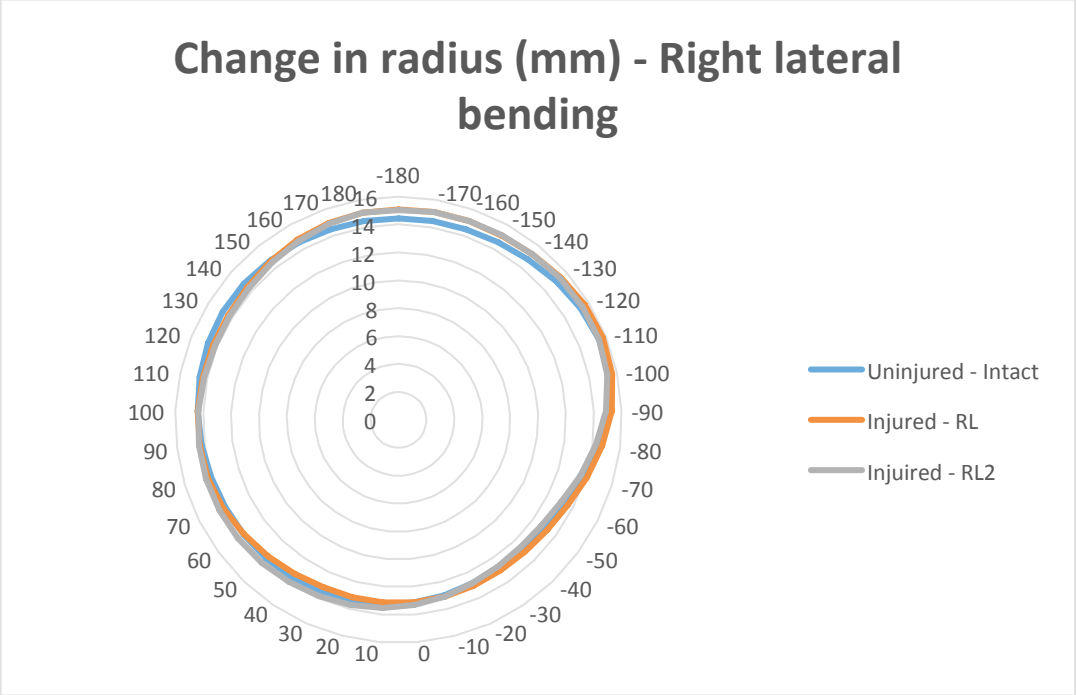

Figure 79: Disc periphery of the specimen in the direction of right lateral bending for different test conditions (Uninjured represents case 1, injury 1 represents case 2, injury 2 represents case 3)-FSU3

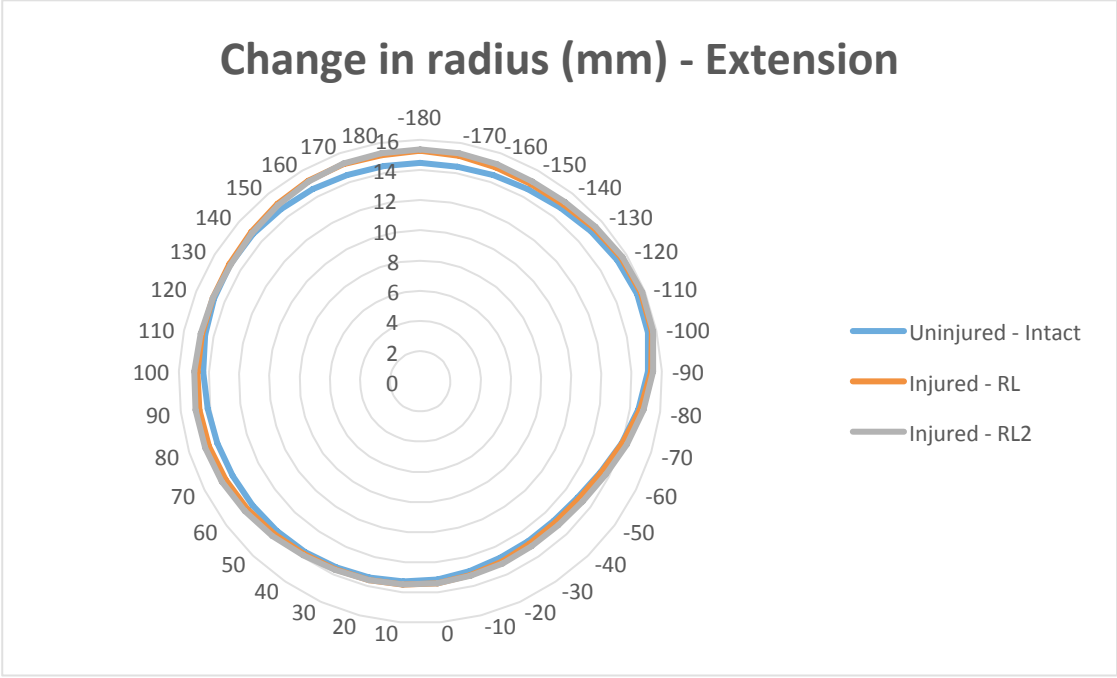

Figure 80: FSU 3 Disc periphery of the specimen in the direction of extension for different test conditions. Uninjured represents case 1, injury 1 represents case 2, injury 2 represents case 3

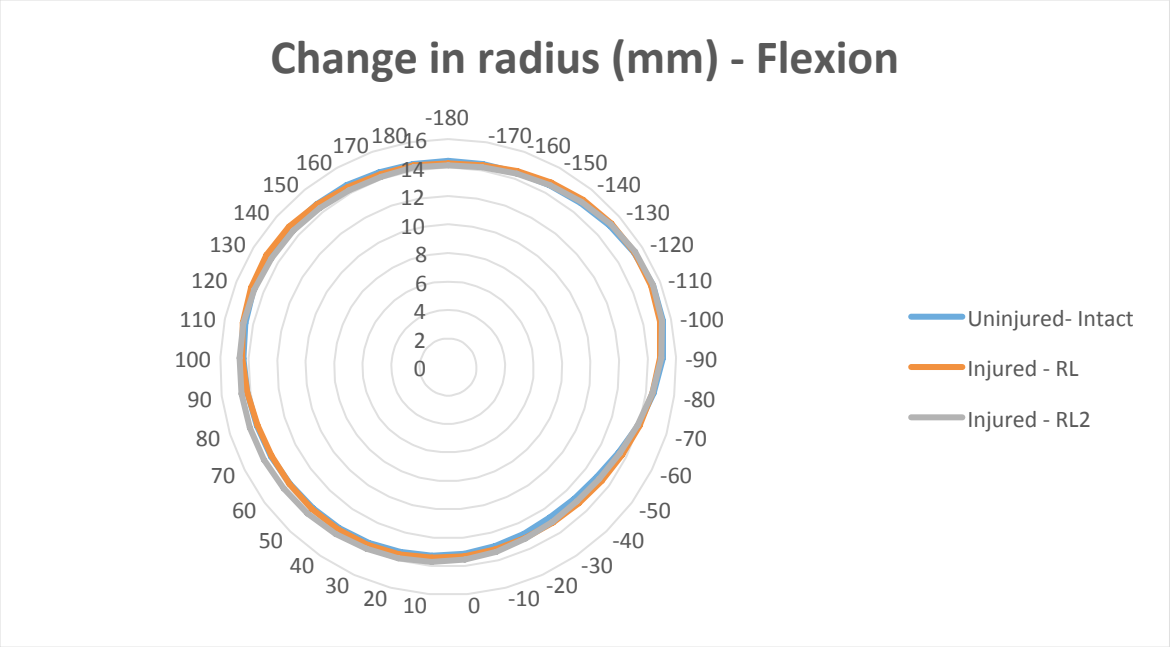

Figure 81: Disc periphery of the specimen in the direction of flexion for different test conditions (Uninjured represents case 1, injury 1 represents case 2, injury 2 represents case 3)-FSU3

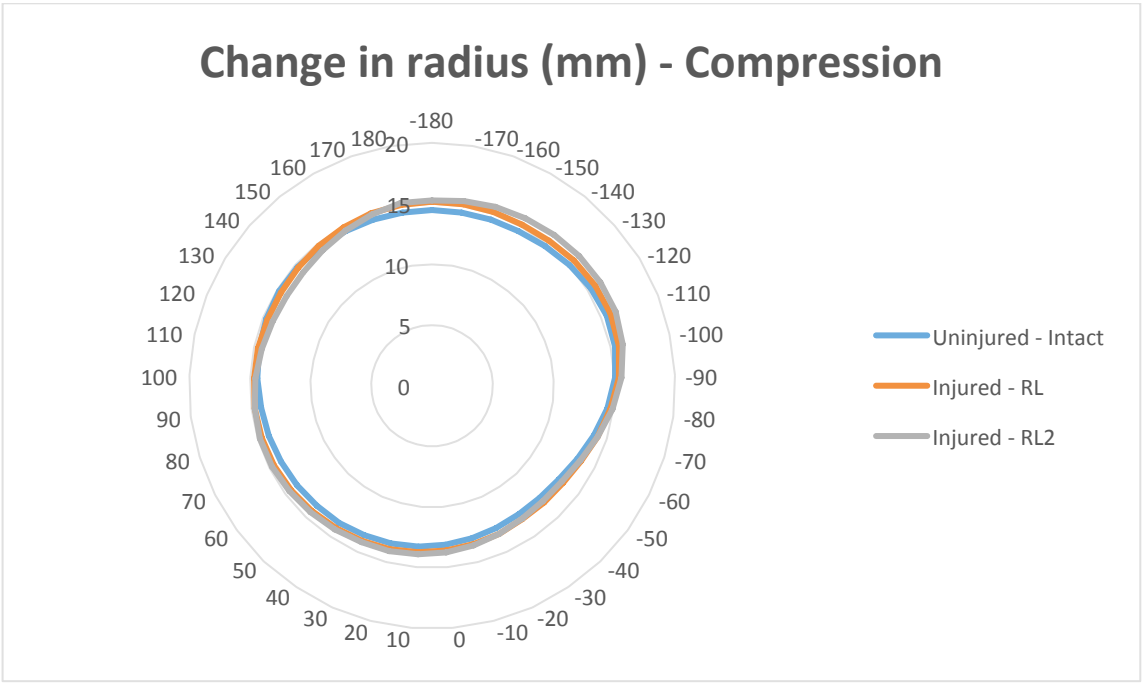

Figure 82: FSU 3 Disc periphery of the specimen in the direction of compression for different test conditions (Uninjured represents case 1, injury 1 represents case 2, injury 2 represents case 3)

FSU 4: Results of specimen 4

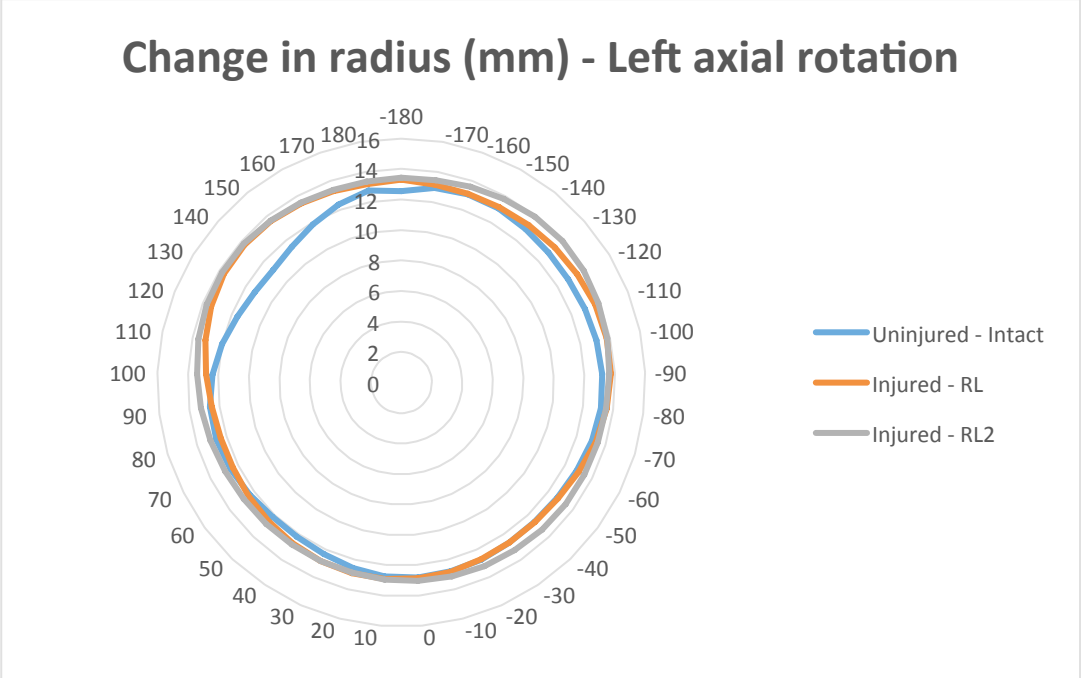

Figure 83: Disc periphery of the specimen in the direction of left axial rotation for different test conditions (Uninjured represents case 1, injury 1 represents case 2, injury 2 represents case 3)-FSU4

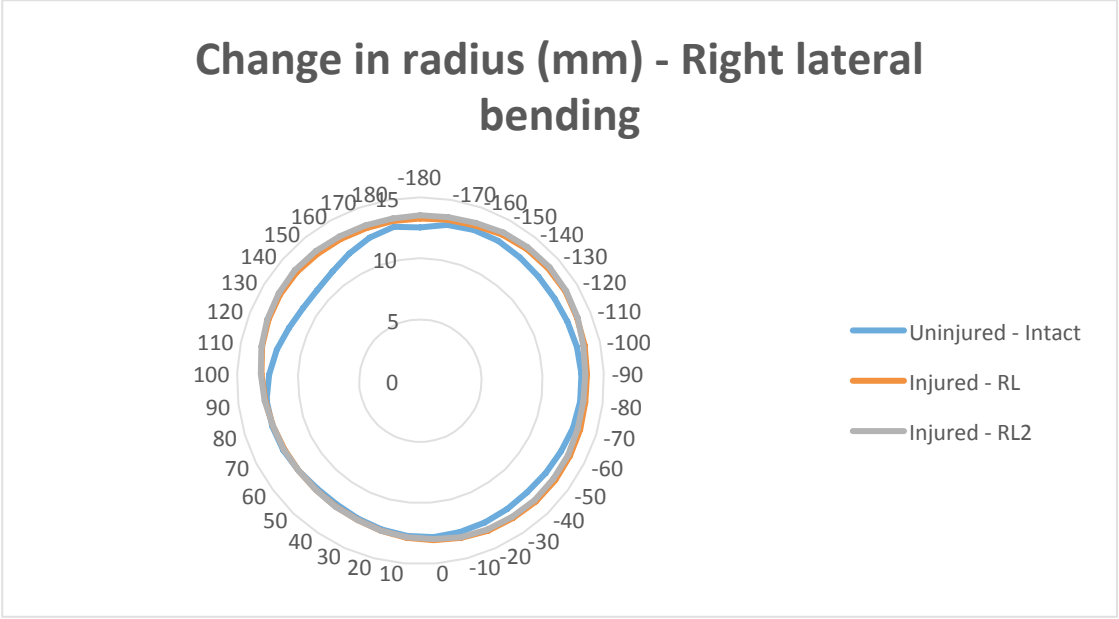

Figure 84: Disc periphery of the specimen in the direction of right lateral bending for different test conditions (Uninjured represents case 1, injury 1 represents case 2, injury 2 represents case 3)-FSU4

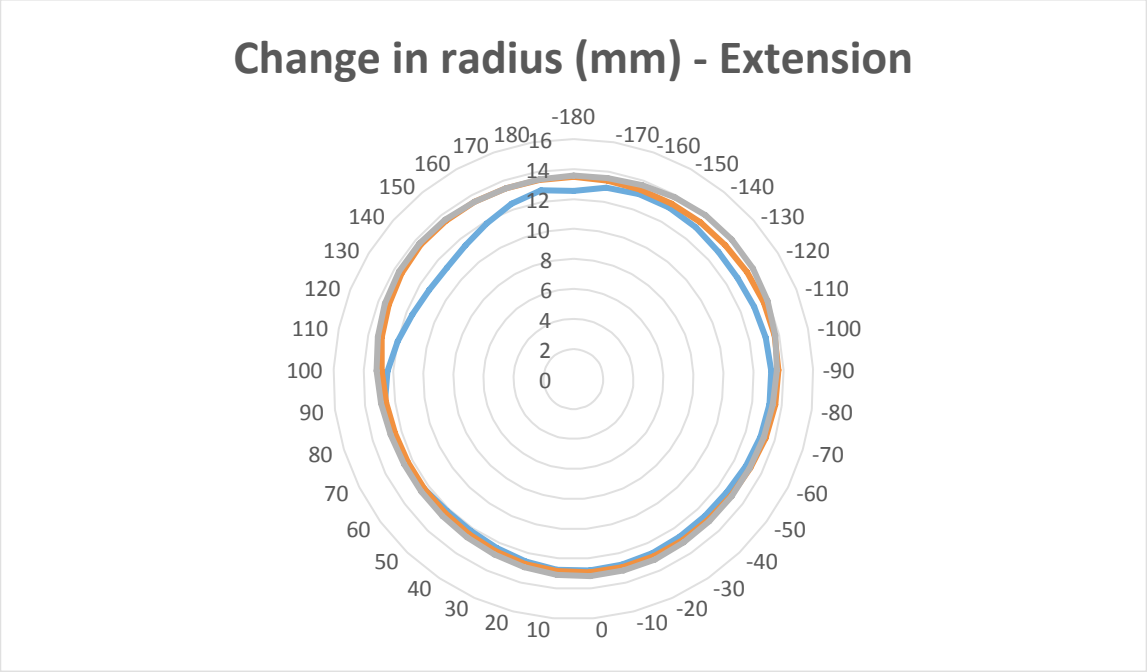

Figure 85: Disc periphery of the specimen in the direction of extension for different test conditions. Uninjured represents case 1, injury 1 represents case 2, injury 2 represents case 3-FSU4

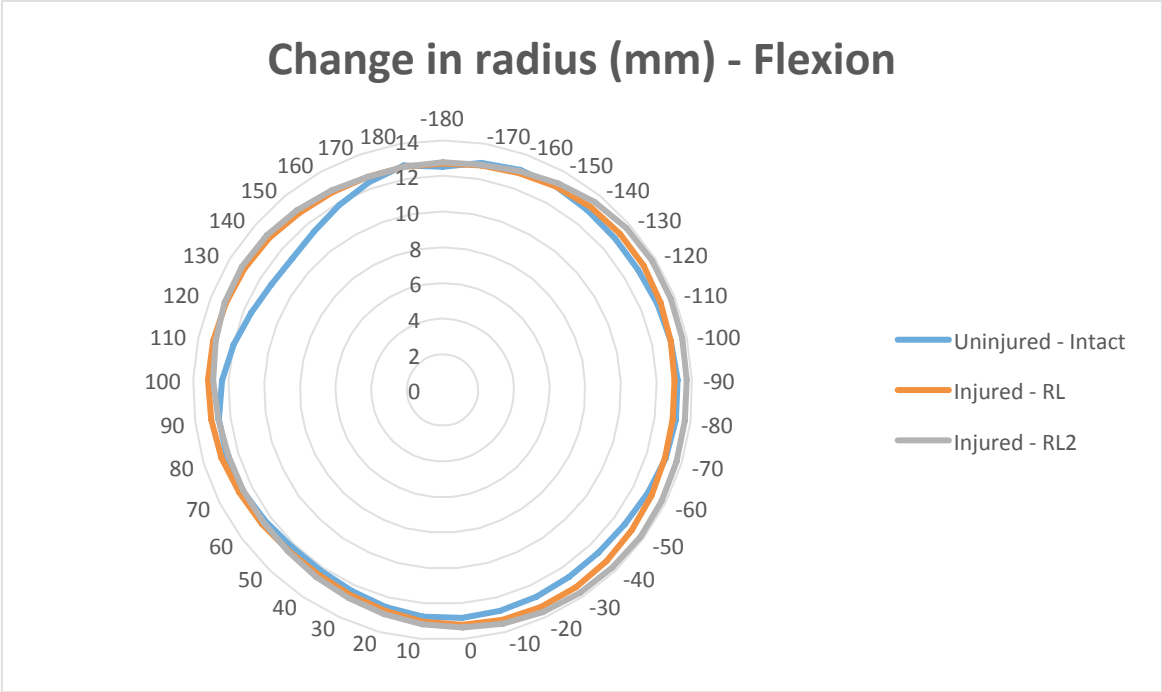

Figure 86: Disc periphery of the specimen in the direction of flexion for different test conditions (Uninjured represents case 1, injury 1 represents case 2, injury 2 represents case 3-FSU4

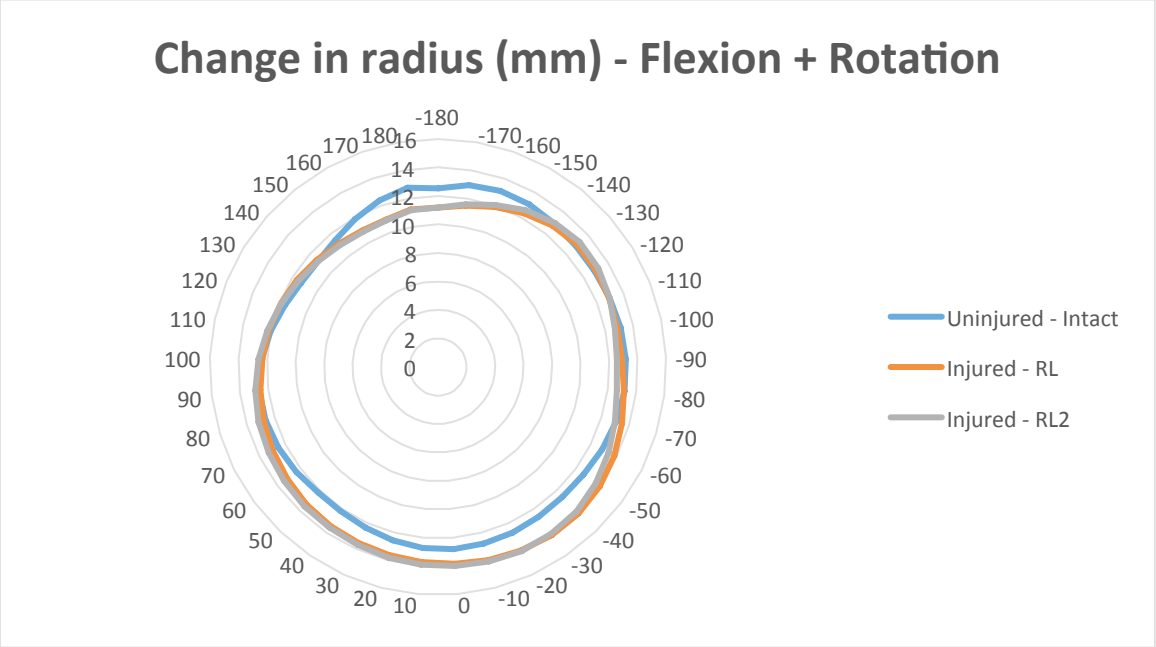

Figure 87: Disc periphery of the specimen in the direction of flexion + rotation for different test conditions (Uninjured represents case 1, injury 1 represents case 2, injury 2 represents case 3)-FSU4

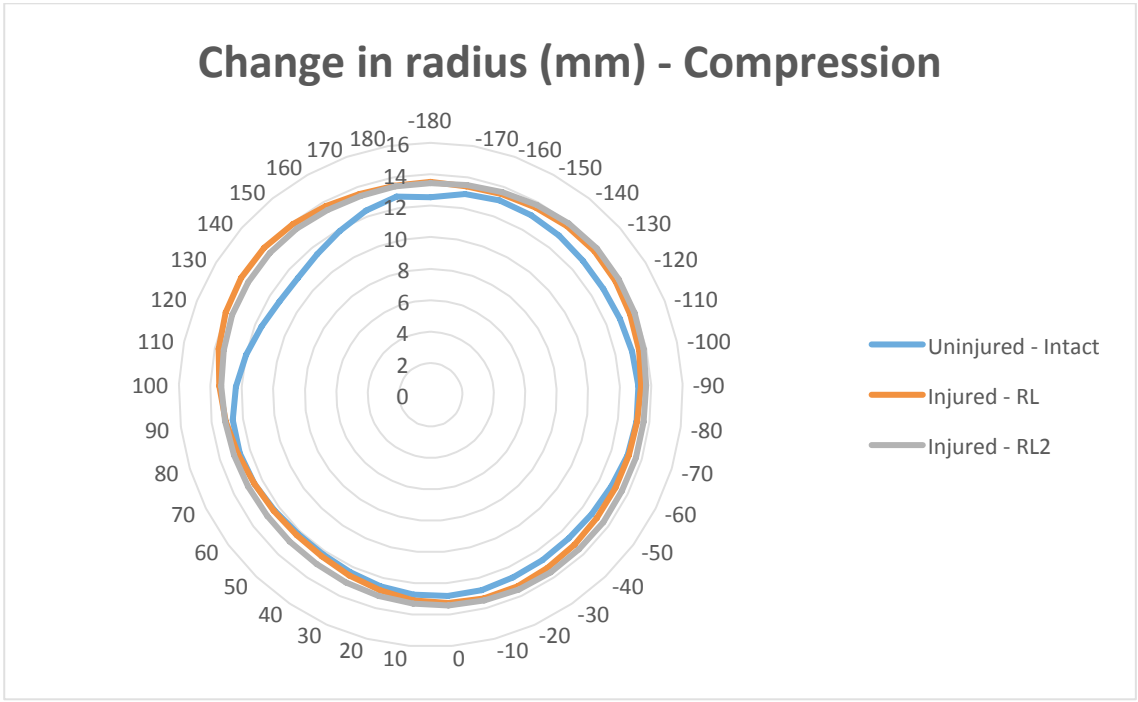

Figure 88: Disc periphery of the specimen in the direction of compression for different test conditions (Uninjured represents case 1, injury 1 represents case 2, injury 2 represents case 3)-FSU4

FSU 1	
After performing left axial rotation	Mean value of Change in radial starin of the disc when compared with radial strain in neutral position
Case 1	0.00221
Case 2	0.00654
Case 3	0.00032
After performing right lateral bending	Mean value of Change in radial starin of the disc when compared with radial strain in neutral position
Case 1	0.00207
Case 2	0.00367
Case 3	0.00246
After performing extension	Mean value of Change in radial starin of the disc when compared with radial strain in neutral position
Case 1	0.01602
Case 2	0.00235
Case 3	0.00178
After performing flexion	Mean value of Change in radial starin of the disc when compared with radial strain in neutral position
Case 1	0.00018
Case 2	0.00156
Case 3	0.00105
After performing flexion+rotation	Mean value of Change in radial starin of the disc when compared with radial strain in neutral position
Case 1	0.00033
Case 2	0.00076
Case 3	0.00017
Afetr performing compression	Mean value of Change in radial starin of the disc when compared with radial strain in neutral position
Case 1	0.03572
Case 2	0.02527
Case 3	0.04292

Figure 89: Showing results of FSU1 mean value of change in radial strain of the disc in three test cases after each DOF

FSU 2	
After performing left axial rotation	Mean value of Change in radial starin of the disc when compared with radial strain in neutral position
Case 1	0.00774
Case 2	0.01067
Case 3	0.00306
After performing right lateral bending	Mean value of Change in radial starin of the disc when compared with radial strain in neutral position
Case 1	0.00166
Case 2	0.00044
Case 3	0.00077
After performing extension	Mean value of Change in radial starin of the disc when compared with radial strain in neutral position
Case 1	0.01753
Case 2	0.01177
Case 3	0.00672
After performing flexion	Mean value of Change in radial starin of the disc when compared with radial strain in neutral position
Case 1	0.0027
Case 2	0.00301
Case 3	0.0226
After performing flexion+rotation	Mean value of Change in radial starin of the disc when compared with radial strain in neutral position
Case 1	0.00262
Case 2	0.00465
Case 3	0.00467
Afetr performing compression	Mean value of Change in radial starin of the disc when compared with radial strain in neutral position
Case 1	0.09045
Case 2	0.03841
Case 3	0.02983

Figure 90: Showing results of FSU2 mean value of change in radial strain of the disc in three test cases after each DOF

FSU 3	
After performing left axial rotation	Mean value of Change in radial starin of the disc when compared with radial strain in neutral position
Case 1	0.00621
Case 2	0.00848
Case 3	0.00596
After performing right lateral bending	Mean value of Change in radial starin of the disc when compared with radial strain in neutral position
Case 1	0.00254
Case 2	0.00732
Case 3	0.0039
After performing extension	Mean value of Change in radial starin of the disc when compared with radial strain in neutral position
Case 1	0.0027
Case 2	0.01772
Case 3	0.00558
After performing flexion	Mean value of Change in radial starin of the disc when compared with radial strain in neutral position
Case 1	0.00368
Case 2	0.00385
Case 3	0.00212
After performing flexion+rotation	Mean value of Change in radial starin of the disc when compared with radial strain in neutral position
Case 1	
Case 2	0.0028
Case 3	0.01137
Afetr performing compression	Mean value of Change in radial starin of the disc when compared with radial strain in neutral position
Case 1	0.03072
Case 2	0.03072
Case 3	0.02471

Figure 91: Showing results of FSU3 mean value of change in radial strain of the disc in three test cases after each DOF

FSU 4	
After performing left axial rotation	Mean value of Change in radial starin of the disc when compared with radial strain in neutral position
Case 1	0.00483
Case 2	0.00027
Case 3	0.00361
After performing right lateral bending	Mean value of Change in radial starin of the disc when compared with radial strain in neutral position
Case 1	0.00485
Case 2	0.00438
Case 3	0.00037
After performing extension	Mean value of Change in radial starin of the disc when compared with radial strain in neutral position
Case 1	0.01614
Case 2	0.00159
Case 3	0.00085
After performing flexion	Mean value of Change in radial starin of the disc when compared with radial strain in neutral position
Case 1	0.00347
Case 2	0.00159
Case 3	0.00178
After performing flexion+rotation	Mean value of Change in radial starin of the disc when compared with radial strain in neutral position
Case 1	0.00051
Case 2	0.00181
Case 3	0.00294
Afetr performing compression	Mean value of Change in radial starin of the disc when compared with radial strain in neutral position
Case 1	0.08914
Case 2	0.02946
Case 3	0.02121

Figure 92: Showing results of FSU4 mean value of change in radial strain of the disc in three test cases after each DOF

After performing left axial rotation	Average Value of the change in radial strain of the disc when compared with disc radial strain in neutral position
Case 1	0.0052475
Case 2	0.00649
Case 3	0.0032375

After performing right lateral bending	Average Value of the change in radial strain of the disc when compared with disc radial strain in neutral position
Case 1	0.00278
Case 2	0.0039525
Case 3	0.001875

After performing extension	Average Value of the change in radial strain of the disc when compared with disc radial strain in neutral position
Case 1	0.0130975
Case 2	0.0083575
Case 3	0.0037325

After performing flexion	Average Value of the change in radial strain of the disc when compared with disc radial strain in neutral position
Case 1	0.0025075
Case 2	0.0025025
Case 3	0.0068875

After performing flexion+rotation	Average Value of the change in radial strain of the disc when compared with disc radial strain in neutral position
Case 1	0.001153333
Case 2	0.002505
Case 3	0.0047875

Afetr performing compression	Average Value of the change in radial strain of the disc when compared with disc radial strain in neutral position
Case 1	0.0615075
Case 2	0.030965
Case 3	0.0296675

Figure 93: Showing the average value of the change in radial strain of all the specimens in three testing cases in 6DOF

10.4 Appendix D

DLT Method for the 3D Reconstruction a Point on an Image:

DLT (Direct Linear Transformation) method is an old method that is usually applied using the image coordinates to calculate the space points. This method is established on the corresponding points that can be seen with the help using two or more cameras. This calculation depends on the availability of 3D point's coordinates in space. Using the area coordinates, we can find out the values of coefficients of transformation. These coefficients of transformation are named as DLT coefficients. With the help of using these coordinates, we can find out the space coordinates of an arbitrary point, which can be seen in the regulated space. The first step of this procedure involves the regulated space. From every camera view, we have to register the coordinates of the area. The parameters are used as the input to find out the DLT coefficients. The help of DLT transformation coefficients can calculate the space coordinates.

There are 2 of the most serious registrations of the area coordinates present during this process:

First critical registration is at the time of the space calibration

Second critical registration is at the time of input from the calculation of the space coordinates

These registrations are critically important, and they must be dealt with maximum precision.

Saving the image with the help of camera is just like mapping an object point O, which is present in the object space on the image point "I" in the plane of the film (Figure 94) (Kwon3d.com, 2017).

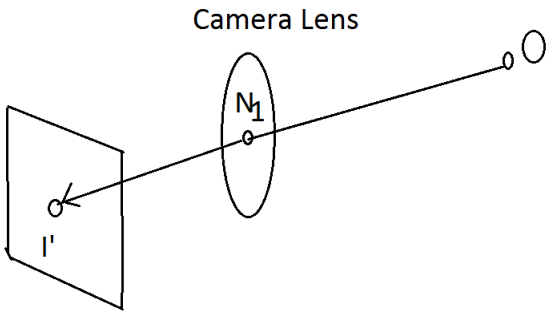

Figure 94: Projecting image onto camera lens (Kwon3d.com, 2017)

To save the image digitally, the recorded image must be projected again on the image I present in the projection plane. (Figure 95)

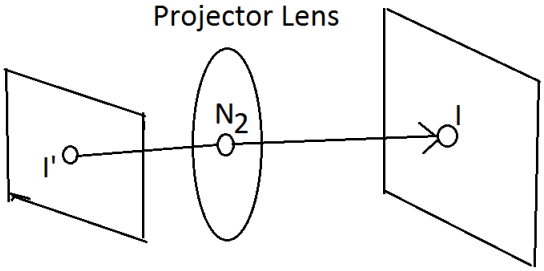

Figure 95: Recorded image projected back in projection plane (Kwon3d.com, 2017)

For the purpose to keep things simple. It is conceivable that we can relate the projected image and the present object directly. (Figure 96)

The object O can be directly mapped into the projected image. The plane that projects are known as the image plane. Point N is the centre of the projection or can also be seen as a new node.

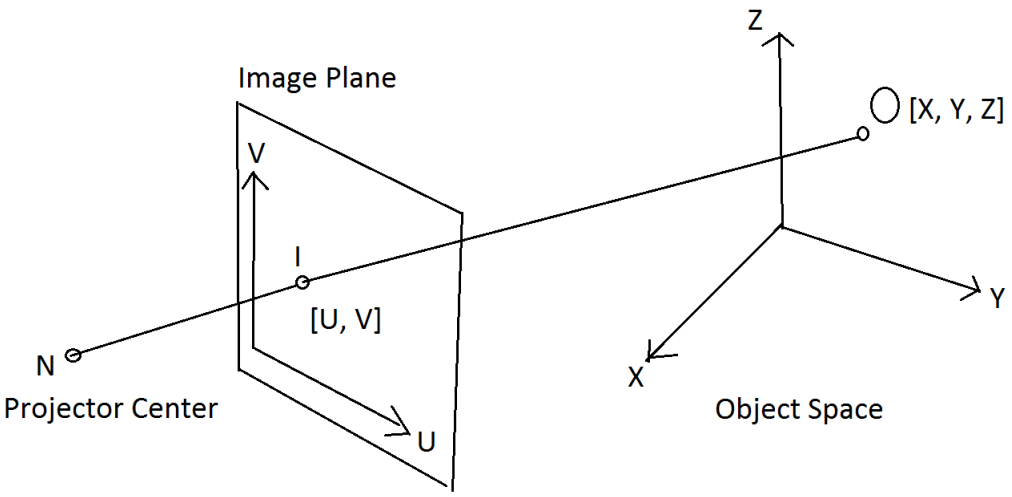

Figure 96: Mapping the projected image

Now let's consider that the location of the center of the projection present in object space reference frame to become [A0, B0, C0] (Figure 97). The vector that is constructed from N to the point O then transforms into [A-A0, B-B0, C-C0].

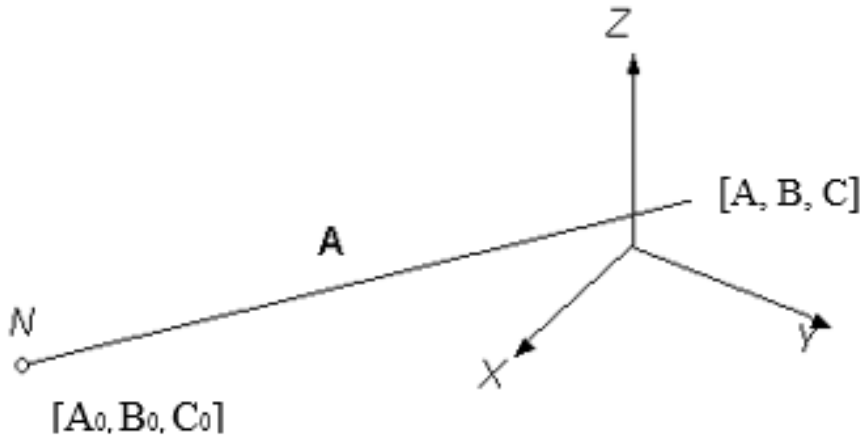

Figure 97: Identifying the coordinates of the mapping points in 3D

W axis was added to the reference frame just like the third axis so that the image plane becomes 3-dimensional.

The algorithm in 3D DLT:

To convert the 2D DLT algorithm in to 3D DLT algorithm ("ISB Software Resources - Movement Analysis Software"). We just must change the problem dimension. In case of 3D DLT, every correspondence Xi ← → xi

We get the following equation:

$$\begin{bmatrix} 0^T & -w_i X_i^T & y_i X_i^T \\ w_i X_i^T & 0^T & -x_i X_i^T \\ -y_i X_i^T & x_i X_i^T & 0^T \end{bmatrix} \begin{pmatrix} P^1 \\ P^2 \\ P^3 \end{pmatrix} = 0$$

The p matrix represents the 3D data.